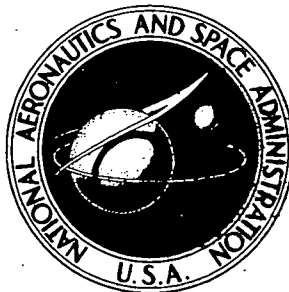


NASA TECHNICAL NOTE



NASA TN D-7367

N74-10014

NASA TN D-7367

CASE FILE
COPY

EXPLORATORY INVESTIGATION AT
MACH NUMBERS FROM 0.40 TO 0.95 OF
THE EFFECTS OF JETS BLOWN OVER A WING

by Lawrence E. Putnam

Langley Research Center

Hampton, Va. 23665

1. Report No. NASA TN D-7367	2. Government Accession No.	3. Recipient's Catalog No.	
4. Title and Subtitle EXPLORATORY INVESTIGATION AT MACH NUMBERS FROM 0.40 TO 0.95 OF THE EFFECTS OF JETS BLOWN OVER A WING		5. Report Date November 1973	
		6. Performing Organization Code	
7. Author(s) Lawrence E. Putnam		8. Performing Organization Report No. L-9067	
		10. Work Unit No. 501-24-06-01	
9. Performing Organization Name and Address NASA Langley Research Center Hampton, Va. 23665		11. Contract or Grant No.	
		13. Type of Report and Period Covered Technical Note	
12. Sponsoring Agency Name and Address National Aeronautics and Space Administration Washington, D.C. 20546		14. Sponsoring Agency Code	
		15. Supplementary Notes	
16. Abstract An exploratory investigation has been made at Mach numbers from 0.40 to 0.95 to determine the effects on lift, drag, and pitching moment of blowing a jet exhaust over the upper surface of a 50° swept leading-edge wing. Also investigated were the effects of varying the longitudinal and vertical location of the nozzle exit on the induced effects of jet blowing.			
17. Key Words (Suggested by Author(s)) Jet effects Jet over wing Induced lift Induced drag Subsonic		18. Distribution Statement Unclassified - Unlimited	
19. Security Classif. (of this report) Unclassified	20. Security Classif. (of this page) Unclassified	21. No. of Pages 69	22. Price* Domestic, \$3.50 Foreign, \$6.00

EXPLORATORY INVESTIGATION AT MACH NUMBERS FROM 0.40 TO 0.95 OF THE EFFECTS OF JETS BLOWN OVER A WING

By Lawrence E. Putnam
Langley Research Center

SUMMARY

An exploratory investigation has been made at Mach numbers from 0.40 to 0.95 to determine the effects on lift, drag, and pitching moment of blowing a jet exhaust over the upper surface of a 50° swept leading-edge wing. Also investigated were the effects of varying the longitudinal and vertical location of the nozzle exit on the induced effects of jet blowing.

The results of the investigation indicate that blowing the jet exhaust over the wing caused an increase in lift and drag at a given angle of attack. Note that the results of this investigation pertain only to the forces and moments acting on the wing and afterbody of the model. No measurements were made of the forces and moments acting on the model forebody and nacelles. The increases in lift and drag are such as to increase the drag coefficient at zero lift, and at Mach numbers of 0.40 and 0.60 to reduce the drag at lift coefficients greater than approximately 0.2. Above a Mach number of 0.60, because of test limitations, insufficient data were obtained to ascertain the effects of jet blowing on the drag at lift coefficients greater than 0.2. These effects of jet blowing generally increase with increasing jet-total-pressure ratio. Increasing the vertical distance of the nacelle above the wing from 0.75 to 1.50 nozzle-exit diameters reduced the interference effects due to jet blowing. Increasing the longitudinal distance of the nozzle exit ahead of the wing from 2.59 to 4.59 nozzle-exit diameters had only small effects on the interference effects due to jet blowing.

INTRODUCTION

The joint DOT-NASA Civil Aviation Research and Development Policy Study (ref. 1) identified noise abatement and traffic congestion relief as the two highest priority needs for aviation and aeronautics research and development. The results of this study have given impetus to research in quiet engine technology (ref. 2, for example), operational procedures such as the use of steep-curved approaches and take-offs, and unorthodox engine locations to reduce the noise perceived on the ground in the vicinity of airports. One such unconventional engine location in which interest has revived is forward and

above the wing. (See ref. 3, for example.) References 4 to 6 indicate that it may be possible with this engine location to take advantage of Coanda turning of the jet exhaust as it passes over the wing to achieve high lift and to use the wing as a barrier to reduce jet noises propagated downward toward the ground during take-off and landing. Other benefits may accrue from locating the engines forward and above the wing, such as reduced landing-gear length and improved mass balance. It may also be possible to improve subsonic cruise performance of jet-transport aircraft by blowing the jet exhaust from forward mounted engines over the wing of the aircraft.

The present exploratory investigation was initiated, therefore, to study the aerodynamic interference effects of jets blowing over a wing at subsonic cruise conditions. In particular, the effects on the aerodynamic characteristics of a 50° swept leading-edge wing of jets exhausting from engine nacelles located 0.75 or 1.50 nozzle-exit diameters above the wing chord plane and 2.59 or 4.59 nozzle-exit diameters ahead of the wing leading edge were experimentally investigated. The tests were made in the Langley 16-foot transonic tunnel at Mach numbers from 0.40 to 0.95 and at angles of attack from -5° to 8° .

SYMBOLS

All force and moment coefficients are with respect to the stability-axis system or the body-axis system. The origin of these axis systems is located on the model center line at fuselage station 81.57 centimeters.

$C_{A,base}$ base-axial-force coefficient, $\frac{\text{Base axial force}}{q_\infty S}$

C_D drag coefficient, $\frac{\text{Drag}}{q_\infty S}$

$C_{D,st}$ drag coefficient at $M = 0$, $\frac{\text{Drag}}{p_\infty S}$

$\Delta C_D = C_{D,jet\ on} - C_{D,jet\ off}$

C_L lift coefficient, $\frac{\text{Lift}}{q_\infty S}$

$C_{L,st}$ lift coefficient at $M = 0$, $\frac{\text{Lift}}{p_\infty S}$

$C_{L\alpha}$ lift-curve slope at $\alpha = 0^\circ$

$C_{L,\alpha=0^\circ}$ lift coefficient at $\alpha = 0^\circ$

$$\Delta C_{L,\alpha=0^0} = (C_{L,\alpha=0^0})_{\text{jet on}} - (C_{L,\alpha=0^0})_{\text{jet off}}$$

C_m pitching-moment coefficient, $\frac{\text{Pitching moment}}{q_\infty S \bar{c}}$

$C_{m,st}$ pitching-moment coefficient at $M = 0$, $\frac{\text{Pitching moment}}{p_\infty S \bar{c}}$

C_{mC_L} longitudinal-stability parameter, $\frac{\partial C_m}{\partial C_L}$ at $C_L = 0$

$C_{T,i}$ aerodynamic ideal-gross-thrust coefficient, $\frac{F_i}{q_\infty S}$

$(C_{T,i})_{st}$ aerodynamic ideal-gross-thrust coefficient at $M = 0$, $\frac{F_i}{p_\infty S}$

c local chord of pylon

\bar{c} mean geometric chord of wing, 32.28 cm

d_b base diameter of nozzles

d_e exit diameter of nozzles

d_m maximum diameter of nacelles

F_i ideal gross thrust for isentropic expansion of measured total-mass-flow rate to free-stream static pressure

h height of nacelle center line above wing chord plane

l longitudinal distance from nozzle exit to wing leading edge measured along nacelle center line

l_n nacelle length

l_{noz} nozzle length

M free-stream Mach number

\dot{m}_j measured total-mass-flow rate

$p_{t,j}$ jet total pressure

p_{∞}	free-stream static pressure
q_{∞}	free-stream dynamic pressure
R	gas constant
r_f	fuselage radius defined in figure 4
r_n	nacelle radius
S	reference wing area, 2599.89 cm ²
$T_{t,j}$	jet total temperature
x	axial distance from fuselage nose
x_n	axial distance from nacelle nose
x_p	axial distance from leading edge of pylon
y,z	rectangular coordinates
y_r,z_r	rectangular coordinates of center of fuselage radius r_f (see fig. 4)
z_p	pylon vertical coordinate
α	angle of attack referenced to wing chord plane, deg
γ	ratio of specific heats
δ	slope of airfoil surface at trailing edge, 3.64°

APPARATUS AND PROCEDURES

Wind Tunnel

The investigation was conducted in the Langley 16-foot transonic tunnel, which is a single-return atmospheric wind tunnel with slotted octagonal test section and continuous air exchange. The wind tunnel has continuously variable airspeed up to a Mach number of 1.30. Test-section plenum suction is used for speeds above a Mach number of 1.10.

By using calibrations of the wind tunnel, the test-section-wall divergence is adjusted as a function of airstream dewpoint to eliminate any longitudinal static-pressure gradients in the test section that might occur because of condensation of atmospheric moisture.

Model, Support System, and Instrumentation

A sketch of the model used in the investigation is shown in figure 1. The model was supported in the wind tunnel with the sting-strut system shown in the photographs of figure 2 and the sketch of figure 3. The strut which attached to the nonmetric forebody of the model had a 45° swept leading edge and a 5-percent-thick (streamwise) hexagonal airfoil. The sting-strut was located in the wind tunnel such that the center line of the tunnel and the center line of the model at zero angle of attack coincided.

The model consisted of the nonmetric forebody, two sets of nonmetric engine nacelles and pylons which attached to the forebody, the metric afterbody, and the metric wing. The afterbody and wing were mounted on a six-component strain-gage balance which was attached to the model forebody. This strain-gage balance was used to measure the aerodynamic forces and moments on the afterbody and wing. (Note, as shown in fig. 1, that the metric portion of the model starts at fuselage station 68.58 cm.) A Teflon strip inserted into grooves machined into the afterbody shell and the forebody was used as a seal to prevent internal flow into the model at the gap between the forebody and afterbody. The Teflon strip, because of its low coefficient of friction, minimized axial restraint on the balance. Sixteen pressure orifices were located in the vicinity of the metric break station for use in determining the internal static pressure at the break and the external static pressures acting on the forward rim of the afterbody outside the seal. Four pressure orifices were located at the base of the afterbody for determining fuselage base pressure.

The 50° swept leading-edge wing had an aspect ratio of 3.0, a taper ratio of 0.3, and an NACA 64A006 (streamwise) airfoil. The fuselage, which had an effective fineness ratio of 5.68, had essentially rectangular cross sections with rounded corners. Details of the fuselage cross section at various longitudinal stations are presented in figure 4. The engine nacelle simulators had circular-arc boattail nozzles and were attached to pylons which were in turn attached to the nonmetric forebody of the model. (See fig. 5.) Provisions were made to change the length of the nacelles from 35.560 cm to 45.720 cm by inserting a cylindrical section into the nacelle just ahead of the nozzle. Provisions were also made to change the vertical location of the nacelle-pylon combination as shown in figure 1 from 3.81 cm to 7.62 cm above the wing chord plane.

A continuous flow of dry high-pressure air at a stagnation temperature of approximately 300 K was used to simulate the jet exhaust from the engine nacelles. The air is ducted through the sting-strut system to a plenum located in the model forebody. From

this plenum the high-pressure air is ducted through the pylons into the engine nacelles. (See fig. 5.) A perforated flow smoothing plate and a set of flow straightening vanes were located downstream of the point where the high-pressure air is dumped in the engine-nacelle simulators. A total-pressure probe and a total-temperature probe were located in each nacelle simulator downstream of the flow straightening vanes. A turbine flow-meter was used to obtain the mass-flow rate to the nozzles.

Tests

This investigation was conducted at Mach numbers of 0.40, 0.60, 0.70, 0.80, 0.90, and 0.95 at a sideslip angle of 0° . Because of strain-gage-balance load limits the test angle-of-attack range varied with Mach number. The angle-of-attack range was -5° to 8° at $M = 0.40$ and decreased to -3.5° to 2.5° at $M = 0.95$. The Reynolds number, based on the wing mean geometric chord, varied from 2.6×10^6 at $M = 0.40$ to 4.4×10^6 at $M = 0.95$. The ratio of the jet total pressure to free-stream static pressure was varied from approximately 1 at the jet-off condition to approximately 7.7, depending on free-stream Mach number. Tests were made with the nacelles located 0.75 and 1.50 nozzle-exit diameters above the wing chord plane. At each nacelle vertical position, tests were made with and without the nacelle cylindrical extension such that the nozzle-exit location varied from 2.59 to 4.59 nozzle-exit diameters ahead of the wing leading edge. Additional tests were made to determine the aerodynamic characteristics of the wing and afterbody with the nacelles and pylons removed from the nonmetric forebody.

Boundary-Layer Transition

All tests of the present investigation were made with fixed transition to minimize changes in the aerodynamic forces and moments owing to changes in the extent of laminar flow on the model. Transition strips, 0.13 cm wide, were located on the upper and lower surfaces of each pylon and the wing, on the nose of each nacelle, and on the nose of the fuselage. The transition strips on the pylons were 1.272 cm aft of the pylon leading edge, and the transition strips on the nacelles and fuselage were located 2.54 cm aft of the nose of each component. The transition strips on the wing were located on a straight line from 5 percent of the wing chord at the wing-fuselage junction to 10 percent of the wingtip chord. These transition strips consisted of No. 100 (0.015-cm nominal particle size) silicon carbide grit with a suitable adhesive. The grit size and location of the transition strips were selected according to the recommendations of references 7 and 8.

Data Reduction and Corrections

In the present investigation the strain-gage balance measured the total forces and moments on the afterbody and wing of the configuration. In addition to the external skin

friction and the external pressure forces, the axial force measured by the balance included pressure tare forces that act on the afterbody forward rim just outside the metric-gap seal and on the inside of the afterbody shell. The measured axial force was therefore corrected for these pressure tares by subtracting the product of the axial projection of these areas and the average difference between the local and free-stream static pressures. The measured axial force was also corrected for the base pressures acting on the base of the afterbody. The base-axial-force coefficients are presented in figures 6 and 7.

The angle of attack of the model afterbody has been corrected for sting-strut and balance deflections due to aerodynamic loads. Note that, because of the location of the balance in the model, the balance deflection due to aerodynamic loads on the afterbody and wings causes the metric portion of the model to be at a different angle of attack than the nonmetric forebody. (The maximum difference in forebody and afterbody angle of attack for the tests was approximately 0.7° .) In the present investigation the angle of attack was not corrected for tunnel flow angularity. (In the Langley 16-foot transonic tunnel the upflow angle is on the order of 0.1° .)

Single-probe jet-total-pressure readings in each nacelle tailpipe were corrected to the integrated average exit value for each nozzle as determined from individual pretest rake surveys behind each exit. The average of the two corrected values (right and left) of jet total pressure was used to obtain the ratio of jet total pressure to free-stream static pressure. The integrated total pressures at the left and right nozzle exits generally differed by less than 4 percent. Average total temperatures and average corrected total pressures were also used with total measured mass flow and total exit area to calculate the ideal-gross-thrust coefficients presented in figure 8. The ideal gross thrust was calculated from the following equation by assuming that the measured total-mass-flow rate expanded isentropically to free-stream static pressure:

$$F_i = \dot{m}_j \sqrt{\frac{2\gamma}{\gamma - 1} RT_{t,j} \left[1 - \left(\frac{p_\infty}{p_{t,j}} \right)^{\frac{\gamma-1}{\gamma}} \right]}$$

where

$$\gamma = 1.4$$

RESULTS

Note that all data presented herein pertain only to the forces and moments acting on the wing and afterbody of the model. No measurements were made of the forces and moments acting on the model forebody or on the nacelles and pylons.

The results of the investigation are presented in the following figures:

	Figure
Effects of jet-total-pressure ratio at $M = 0$	9
Effects of jet-total-pressure ratio at constant angles of attack	10
Effects of jet-total-pressure ratio as function of lift coefficient for configuration with nozzle exit in –	
Low-aft position	11
Low-forward position	12
High-aft position	13
High-forward position	14
Summary of effects of jet-total-pressure ratio	15
Effects of nozzle-exit position; jet off	16
Summary of effects of nozzle-exit position; jet off	17
Summary of effects of nozzle-exit position; jet on	18

DISCUSSION

Effects of Jet-Total-Pressure Ratio

At static conditions ($M = 0$), increasing the ratio of jet-exit total pressure to free-stream static pressure caused an increase in the lift coefficient of the wing and afterbody for all nozzle positions. (See fig. 9(a).) The increase in lift coefficient is approximately one-third of the lift that could be developed if the total ideal-gross-thrust vector is turned by the Coanda effect as the jet passes over the wing an amount equal to the angle at the trailing edge of the airfoil of the wing. Flow visualization studies (fig. 9(b)) indicated that with the nozzles in the low position a large area of the wing upper surface was washed by the jet exhaust. The resulting scrubbing drag increased with jet-total-pressure ratio. With the nozzles in the high position only a small area of the wing was washed by the jet exhaust, and as a result no measurable effect of jet-total-pressure ratio on drag coefficient was observed.

At Mach numbers from 0.40 to 0.90, increasing jet-total-pressure ratio also caused an increase in the lift coefficient of the wing and afterbody. (See fig. 10.) The variation of lift with jet-total-pressure ratio at these Mach numbers was essentially unaffected by angle of attack such that at a given jet-total-pressure ratio only small differences in lift-curve slope between the jet-on and jet-off conditions occur. (See figs. 11 to 14.) At $M = 0.95$, the lift variation with jet total pressure is dependent on angle of attack; however,

in general, only small changes in lift coefficient with pressure ratio occur at this Mach number.

The pitching-moment coefficient of the wing and afterbody generally decreases with increasing jet-total-pressure ratio at a given angle of attack. These pitching-moment changes combine with the lift changes due to jet-total-pressure ratio such that there is essentially no effect of jet blowing on the variation of pitching-moment coefficient with lift coefficient at all test Mach numbers except 0.95. (See figs. 11 to 14.) At $M = 0.95$, some small reductions in the pitching-moment coefficient at zero lift and some small inconsistent changes in longitudinal stability result from increasing jet-total-pressure ratio.

Associated with the increase in afterbody and wing lift at positive angles of attack is a corresponding increase in drag coefficient with increasing jet-total-pressure ratio. (See fig. 10.) These two effects of jet blowing, increased lift and increased drag at a given angle of attack, are such as to increase the drag coefficient at or near zero lift and to reduce the drag of the wing and afterbody at high-lift conditions. (See figs. 11 to 14.) The increment in drag coefficient ΔC_D at zero lift, which is most likely associated with scrubbing drag on the upper wing surface, is shown in figure 15 to increase with increasing jet-total-pressure ratio. As the Mach number increases up to the transonic-drag-rise Mach number, the increment in drag coefficient at zero lift decreases. Above the transonic-drag-rise Mach number the increment in zero-lift-drag coefficient increased with increasing Mach number. At Mach numbers of 0.40 and 0.60 jet blowing caused a reduction in drag coefficient at lift coefficients above approximately 0.2. The reduction corresponds to a favorable drag increment, the magnitude of which generally increases with jet-total-pressure ratio. Because of test limitations, data were not obtained at sufficiently high lift coefficients at Mach numbers greater than 0.60 to ascertain whether these favorable effects on drag coefficient will occur at these Mach numbers.

Effects of Nozzle-Exit Location

Jet off. - The location of the nozzle exit had essentially no effect on the lift-curve slope of the wing and afterbody with the jet off. (See figs. 16 and 17.) Nozzle-exit location did, however, cause some small changes in the lift coefficient at zero angle of attack. The lift coefficient at zero angle of attack generally decreased with Mach number. The configuration with the nacelles and pylons in the low position had a greater value of $C_{L,\alpha=0^\circ}$ at each Mach number than the configuration with nacelles and pylons in the high position. The lift-curve slope of the wing and afterbody, when the nacelles and pylons were attached to the forebody, was approximately 20 percent lower than $C_{L\alpha}$ for the wing and afterbody when the nacelles and pylons were off. This reduction in $C_{L\alpha}$ is

associated in part with the induced downwash field of the nacelles and pylons reducing the effective angle of attack of the wing and in part with the reduction in dynamic pressure at the wing because of the wakes of the nacelles and pylons. Note that the reduction in $C_{L\alpha}$ for the wing and afterbody does not imply that $C_{L\alpha}$ for the complete configuration (that is, forebody, nacelles, pylons, wing, and afterbody) has decreased; indeed, calculations made by the method of reference 9 show that the lift-curve slope for the complete configuration would increase as a result of the lift produced by the pylons.

In general, nozzle-exit position had only small effects on the pitching-moment coefficient at zero lift but did cause changes in the aerodynamic-center location of the wing and afterbody. The aerodynamic-center location (fig. 17) for the configurations with the nacelles and pylons in the low position is approximately 4 percent of the mean geometric chord aft of the aerodynamic-center location for the configurations with nacelles and pylons in the high position. Longitudinal location of the nozzle exit had only small effects on the aerodynamic-center location for the wing and afterbody. Locating the nacelles and pylons on the forebody increased the longitudinal stability of the wing and afterbody. This increase in stability is associated with the aforementioned effects of the wake and downwash field of the nacelles and pylons.

Only small effects of nacelle-exit position on the jet-off drag coefficient of the wing and afterbody occur at Mach numbers below 0.80. (See figs. 16 and 17.) Above this Mach number the effects of nozzle-exit position become more pronounced. In general, the configuration with the nozzle exit in the high-aft position has the lowest wing and afterbody drag coefficient at each Mach number and lift coefficient. At Mach numbers below 0.80 the presence of the nacelles and pylons on the forebody caused a small reduction in the drag coefficient at zero lift for the wing and afterbody but caused a substantial increase in drag at lift. At Mach numbers above 0.80 the presence of the nacelles and pylons on the nonmetric forebody caused large reductions in drag coefficient throughout the test lift-coefficient range.

Jet on.- The jet exhaust from the nacelles in the low position ($h/d_e = 0.75$) blowing over the wing produced greater favorable lift interference than the jet exhaust from the nacelles in the high position ($h/d_e = 1.50$). (See fig. 18.) Changing the longitudinal location of the nozzle exit, however, had no substantial effect on the increments in lift coefficient because of blowing the jet exhaust over the wing.

The jet exhaust from the nacelles in the low positions generally caused greater increases in wing and afterbody drag coefficient at zero lift than the jet exhaust from the nacelles in the high positions. However, as a result of the greater interference lift associated with the nacelles in the low position, the favorable effects of the jets blowing over the wing on drag coefficients at lift coefficients above approximately 0.2 were greater for the low than for the high nacelle position. Changing the longitudinal location of the

nozzle exit from $l/d_e = 2.59$ to $l/d_e = 4.59$ had only small effects on the interference drag because of jet blowing at all lift coefficients and Mach numbers.

CONCLUSIONS

An exploratory investigation has been made at Mach numbers from 0.40 to 0.95 to determine the effects on lift, drag, and pitching moment of blowing a jet exhaust over the upper surface of a 50° swept leading-edge wing. Also investigated were the effects of varying the longitudinal and vertical location of the nozzle exit on the induced effects of jet blowing. Note that the results of this investigation pertain only to the forces and moments acting on the wing and afterbody of the model. No measurements were made of the forces and moments acting on the model forebody and nacelles. The results of the investigation indicate the following:

1. Blowing the jet exhaust over the wing caused an increase in lift coefficient and drag coefficient at a given angle of attack and an increase in the drag coefficient at zero lift. At Mach numbers of 0.40 and 0.60 blowing the jet exhaust over the wing caused a reduction in the induced drag at lift coefficients greater than approximately 0.2. Above a Mach number of 0.60, because of test limitations, insufficient data were obtained to ascertain effects of jet blowing on the drag at lift coefficients greater than 0.2.

2. The effects of jet blowing generally increase with increasing jet-total-pressure ratio.

3. Increasing the vertical distance of the nacelle above the wing from 0.75 to 1.50 nozzle-exit diameters reduced the effects of jet blowing.

4. Increasing the longitudinal distance of the nozzle exit ahead of the wing leading edge from 2.59 to 4.59 nozzle-exit diameters had only small effects on the interference effects due to blowing the jet over the wing.

Langley Research Center,
National Aeronautics and Space Administration,
Hampton, Va., August 21, 1973.

REFERENCES

1. Anon.: Civil Aviation Research and Development Policy Study - Report. NASA SP-265, 1971. (Also available as DOT TST-10-4.)
2. Anon.: Aircraft Engine Noise Reduction. NASA SP-311, 1972.
3. Winston, Donald C.: Boeing Delays Its Decision on 7X7. *Aviat. Week & Space Technol.*, vol. 98, no. 16, Apr. 16, 1973, pp. 24-27.
4. Riebe, John M.; and Davenport, Edwin E.: Exploratory Wind-Tunnel Investigation To Determine the Lift Effects of Blowing Over Flaps From Nacelles Mounted Above the Wing. NACA TN 4298, 1958.
5. Turner, Thomas R.; Davenport, Edwin E.; and Riebe, John M.: Low-Speed Investigation of Blowing From Nacelles Mounted Inboard and on the Upper Surface of an Aspect-Ratio-7.0 35° Swept Wing With Fuselage and Various Tail Arrangements. NASA MEMO 5-1-59L, 1959.
6. Kettle, D. J.; Kurn, A. G.; and Bagley, J. A.: Exploratory Tests on a Forward-Mounted Overwing Engine Installation. C.P. No. 1207, *Brit. A.R.C.*, 1972.
7. Braslow, Albert L.; and Knox, Eugene C.: Simplified Method for Determination of Critical Height of Distributed Roughness Particles for Boundary-Layer Transition at Mach Numbers From 0 to 5. NACA TN 4363, 1958.
8. Braslow, Albert L.; Hicks, Raymond M.; and Harris, Roy V., Jr.: Use of Grit-Type Boundary-Layer-Transition Trips on Wind-Tunnel Models. NASA TN D-3579, 1966.
9. Margason, Richard J.; and Lamar, John E.: Vortex-Lattice FORTRAN Program for Estimating Subsonic Aerodynamic Characteristics of Complex Planforms. NASA TN D-6142, 1971.

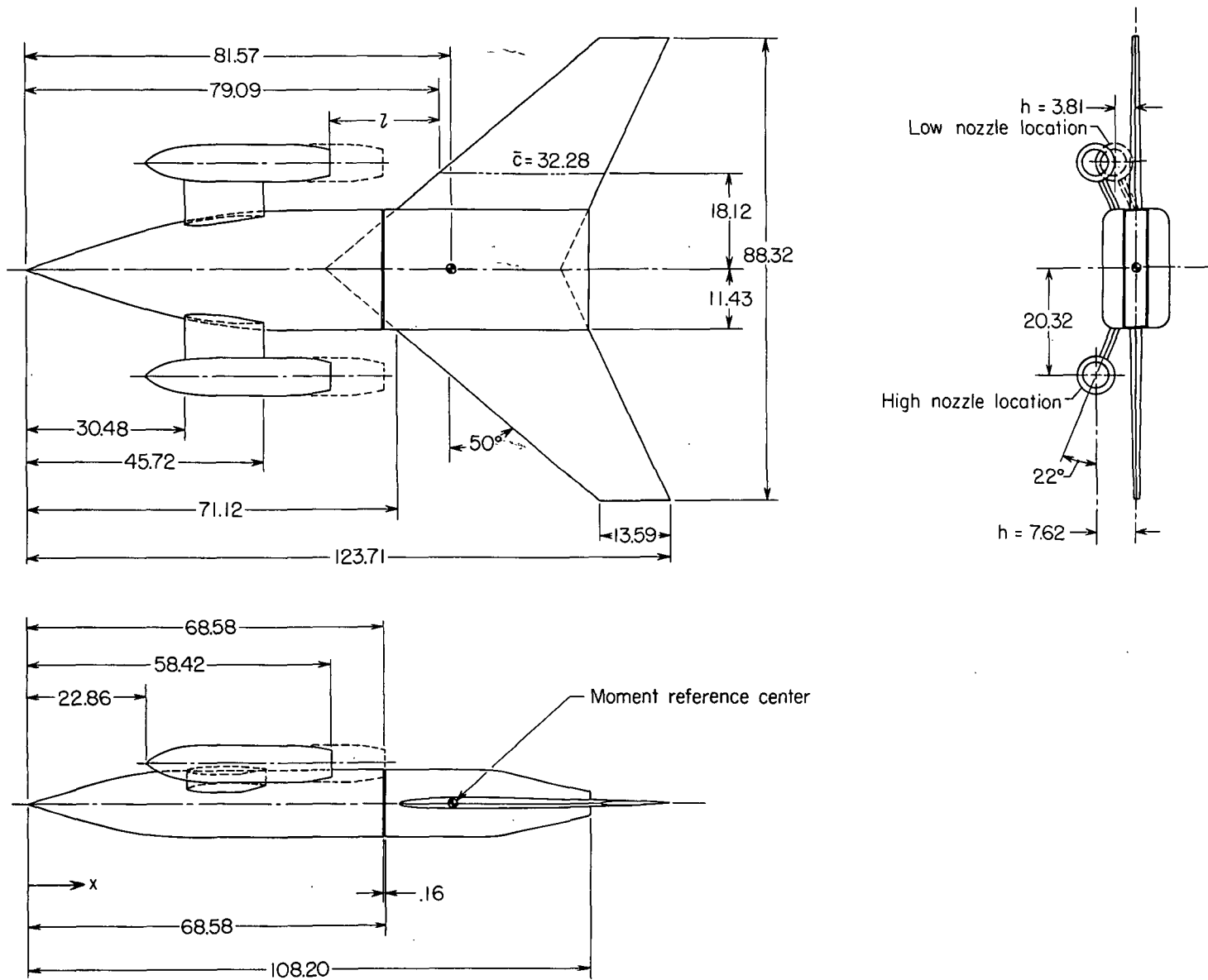
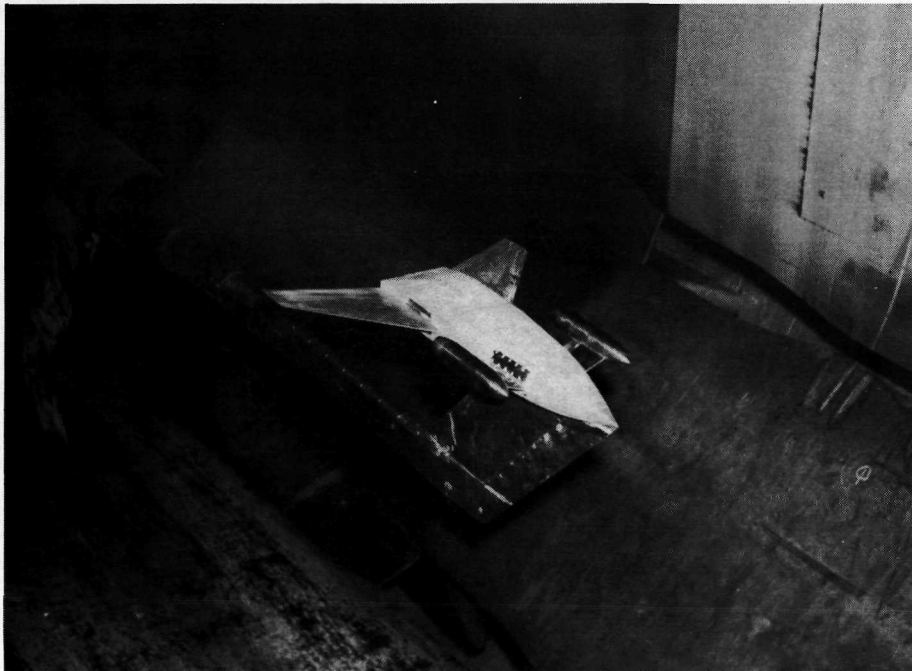


Figure 1.- Drawing of model. (All dimensions are in centimeters unless otherwise noted.)



L-72-3075

(a) Top-rear view of configuration with nozzle exits in high-forward position.



L-72-2849

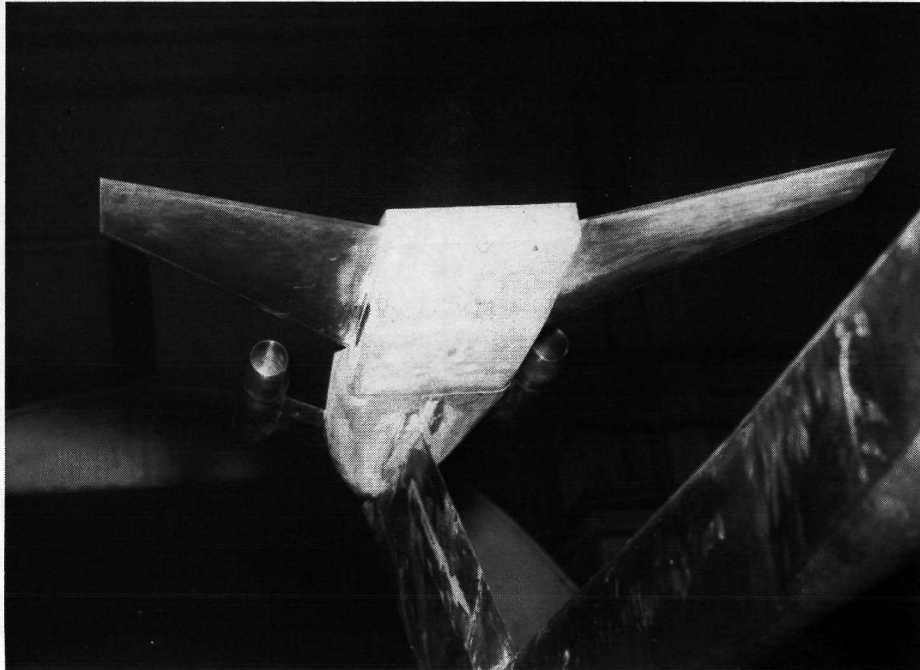
(b) Top-front view of configuration with nozzle exits in low-forward position.

Figure 2. - Photographs of model.



L-72-2852

(c) Bottom-front view of configuration with nozzle exits in low-forward position.



L-72-2850

(d) Bottom-rear view of configuration with nozzle exits in low-forward position.

Figure 2.- Concluded.

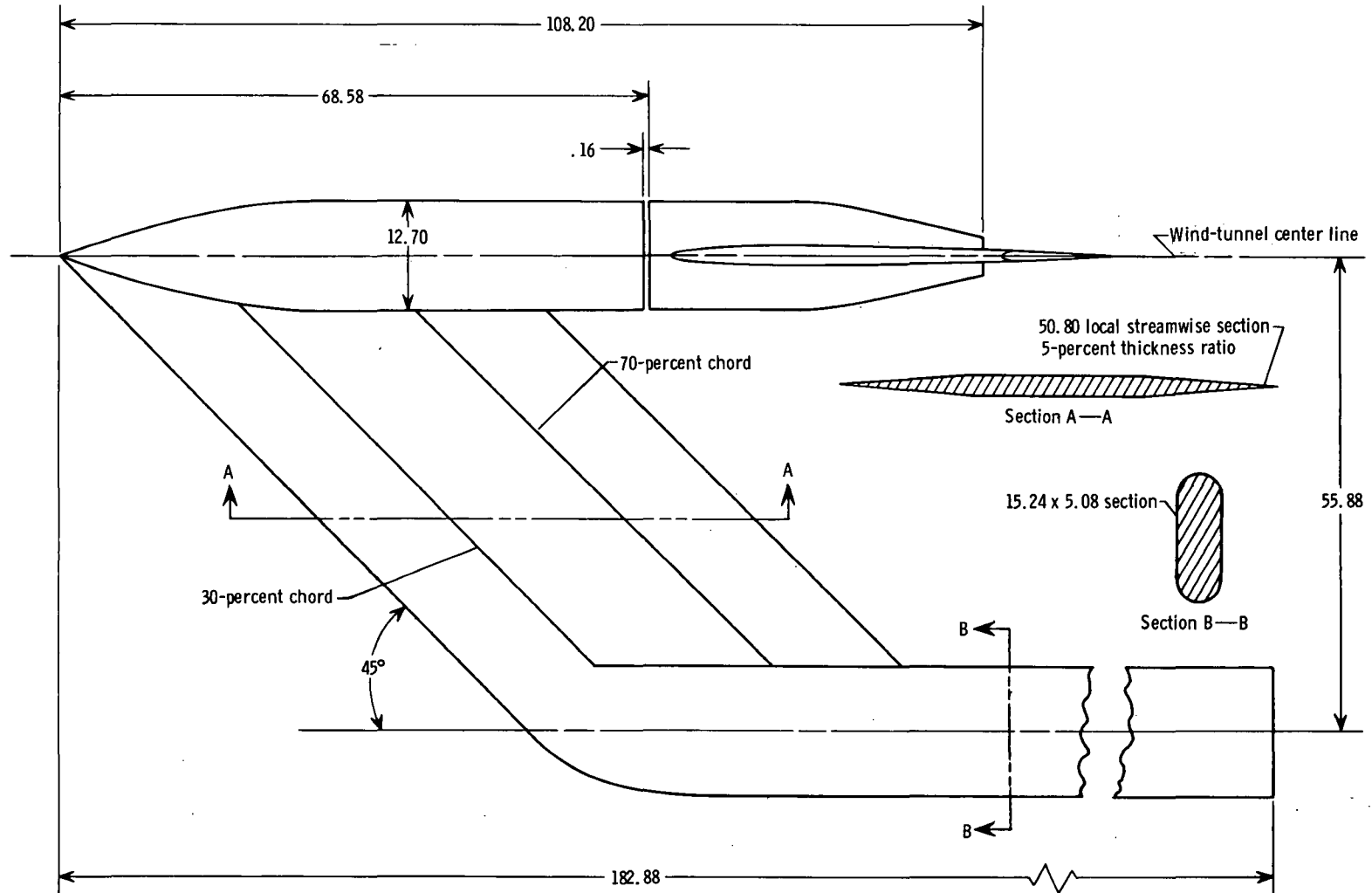
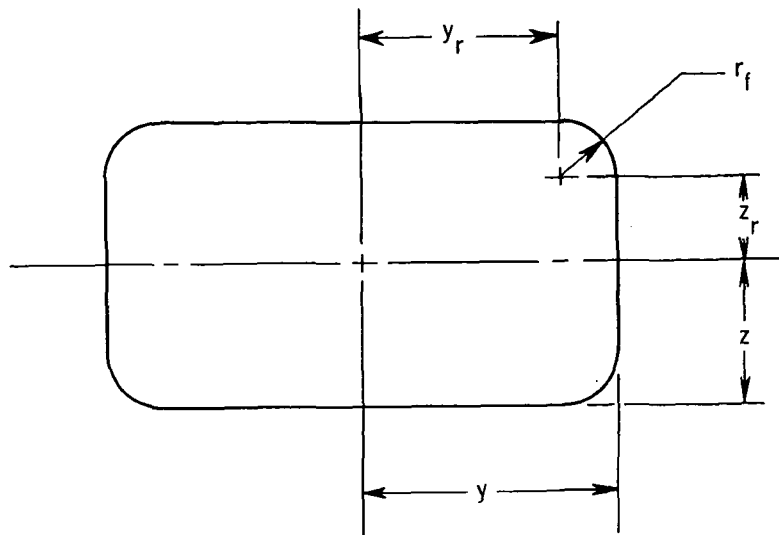


Figure 3.- Details of sting-strut support. (All dimensions are in centimeters unless otherwise noted.)



Typical cross section at fuselage station x

x	y	z	r _f	y _r	z _r
0	0	0	0	0	0
2.540	.916	.814	.814	.102	0
5.080	1.815	1.602	1.602	.102	0
7.620	2.694	2.359	2.359	.335	0
10.160	3.552	3.080	3.080	.472	0
15.240	5.192	4.379	4.379	.014	0
20.320	5.950	5.420	5.420	1.292	0
22.860	6.656	5.815	5.842	1.603	0
25.400	8.082	6.108	6.108	1.975	0
30.480	9.270	6.350	6.350	2.920	0
38.100	10.620	6.350	6.350	4.270	0
45.720	11.201	6.350	6.096	5.105	.254
49.530	11.328	6.350	5.334	5.994	1.016
55.880	11.328	6.350	3.937	7.391	2.413
63.500	11.430	6.350	2.540	8.890	3.810
68.420	11.430	6.350	2.540	8.890	3.810
68.580	11.430	6.350	2.540	8.890	3.810
73.660	11.430	6.350	2.540	8.890	3.810
78.740	11.430	6.350	2.540	8.890	3.810
83.820	11.430	6.350	2.540	8.890	3.810
88.900	11.430	6.350	2.540	8.890	3.810
90.170	11.430	6.266	2.563	8.867	3.701
91.008	11.430	6.098	2.464	8.966	3.635
91.440	11.430	6.003	2.403	9.027	3.600
101.600	11.430	3.750	1.026	10.404	2.724
108.204	11.430	2.286	0	11.430	2.286

Figure 4.- Details of fuselage. (All dimensions are in centimeters unless otherwise noted.)

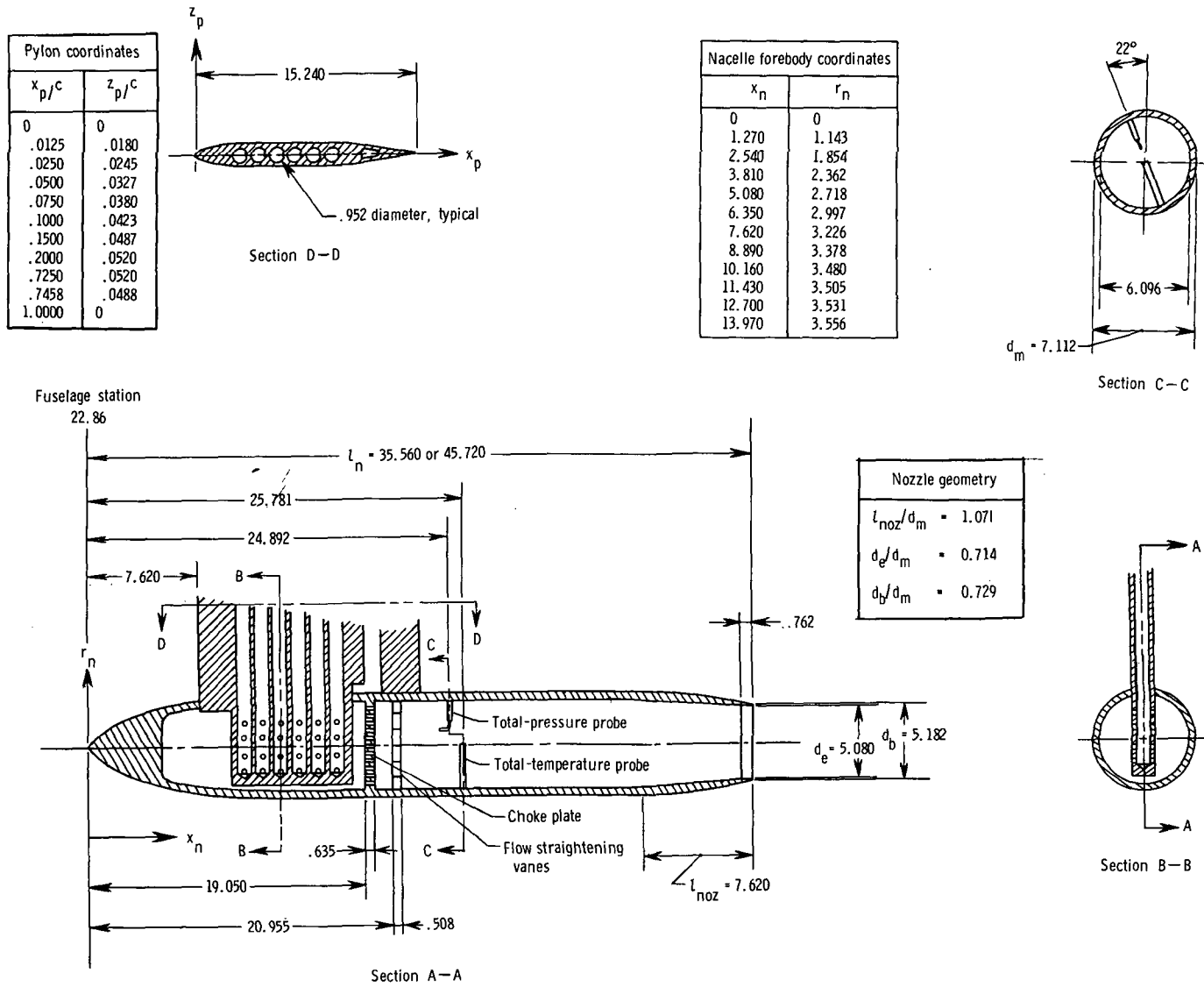


Figure 5.- Details of nacelles and pylons (left nacelle and pylon shown). (All dimensions are in centimeters unless otherwise noted.)

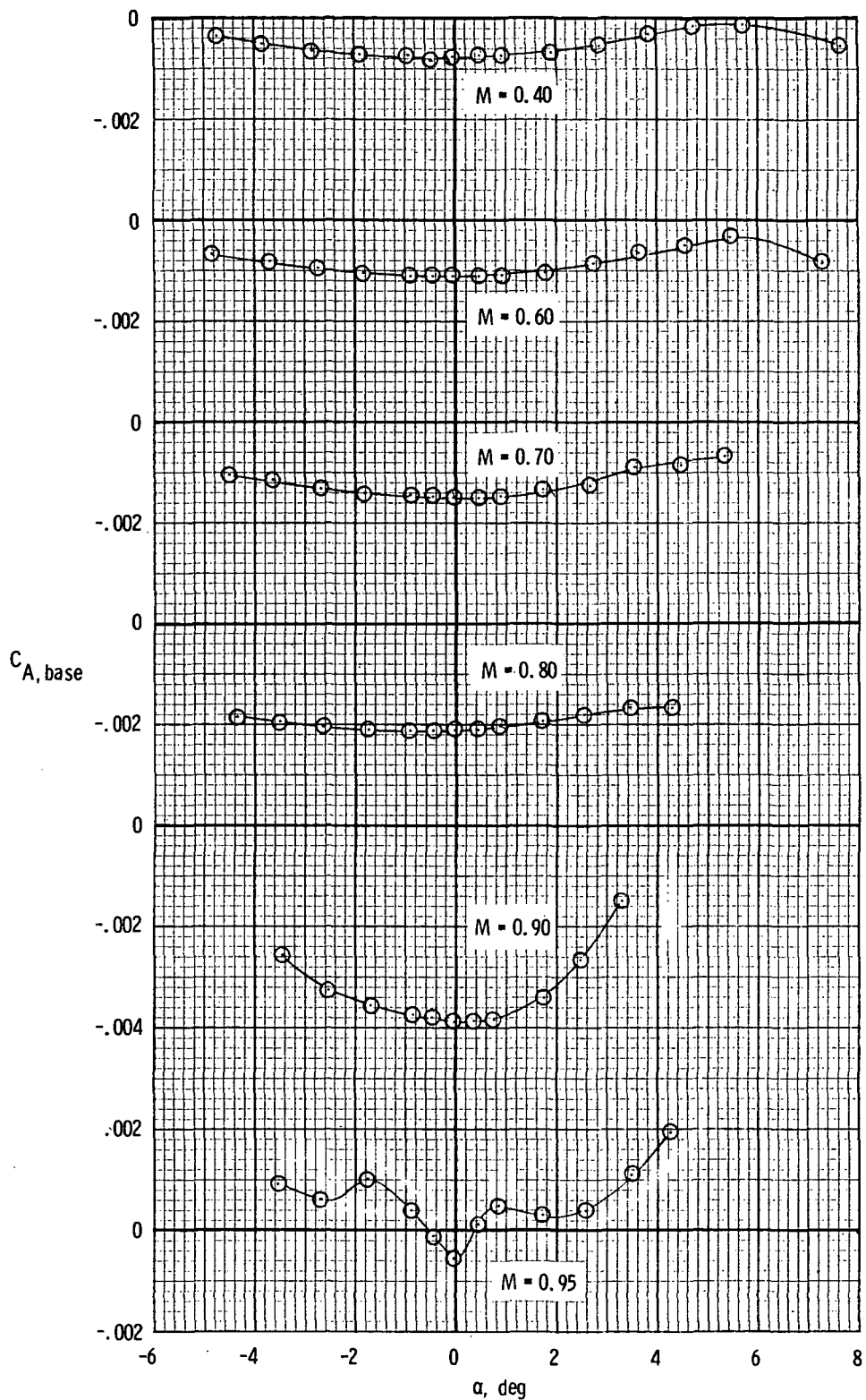


Figure 6.- Variation of base-axial-force coefficient with angle of attack for configuration with wings on and nacelles off.

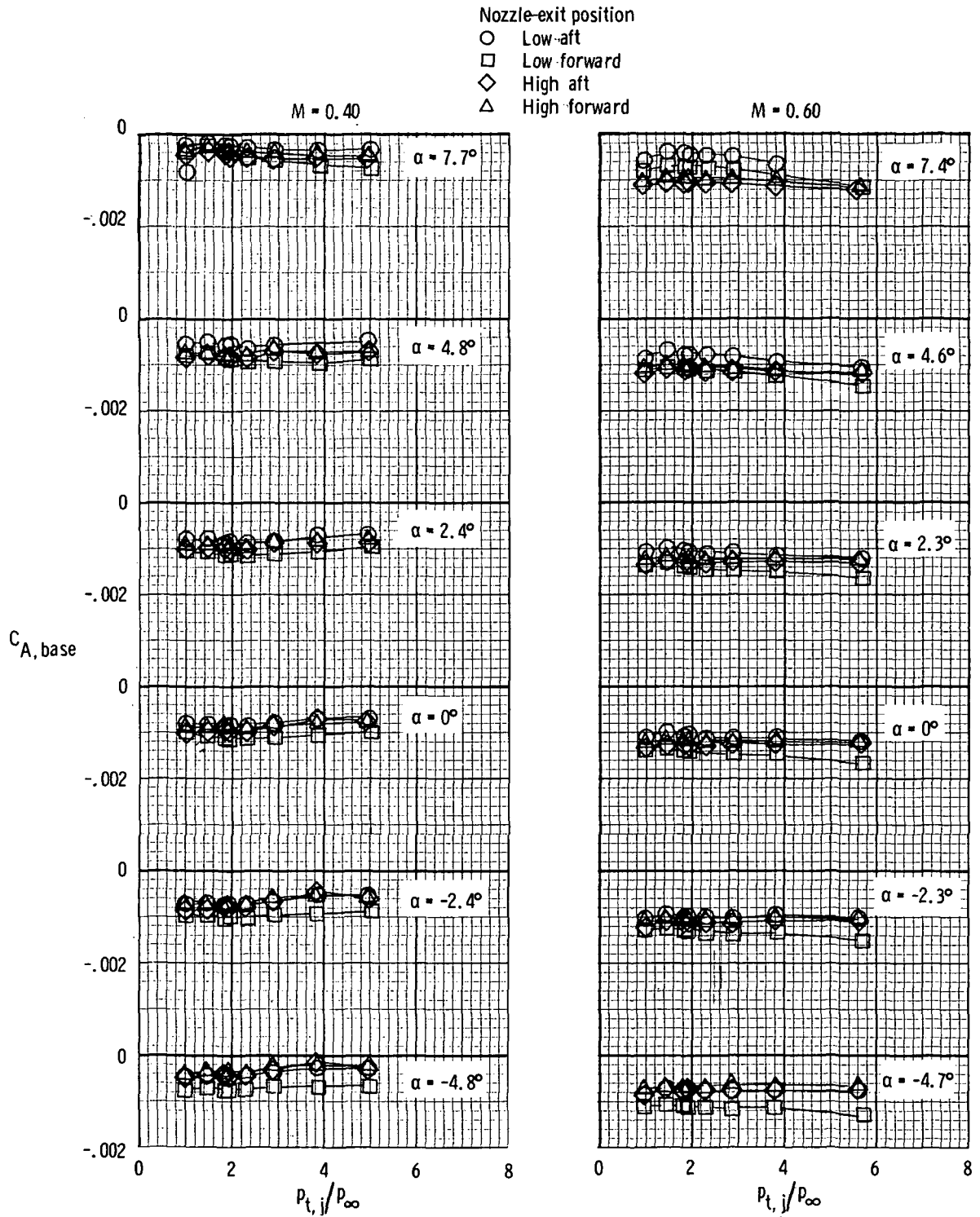
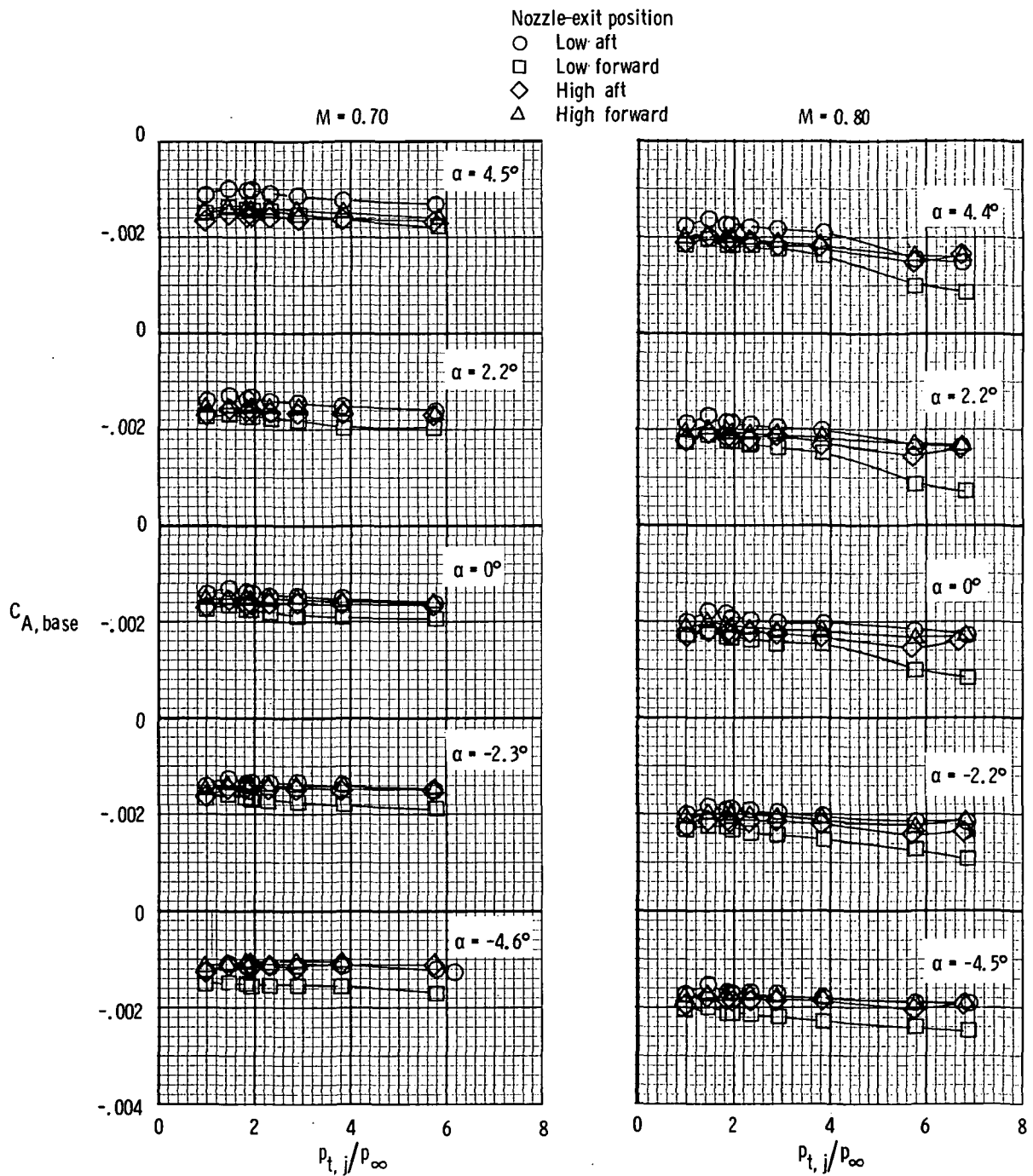
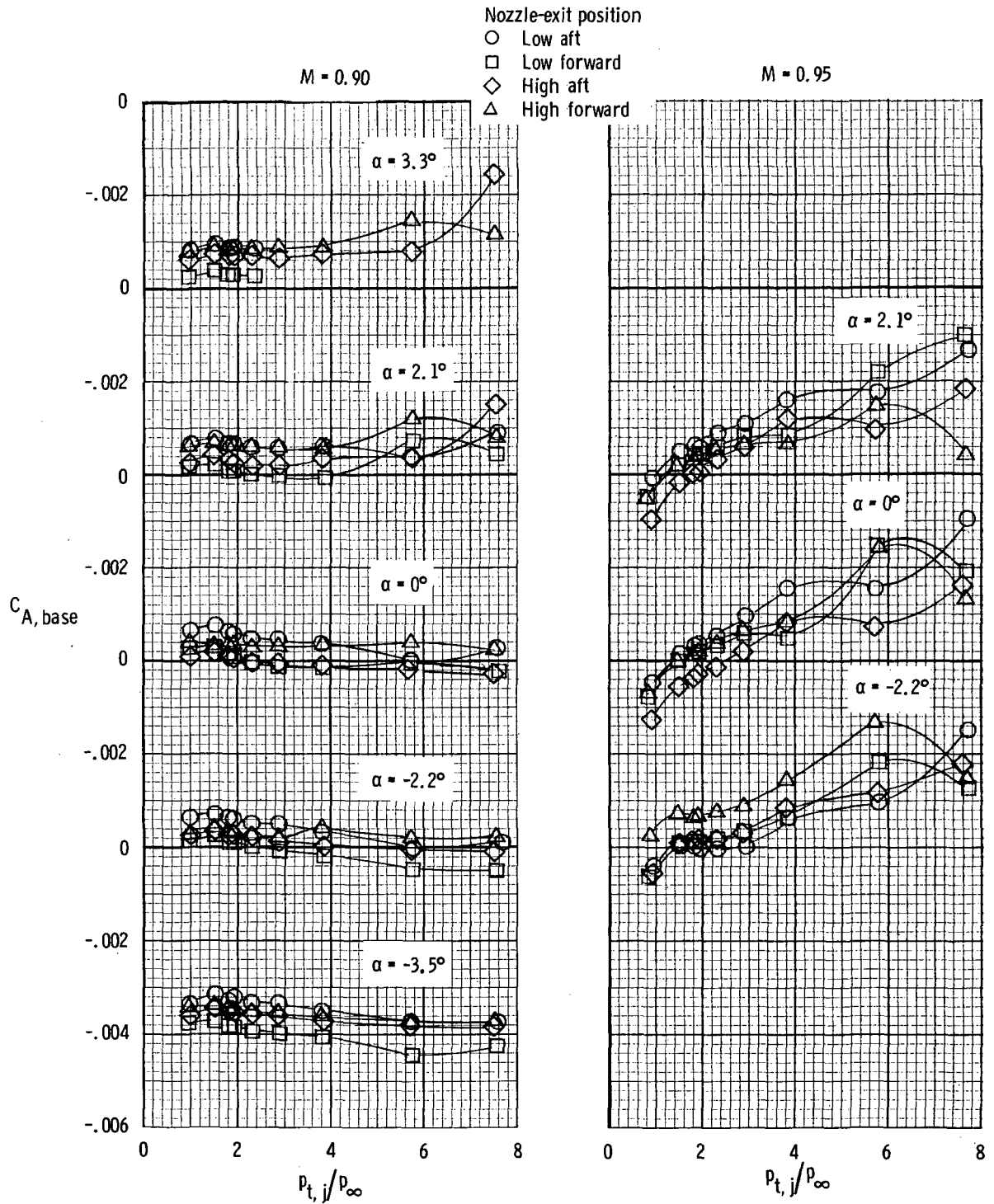


Figure 7.- Variation of base-axial-force coefficient with jet-total-pressure ratio.



(b) $M = 0.70$ and 0.80 .

Figure 7.- Continued.



(c) $M = 0.90$ and 0.95 .

Figure 7.- Concluded.

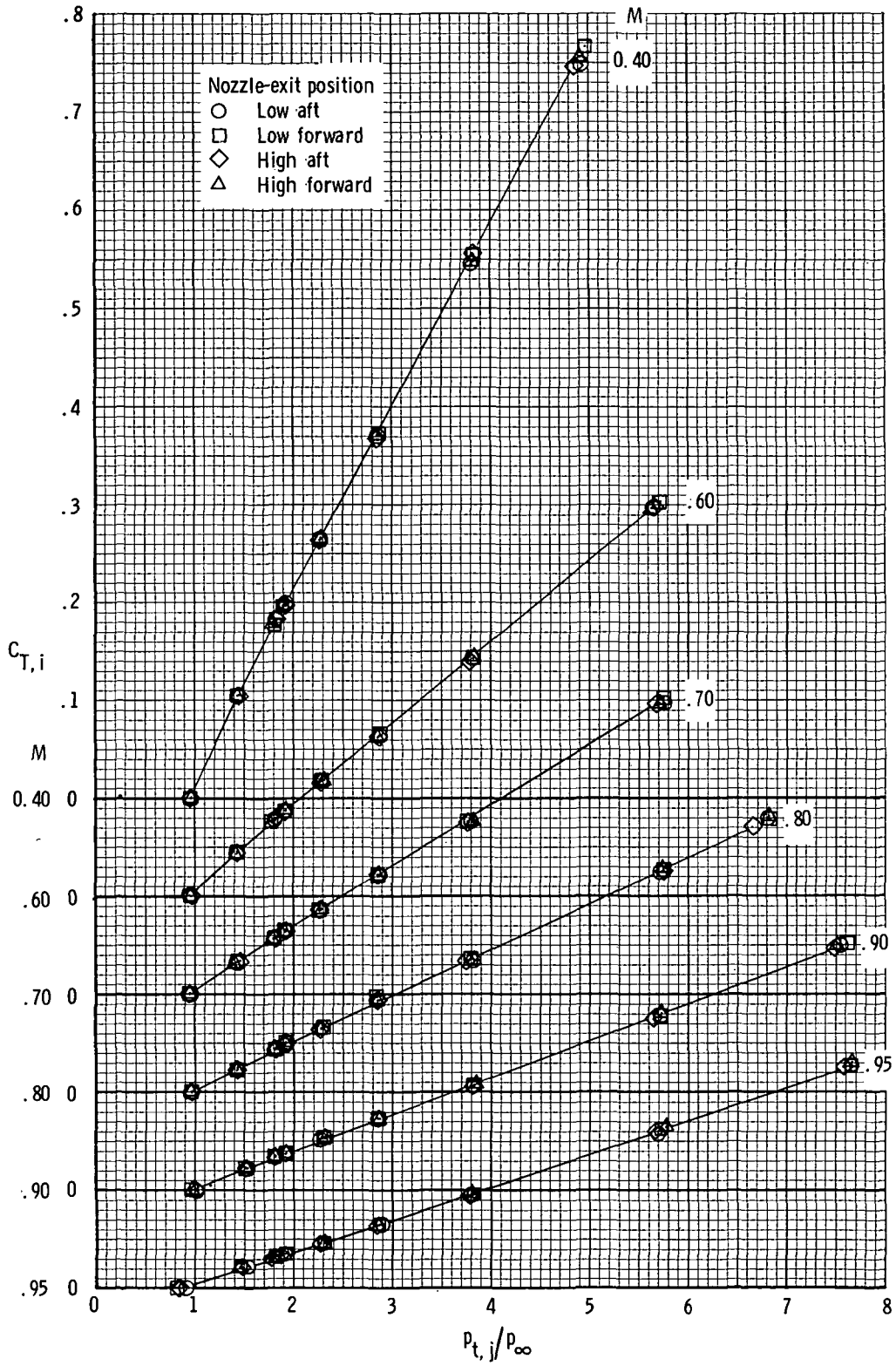
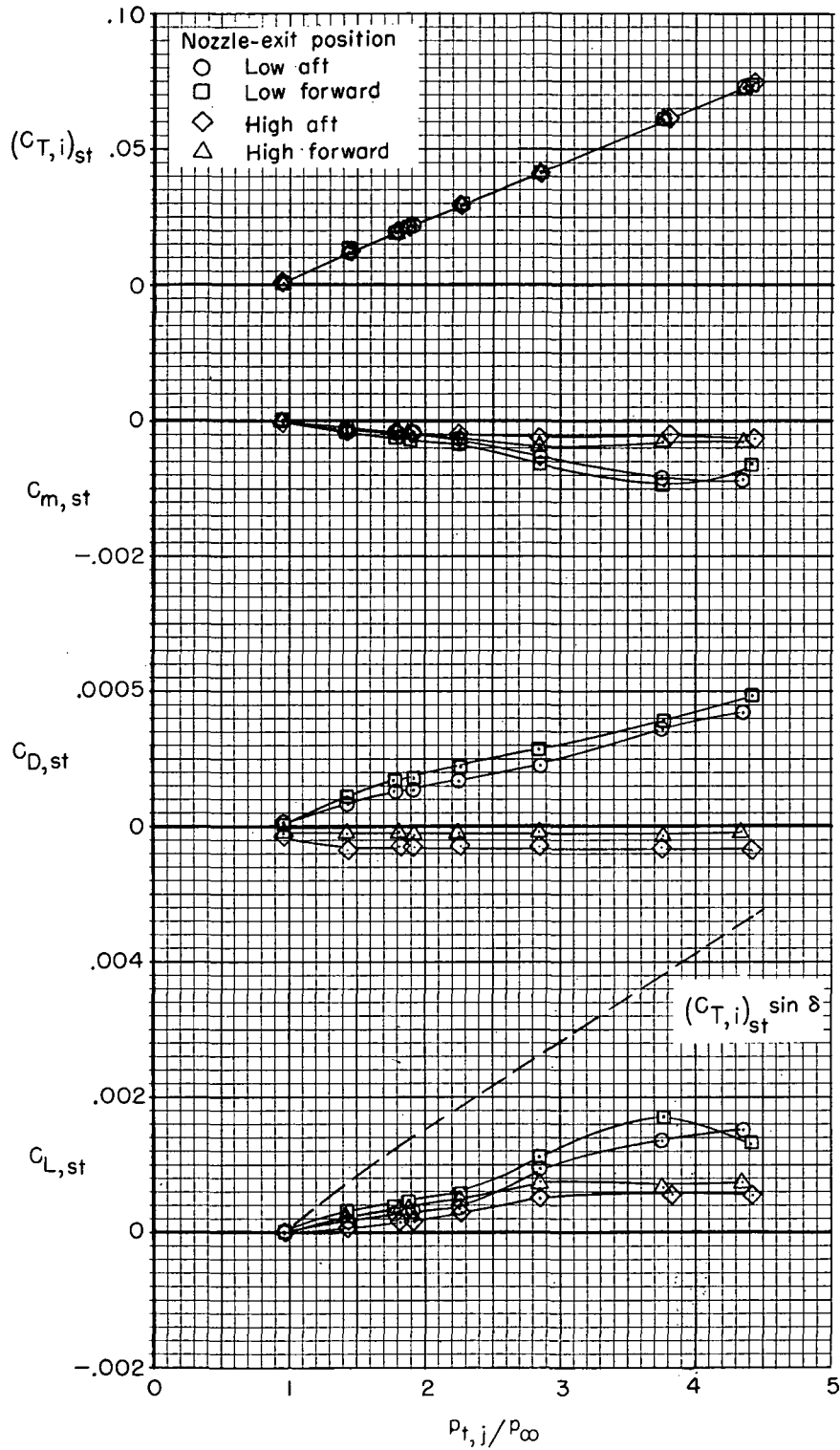
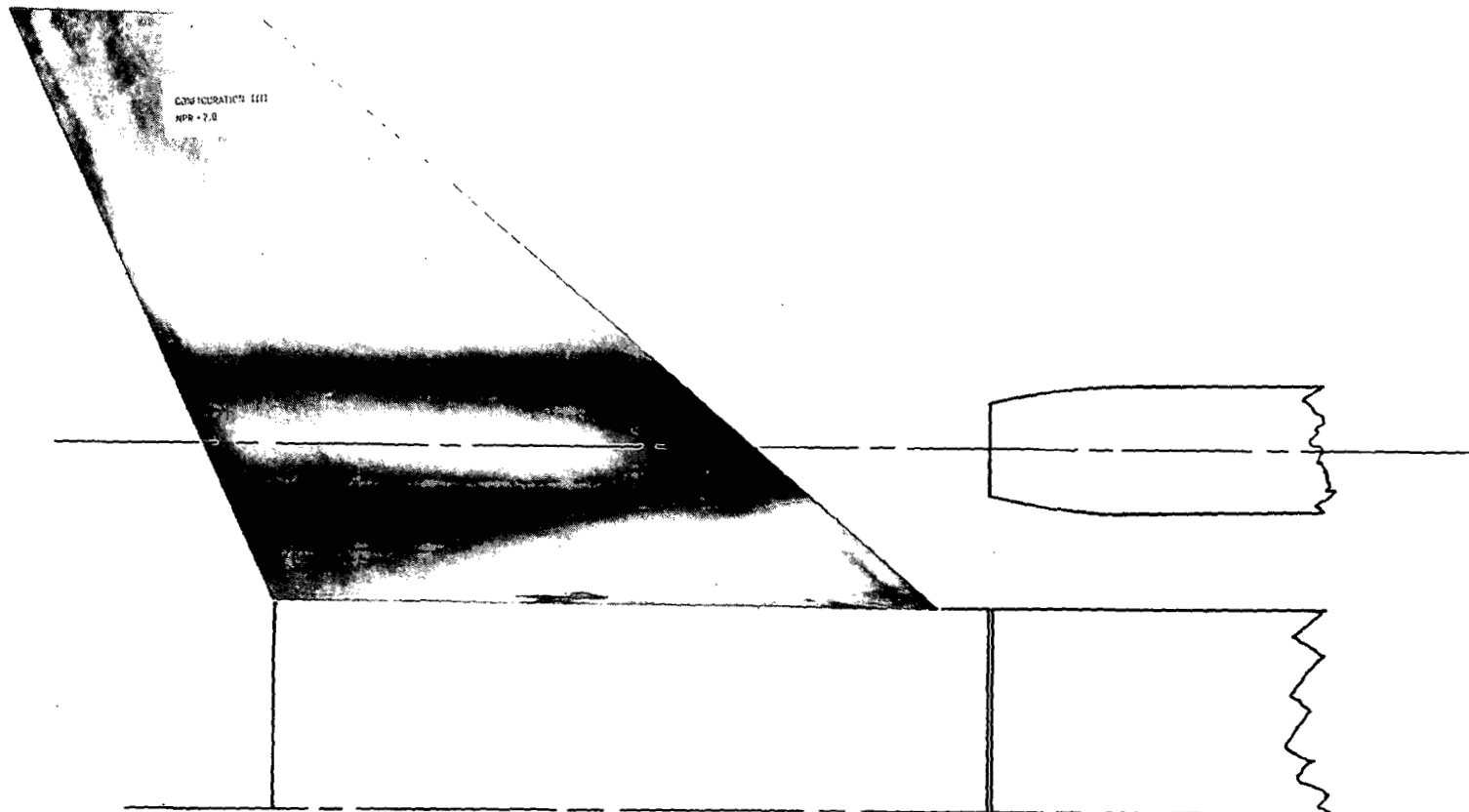


Figure 8.- Variation of ideal-gross-thrust coefficient with jet-total-pressure ratio.



(a) Variation of aerodynamic characteristics with jet-total-pressure ratio.

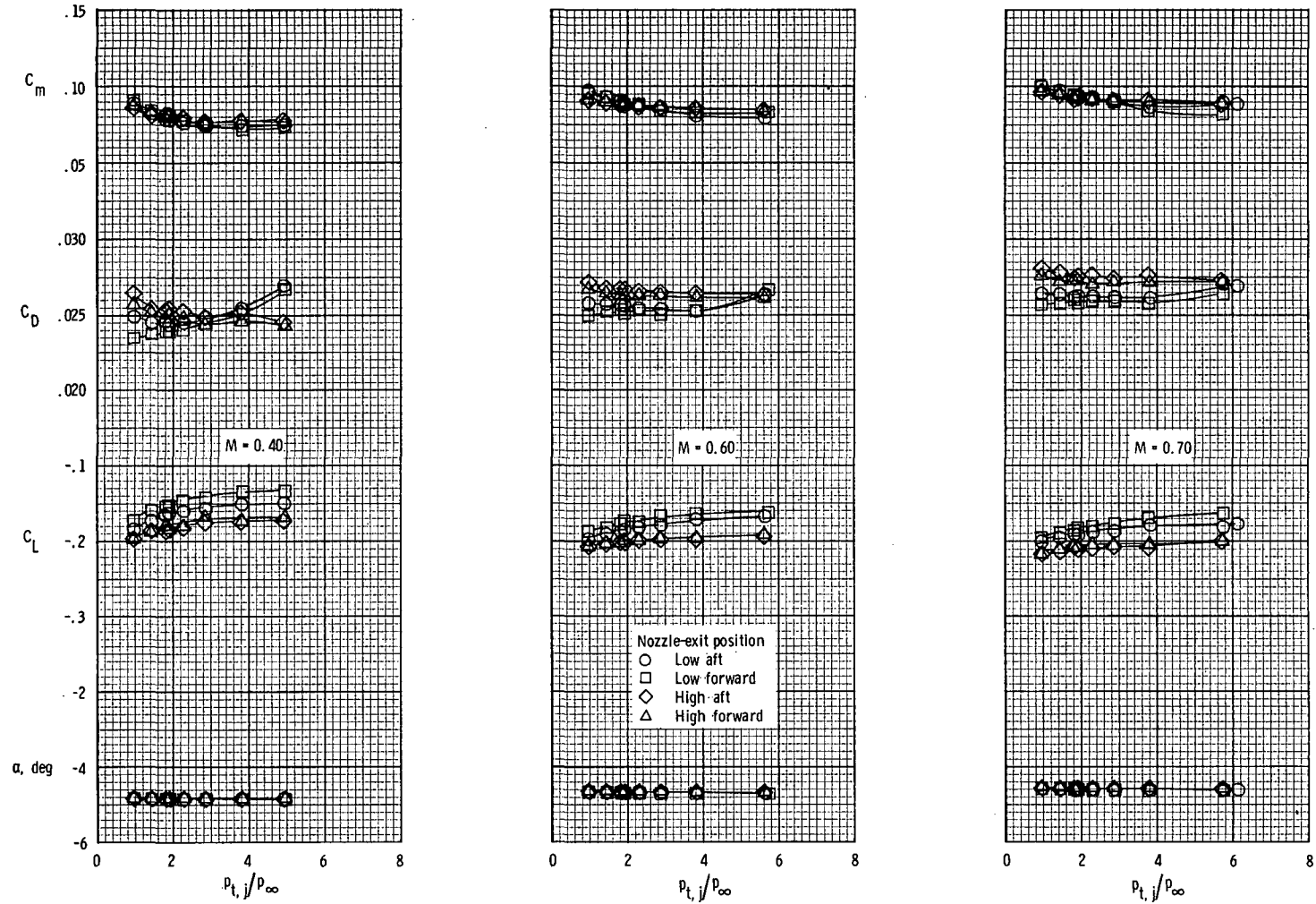
Figure 9.- Effects of blowing jet exhaust over wing at $M = 0$.



L-73-6825

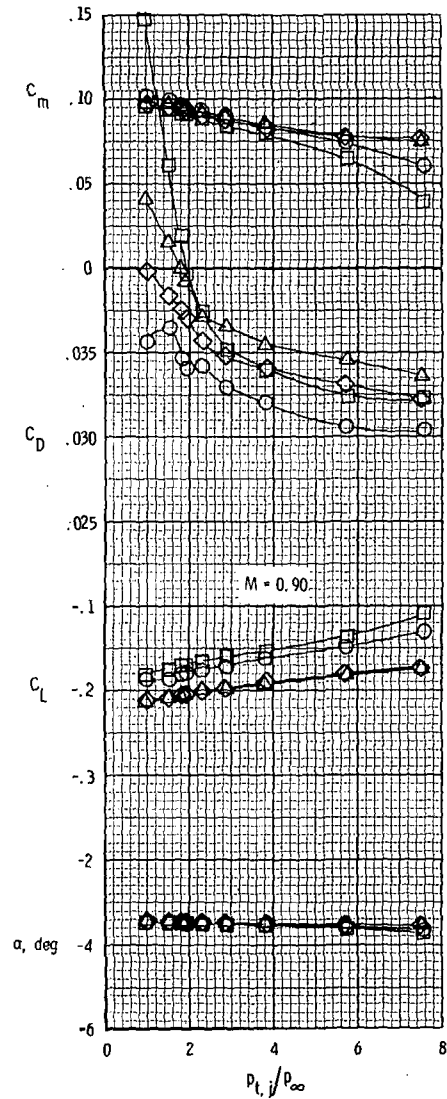
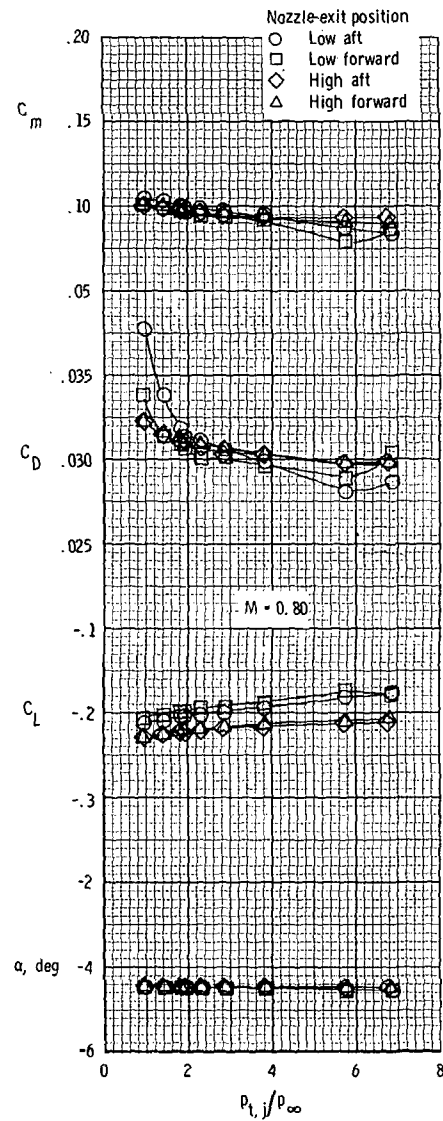
(b) Photograph showing area of wing washed by jet exhaust from nozzle in low-aft position
($h/d_e = 0.75$; $l/d_e = 2.59$) at jet-total-pressure ratio of approximately 2.0.

Figure 9.- Concluded.



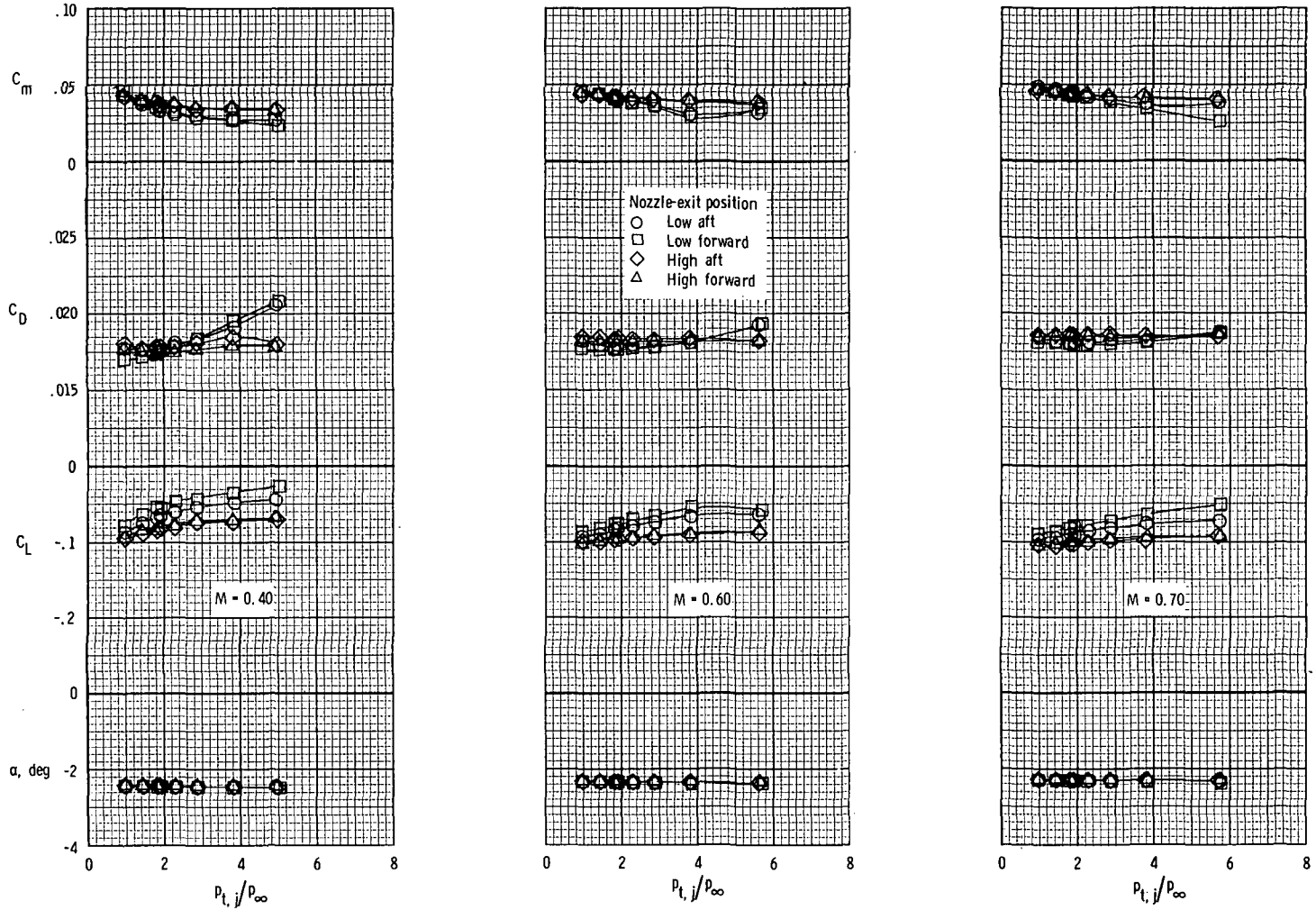
(a) $\alpha \approx -4.6^\circ$ or -3.5° .

Figure 10.- Effects of jet-total-pressure ratio on longitudinal aerodynamic characteristics of wing and afterbody at constant angles of attack.



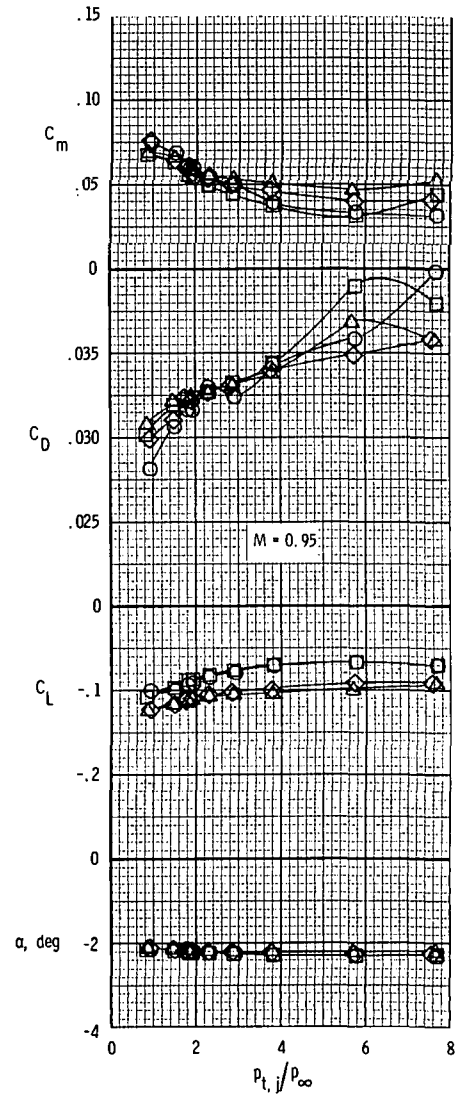
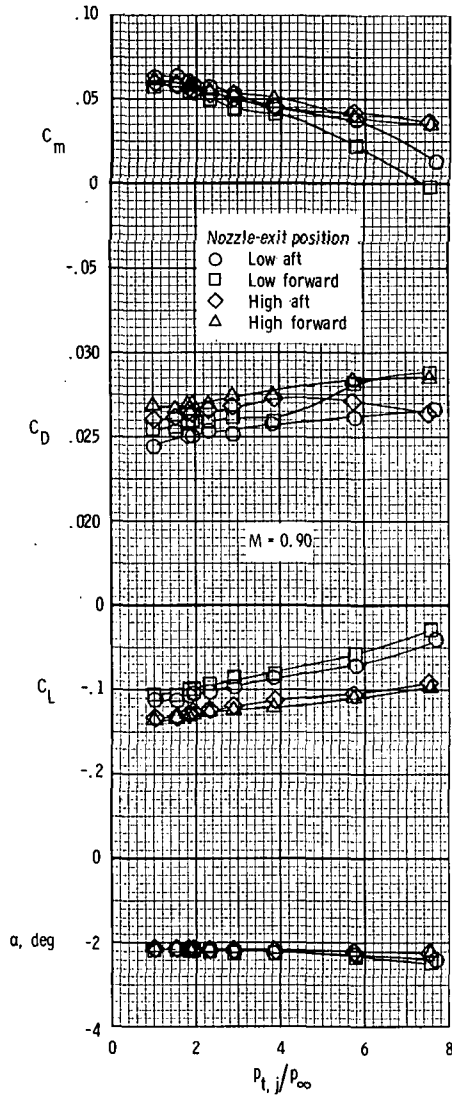
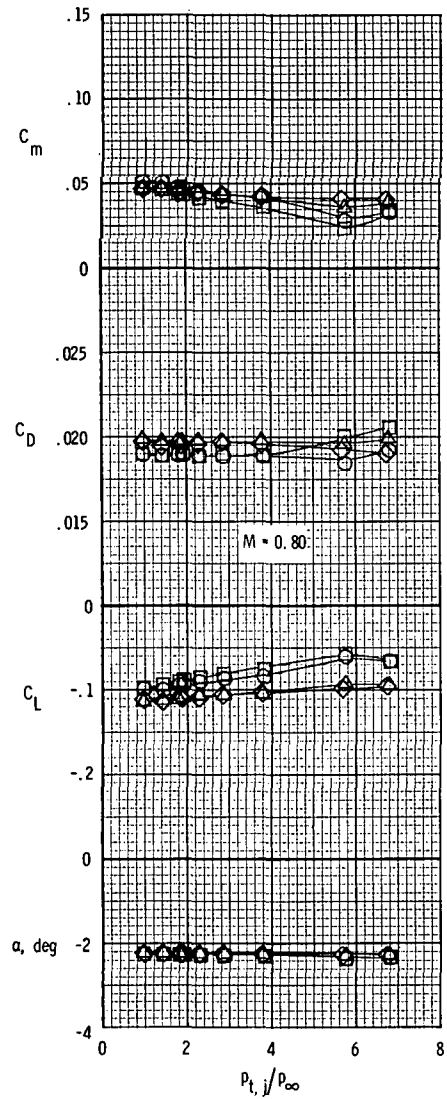
(a) $\alpha \approx -4.6^\circ$ or -3.5° . Concluded.

Figure 10.- Continued.



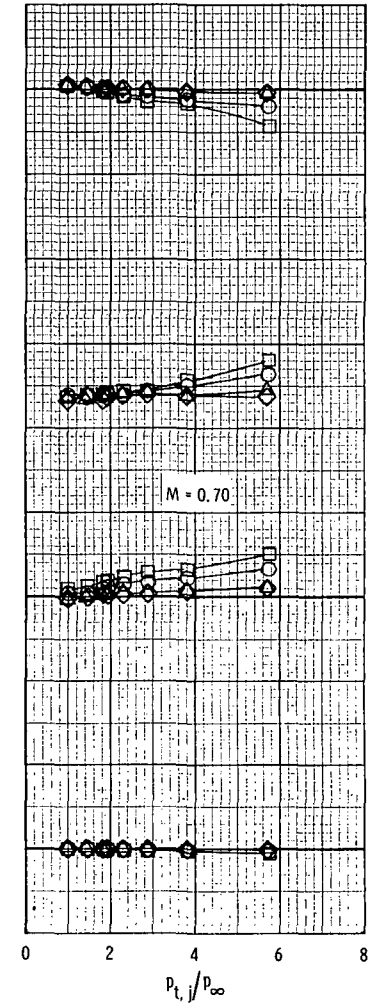
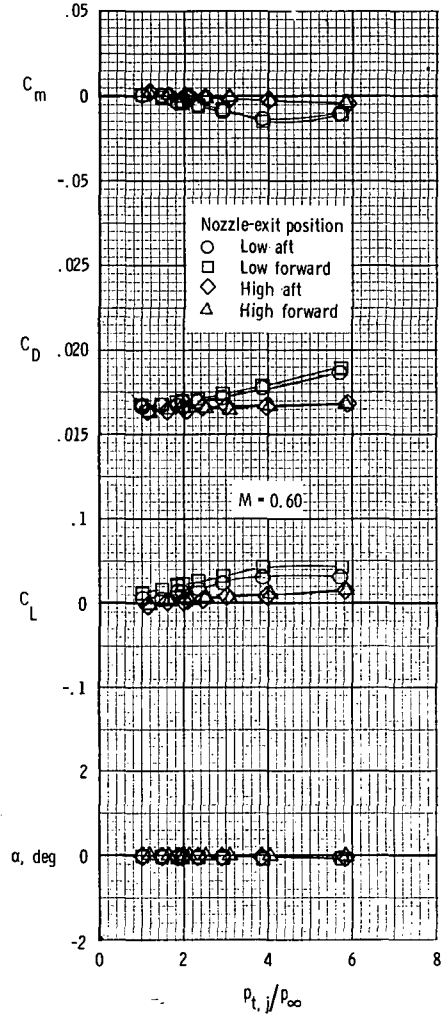
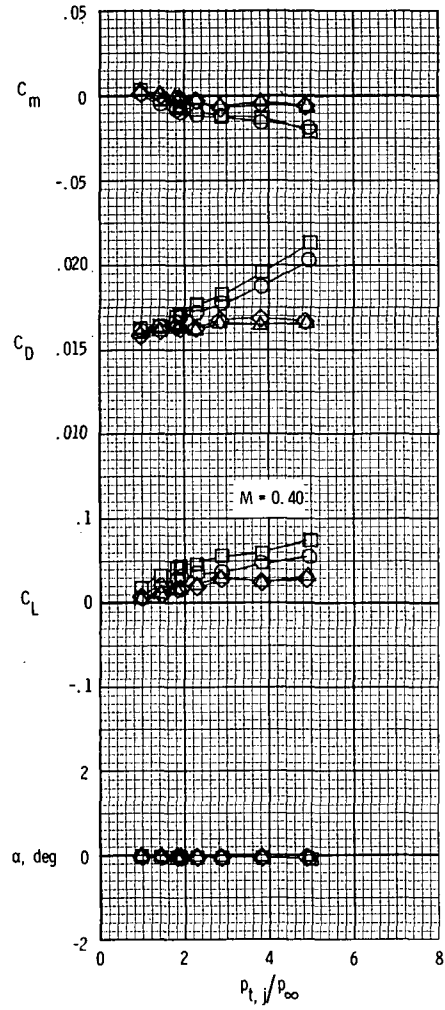
(b) $\alpha \approx -2.3^\circ$.

Figure 10.- Continued.



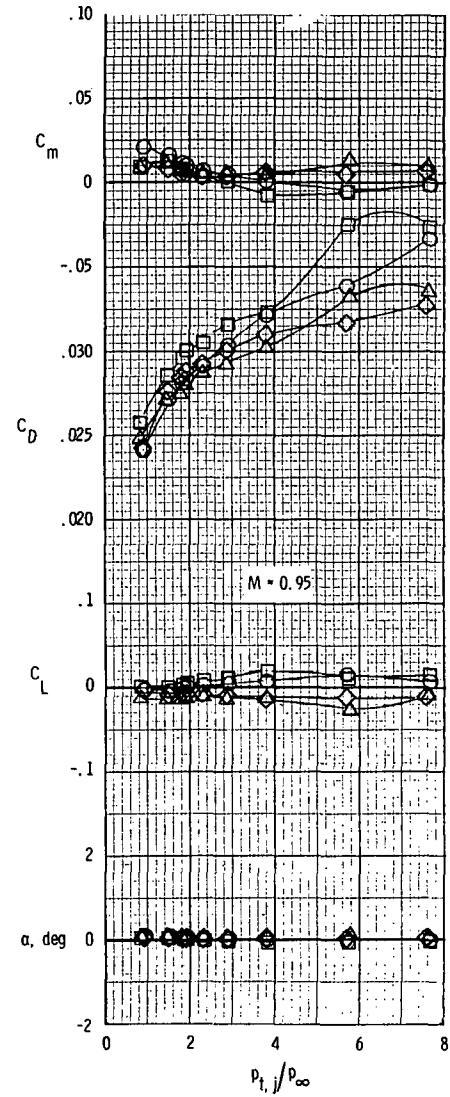
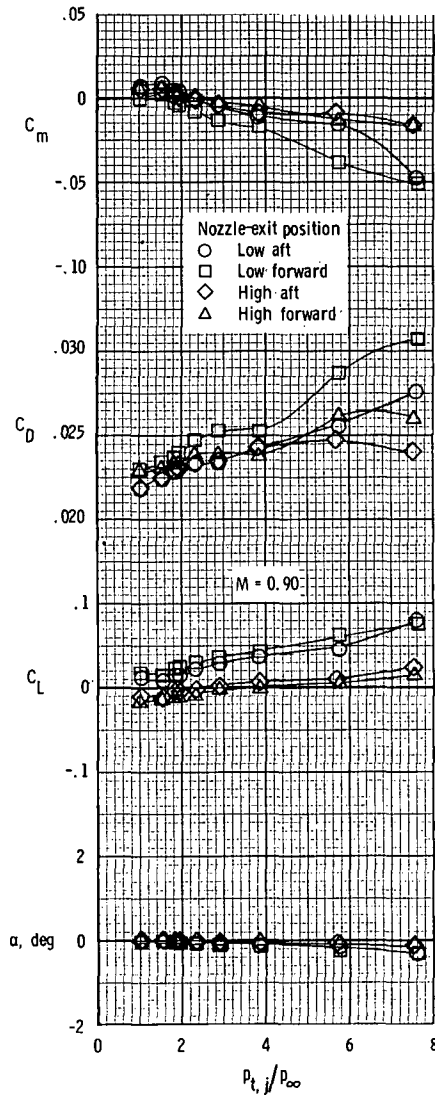
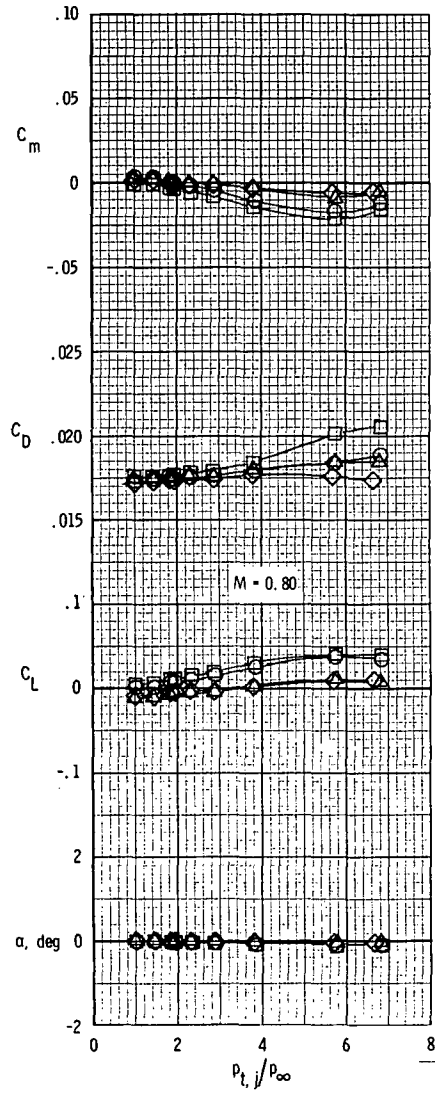
(b) $\alpha \approx -2.3^\circ$. Concluded.

Figure 10.- Continued.



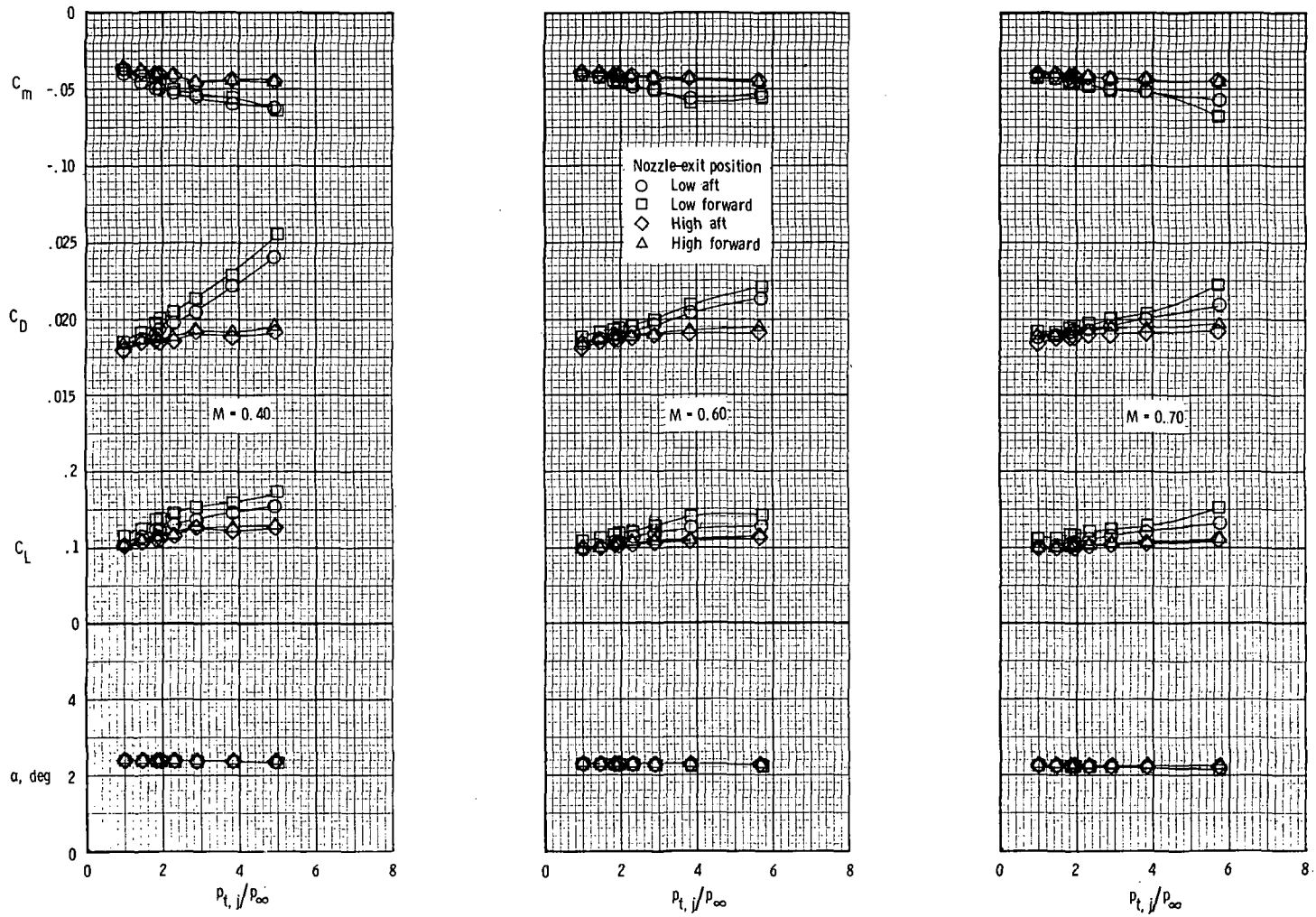
(c) $\alpha \approx 0^\circ$.

Figure 10.- Continued.



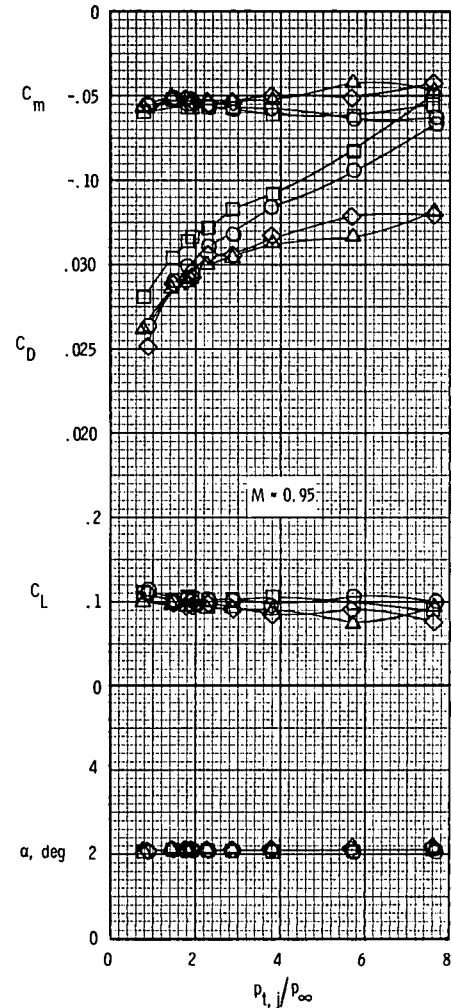
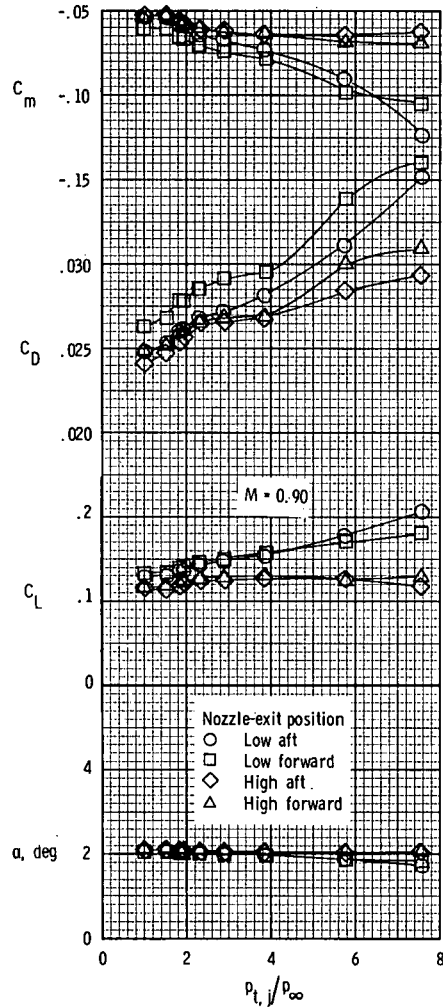
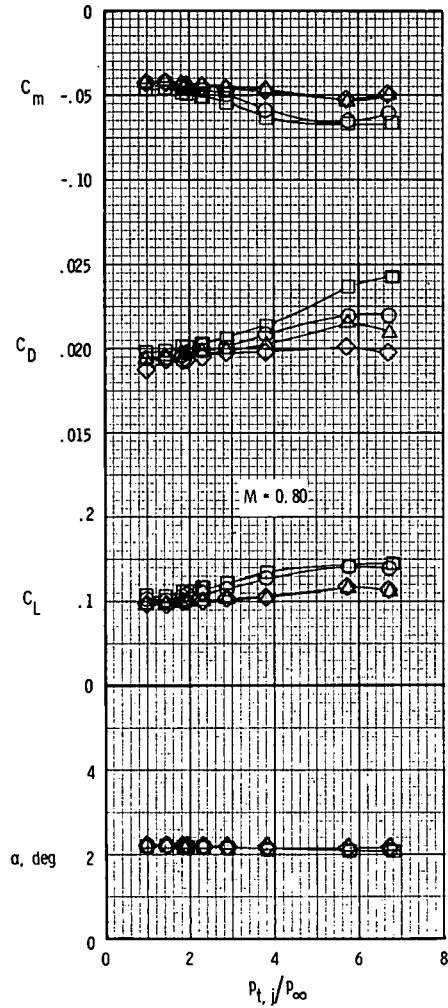
(c) $\alpha \approx 0^\circ$. Concluded.

Figure 10.- Continued.



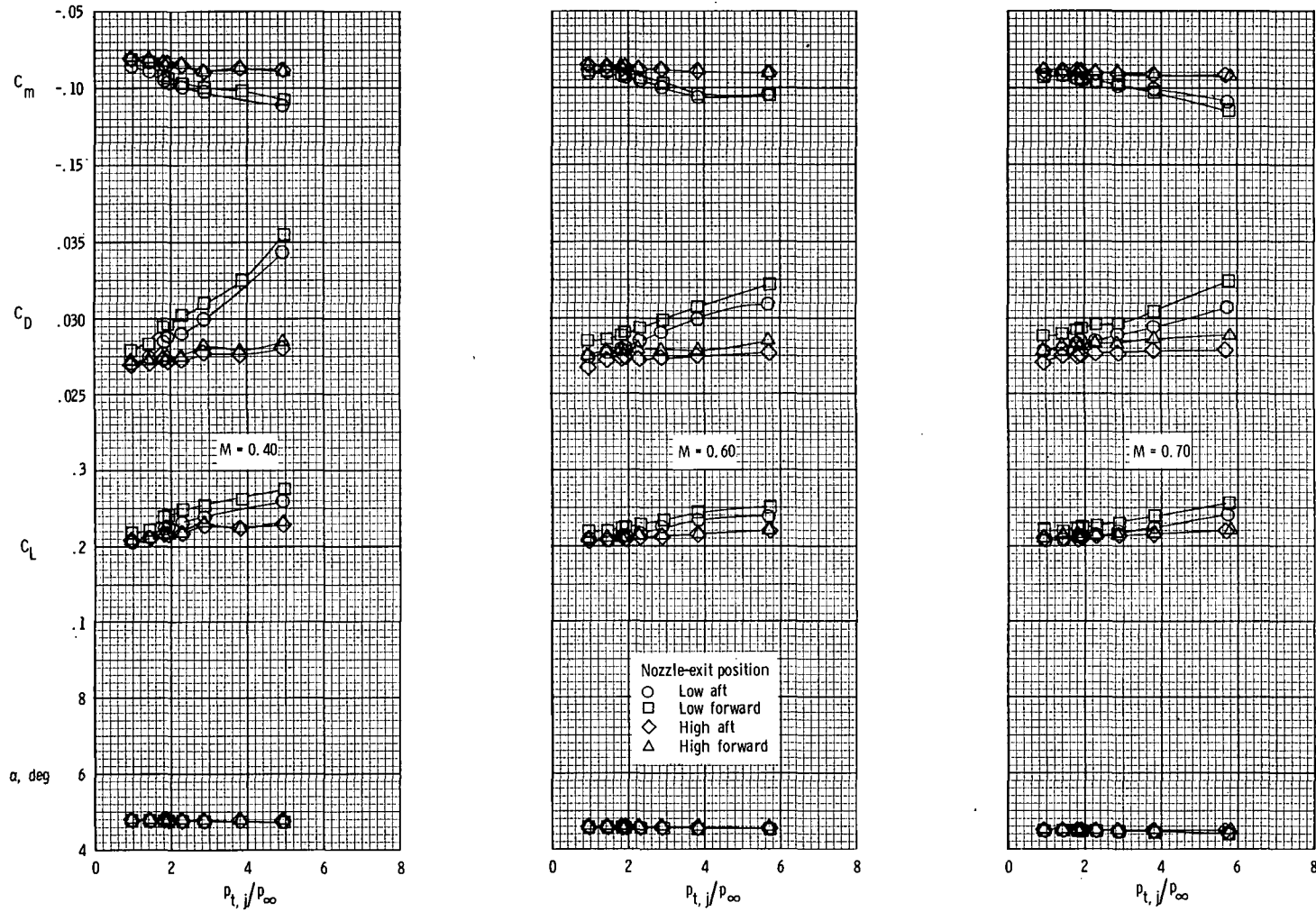
(d) $\alpha \approx 2.2^\circ$.

Figure 10.- Continued.



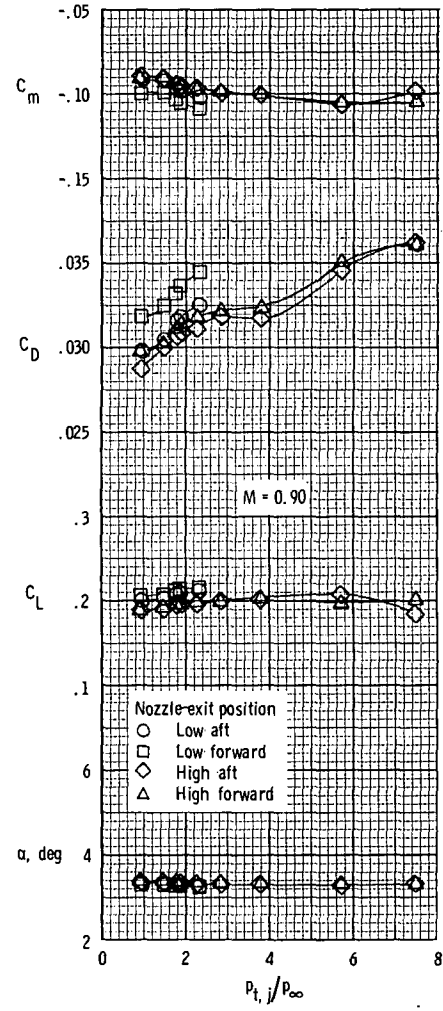
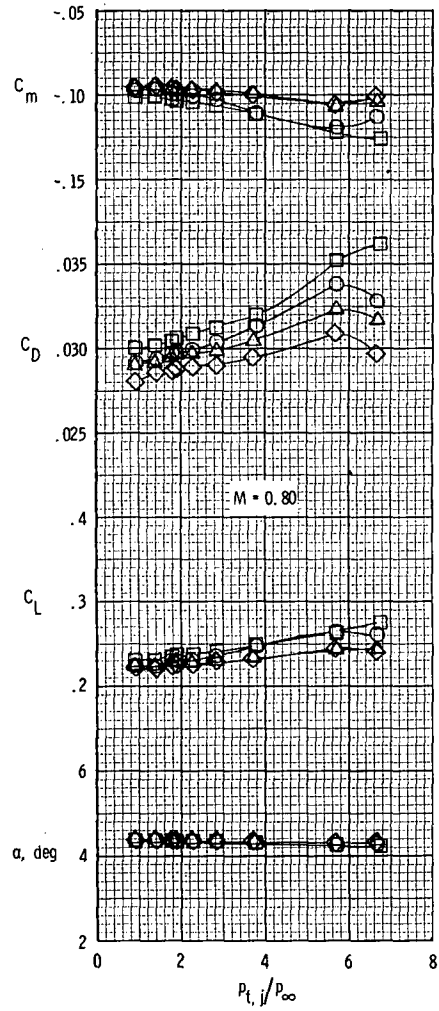
(d) $\alpha \approx 2.2^\circ$. Concluded.

Figure 10.- Continued.



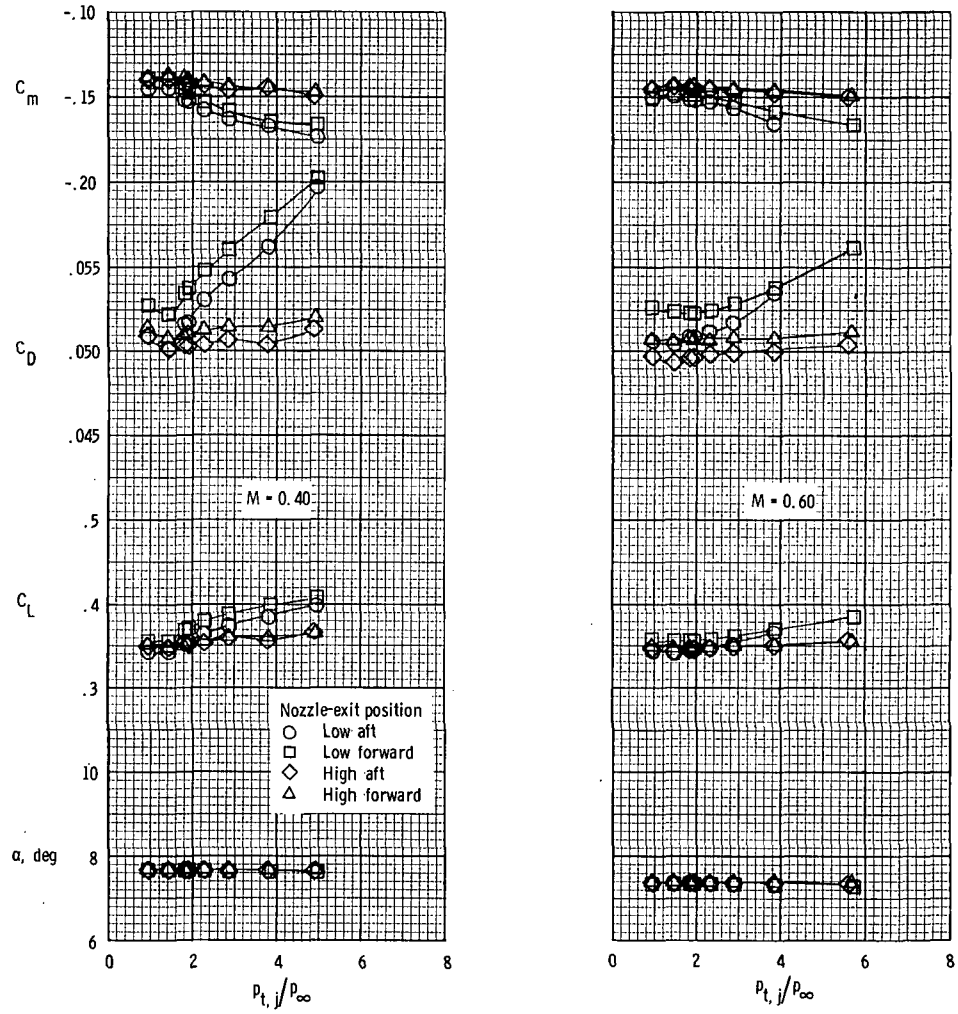
(e) $\alpha \approx 4.6^\circ$ or 3.3° .

Figure 10.- Continued.



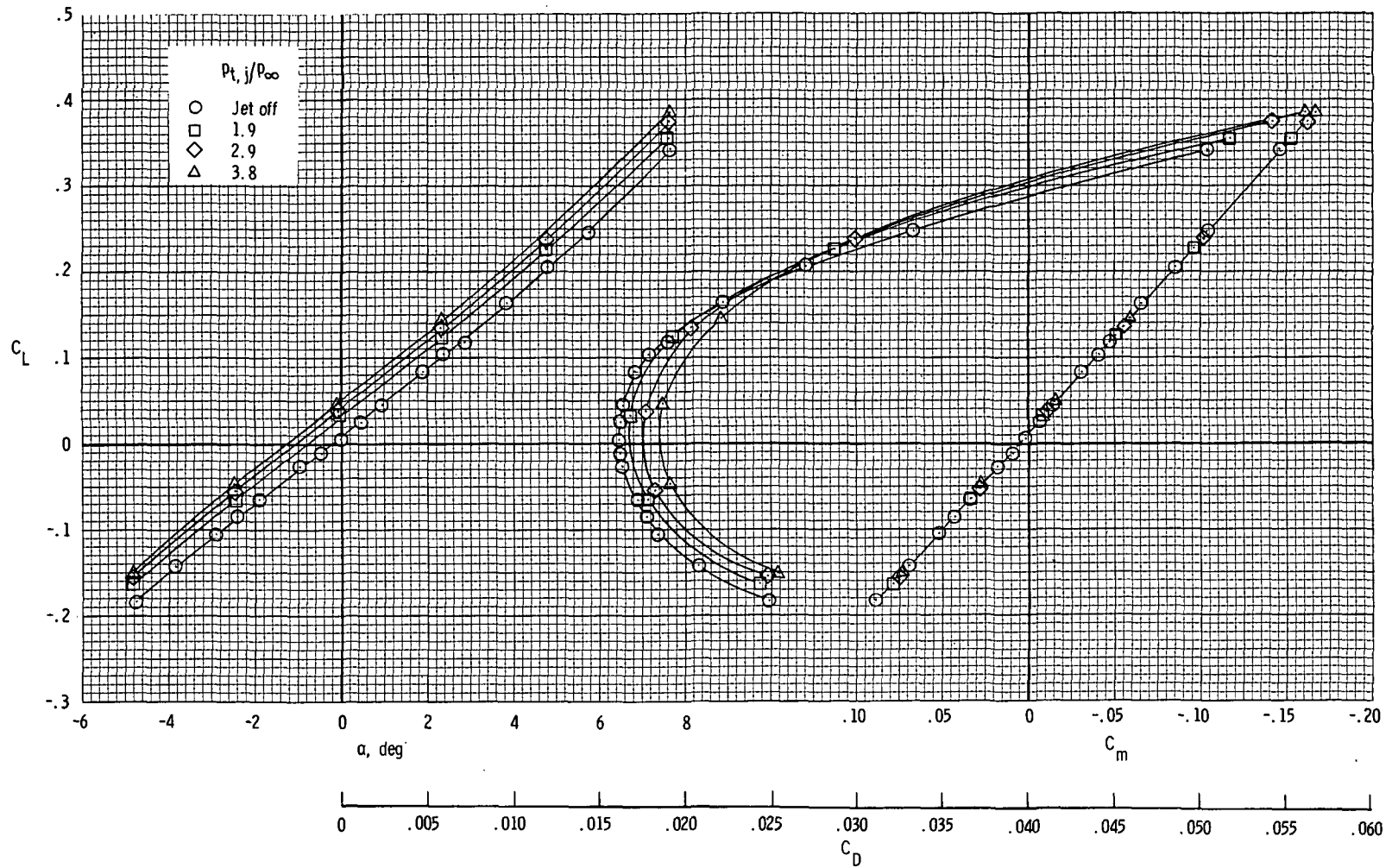
(e) $\alpha \approx 4.6^\circ$ or 3.3° . Concluded.

Figure 10.- Continued.



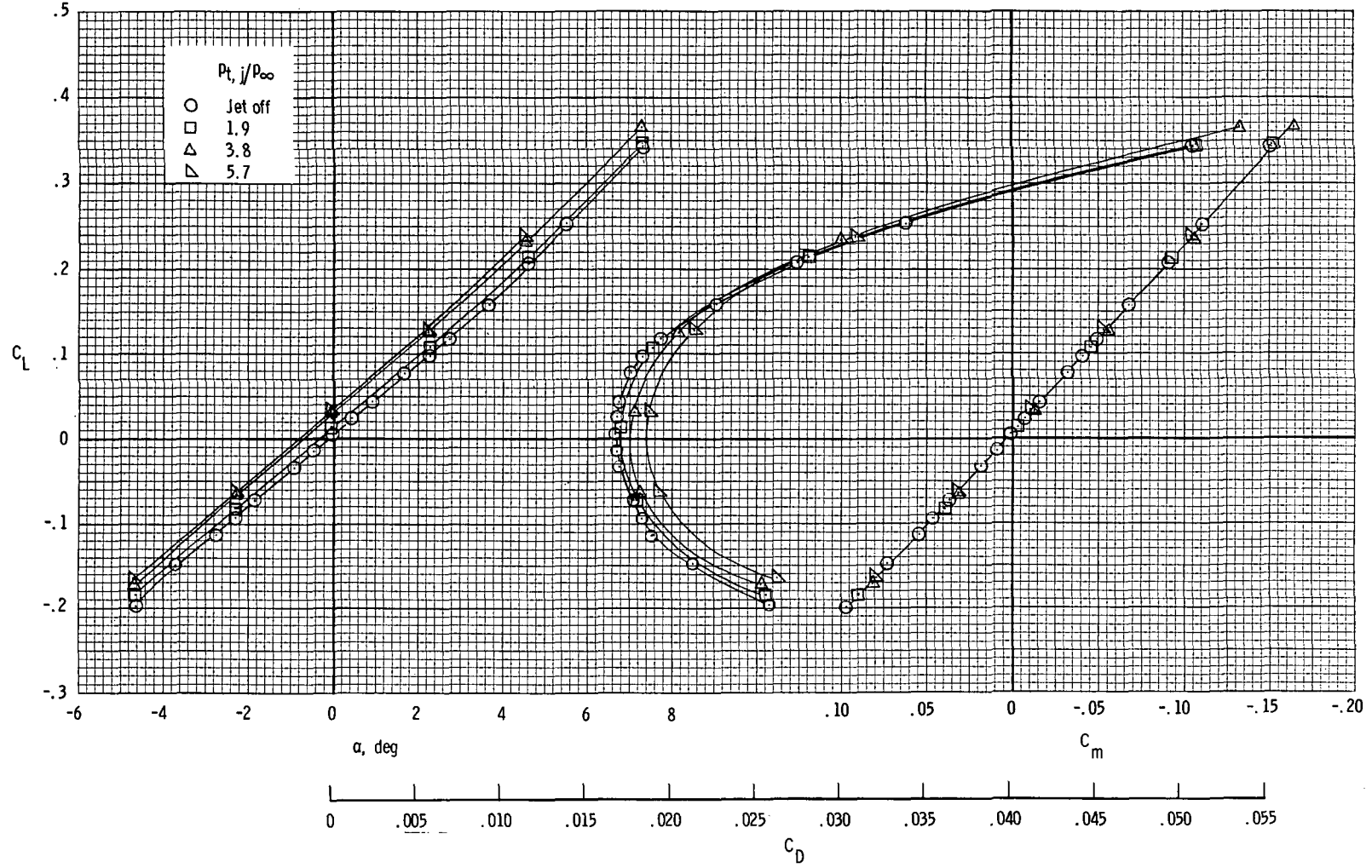
(f) $\alpha \approx 7.5^\circ$.

Figure 10.- Concluded.



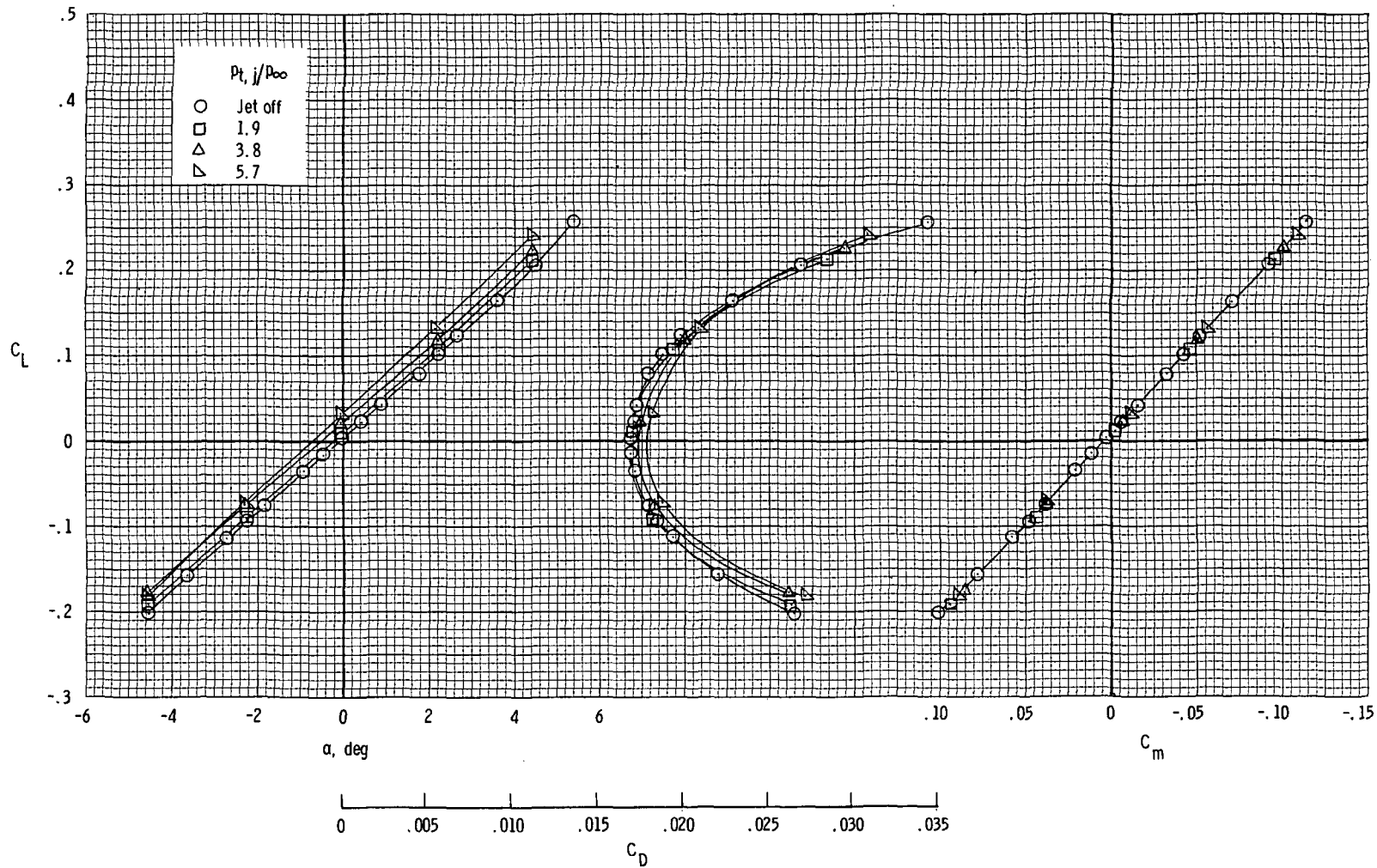
(a) $M = 0.40$.

Figure 11.- Effects of jet-total-pressure ratio on longitudinal aerodynamic characteristics of wing and afterbody of configuration with nozzle exit in low-aft position ($h/d_e = 0.75$; $l/d_e = 2.59$).



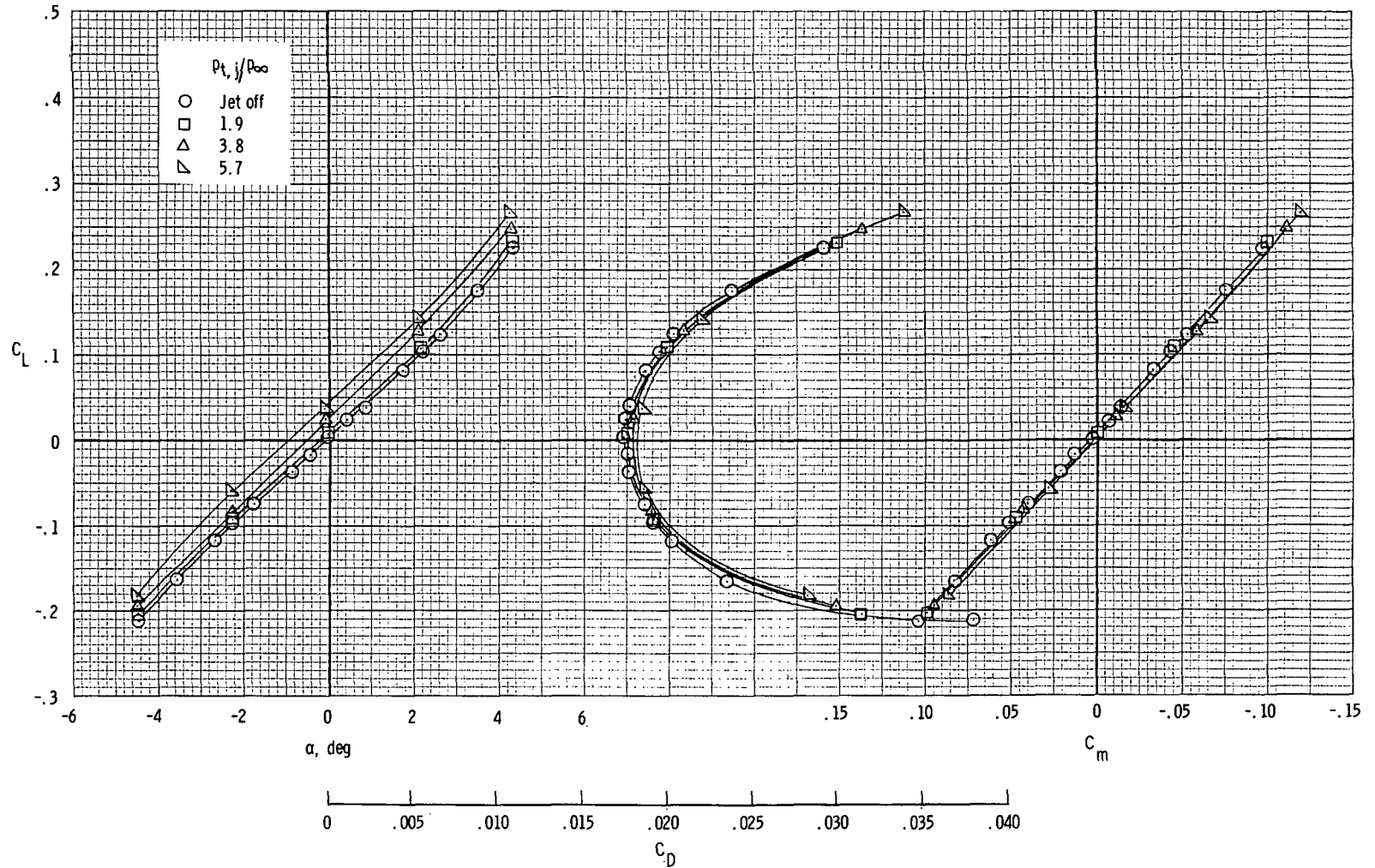
(b) $M = 0.60$.

Figure 11.- Continued.



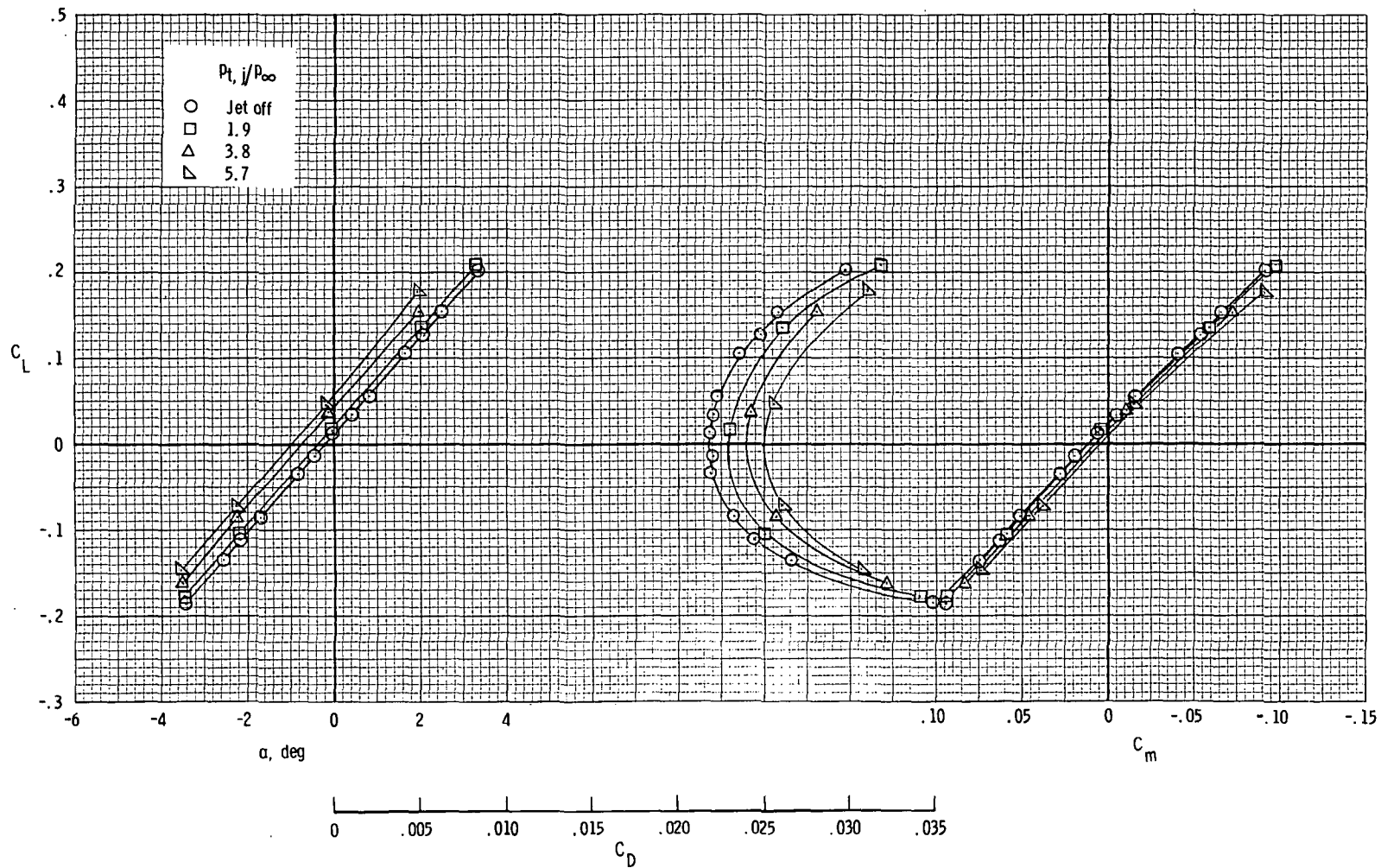
(c) $M = 0.70$.

Figure 11.- Continued.



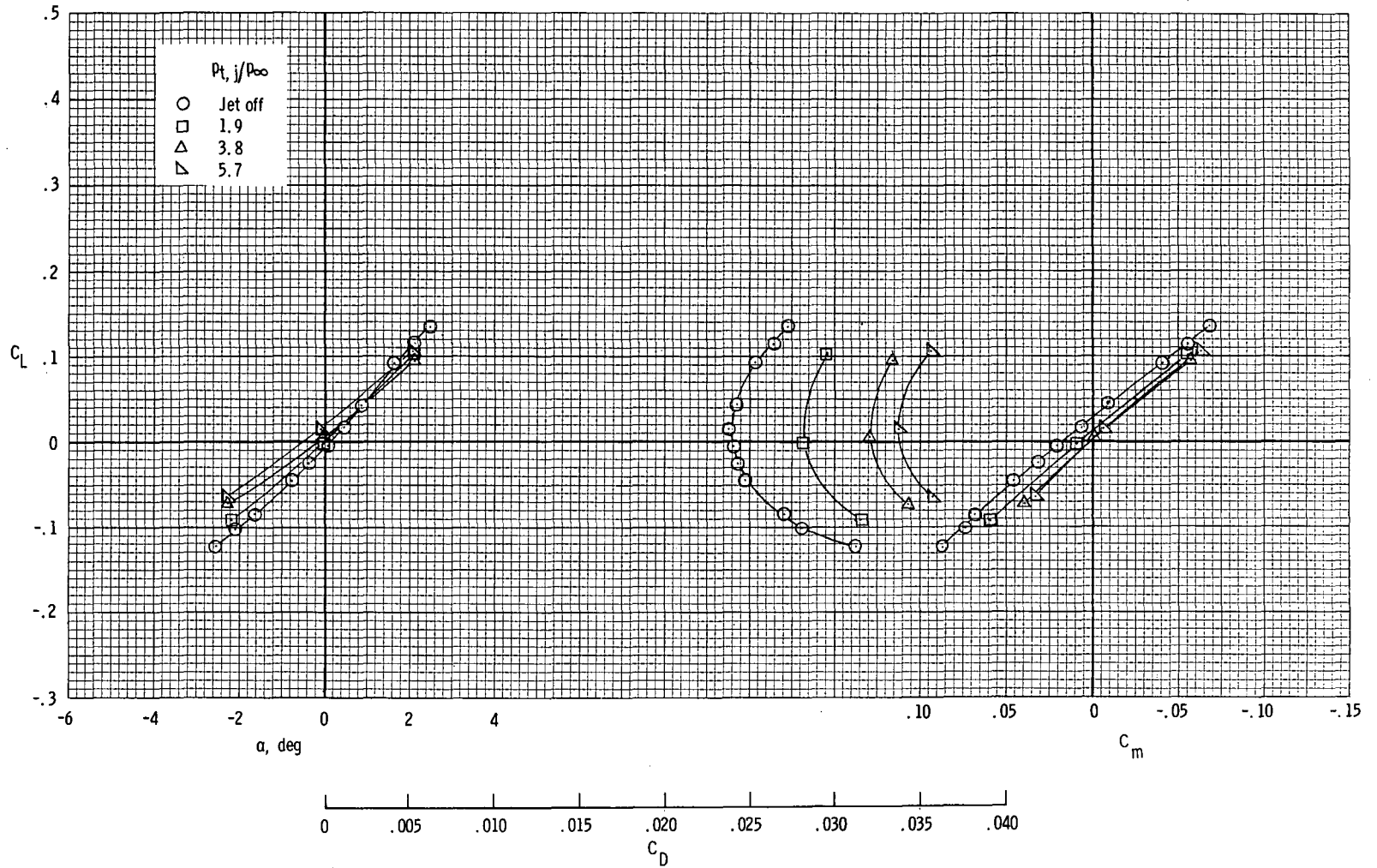
(d) $M = 0.80$.

Figure 11.- Continued.



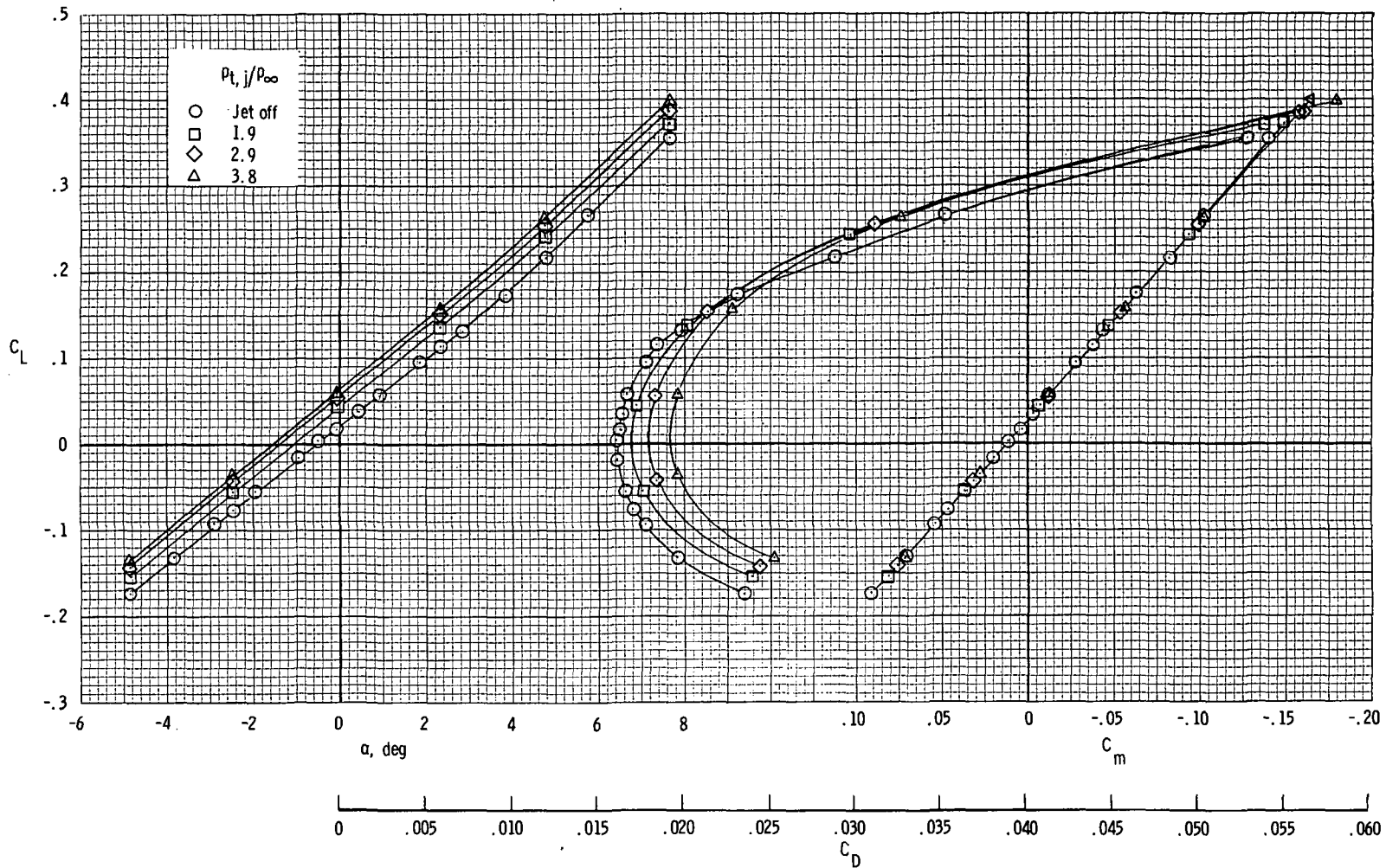
(e) $M = 0.90$.

Figure 11.- Continued.



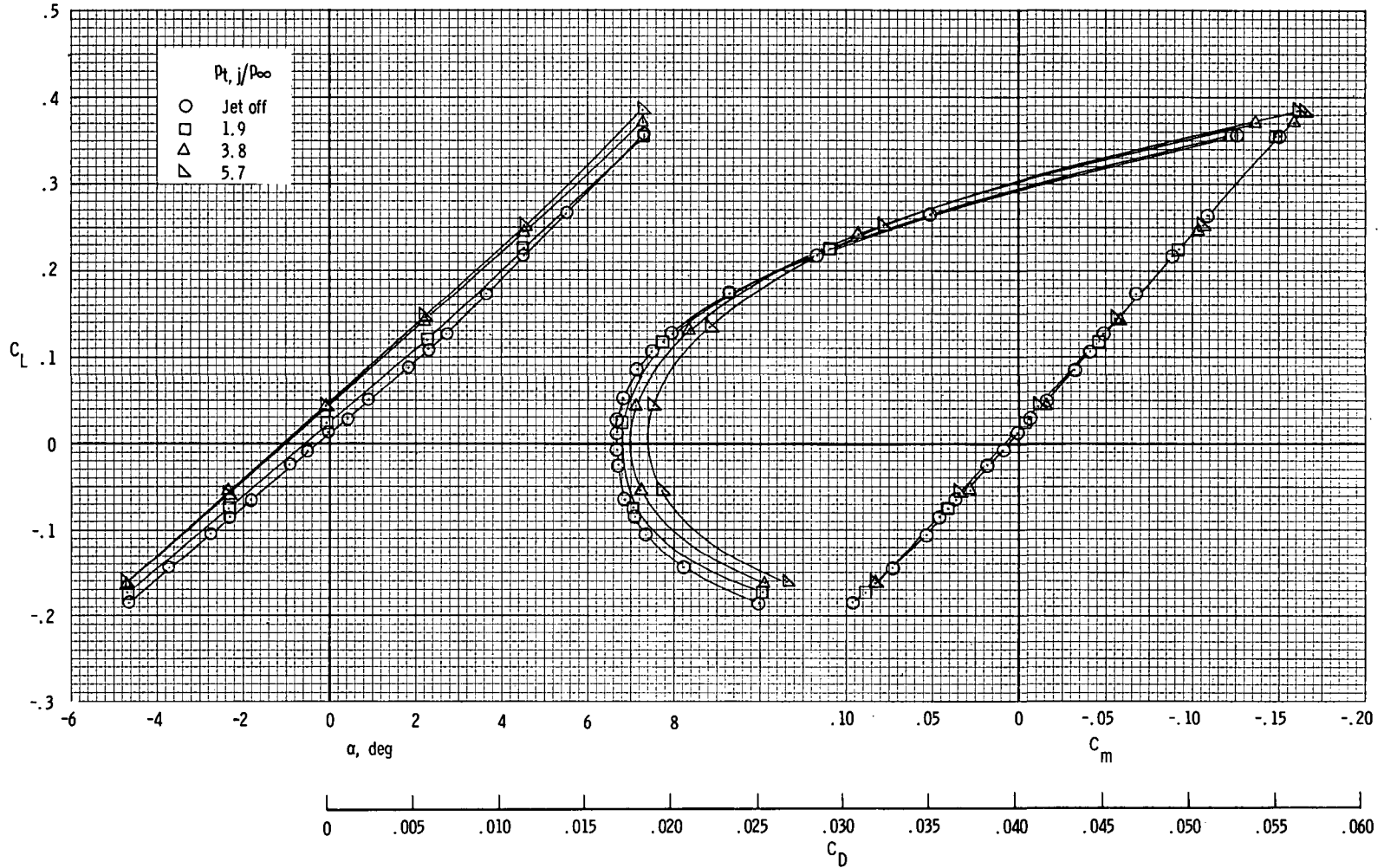
(f) $M = 0.95$.

Figure 11.- Concluded.



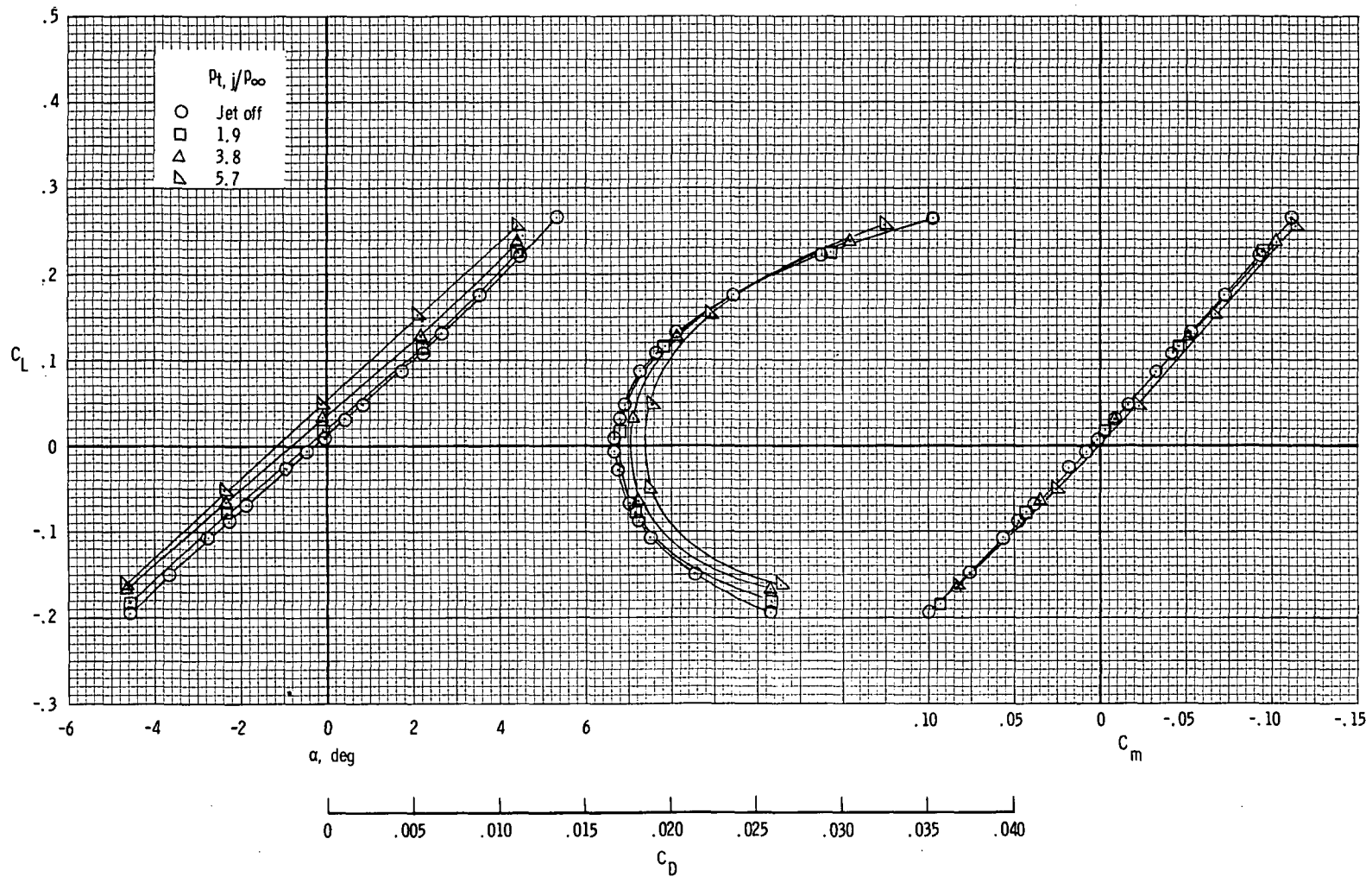
(a) $M = 0.40$.

Figure 12.- Effects of jet-total-pressure ratio on longitudinal aerodynamic characteristics of wing and afterbody of configuration with nozzle exit in low-forward position ($h/d_e = 0.75$; $l/d_e = 4.59$).



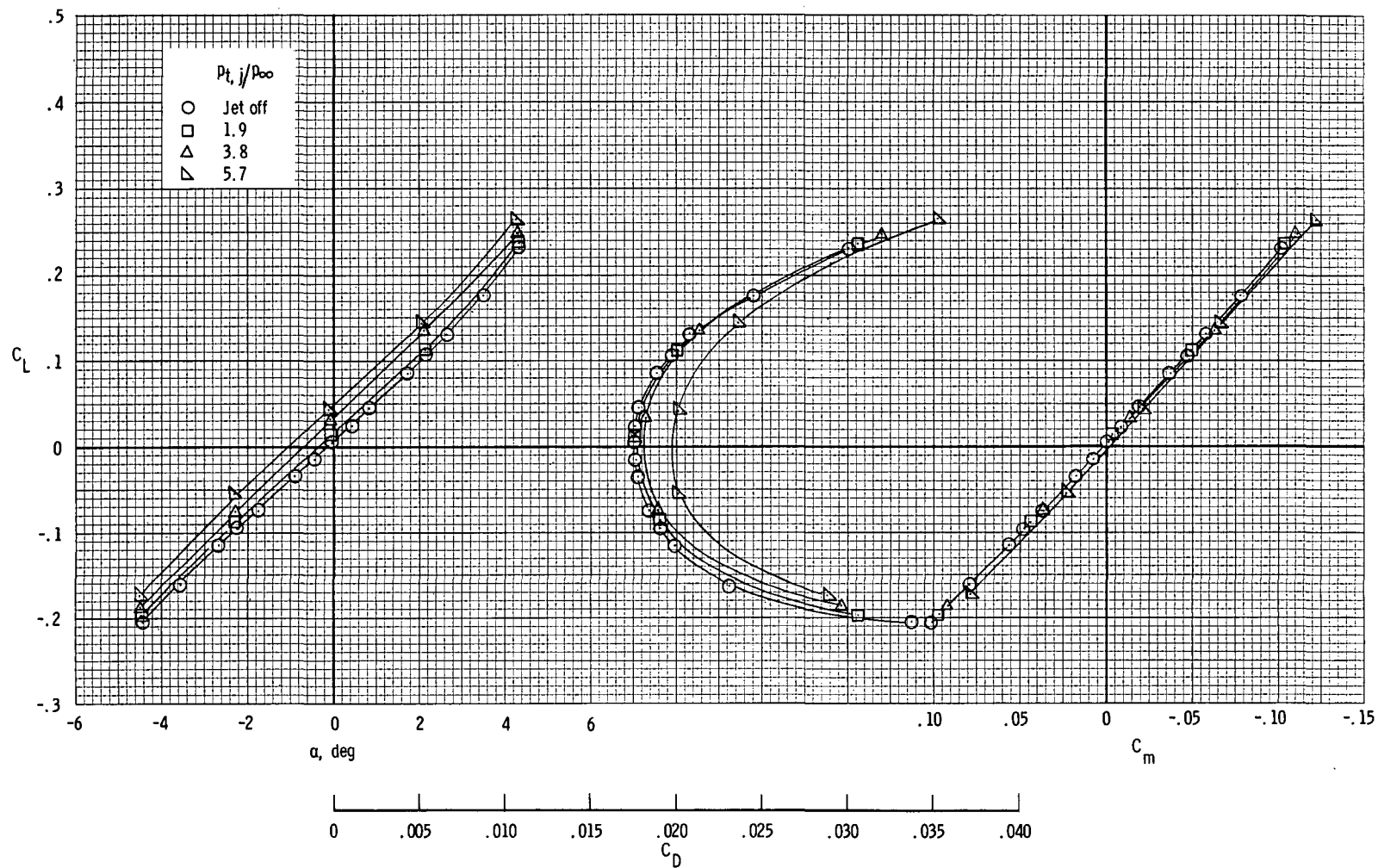
(b) $M = 0.60$.

Figure 12.- Continued.



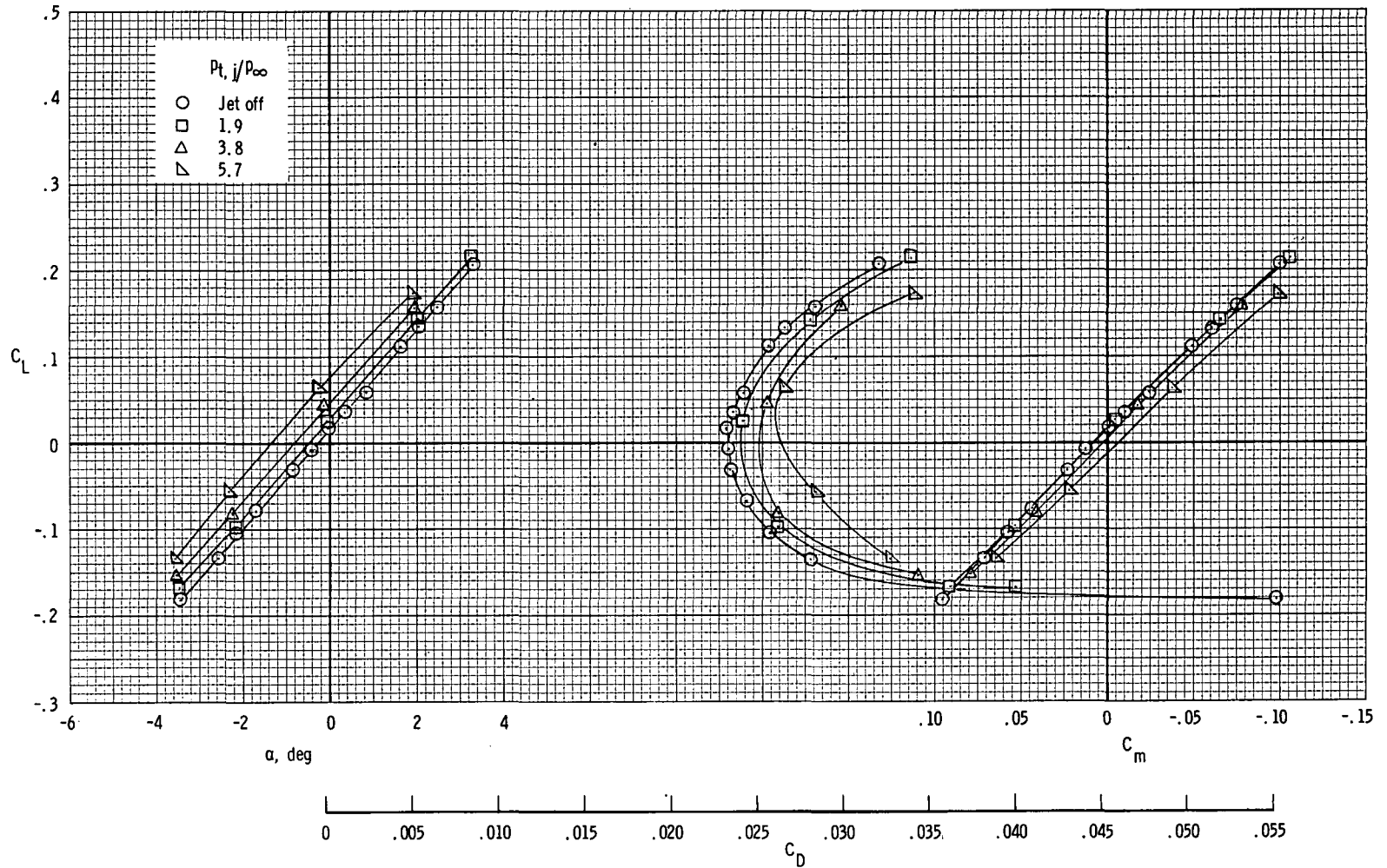
(c) $M = 0.70$.

Figure 12.- Continued.



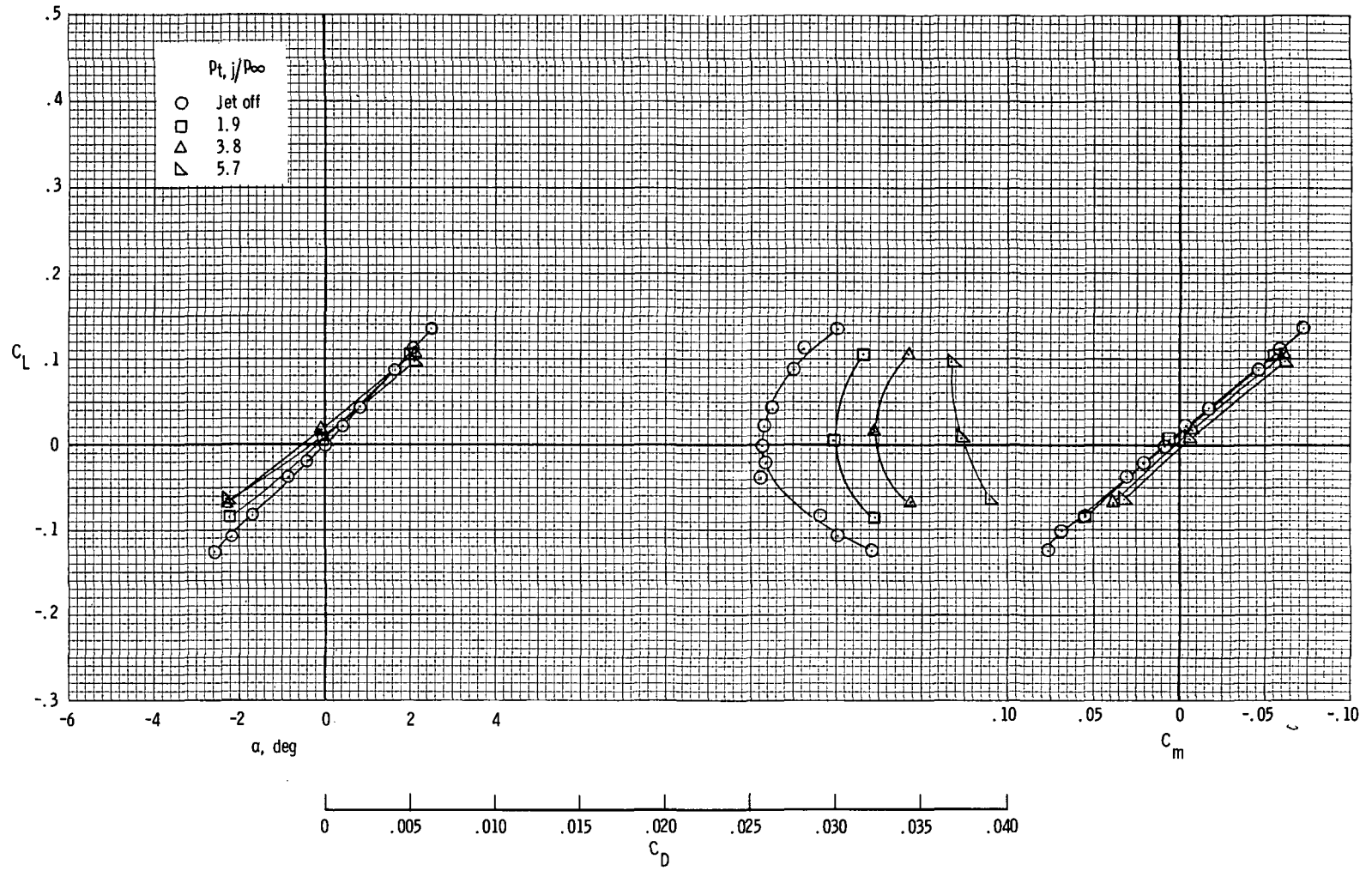
(d) $M = 0.80$.

Figure 12.- Continued.



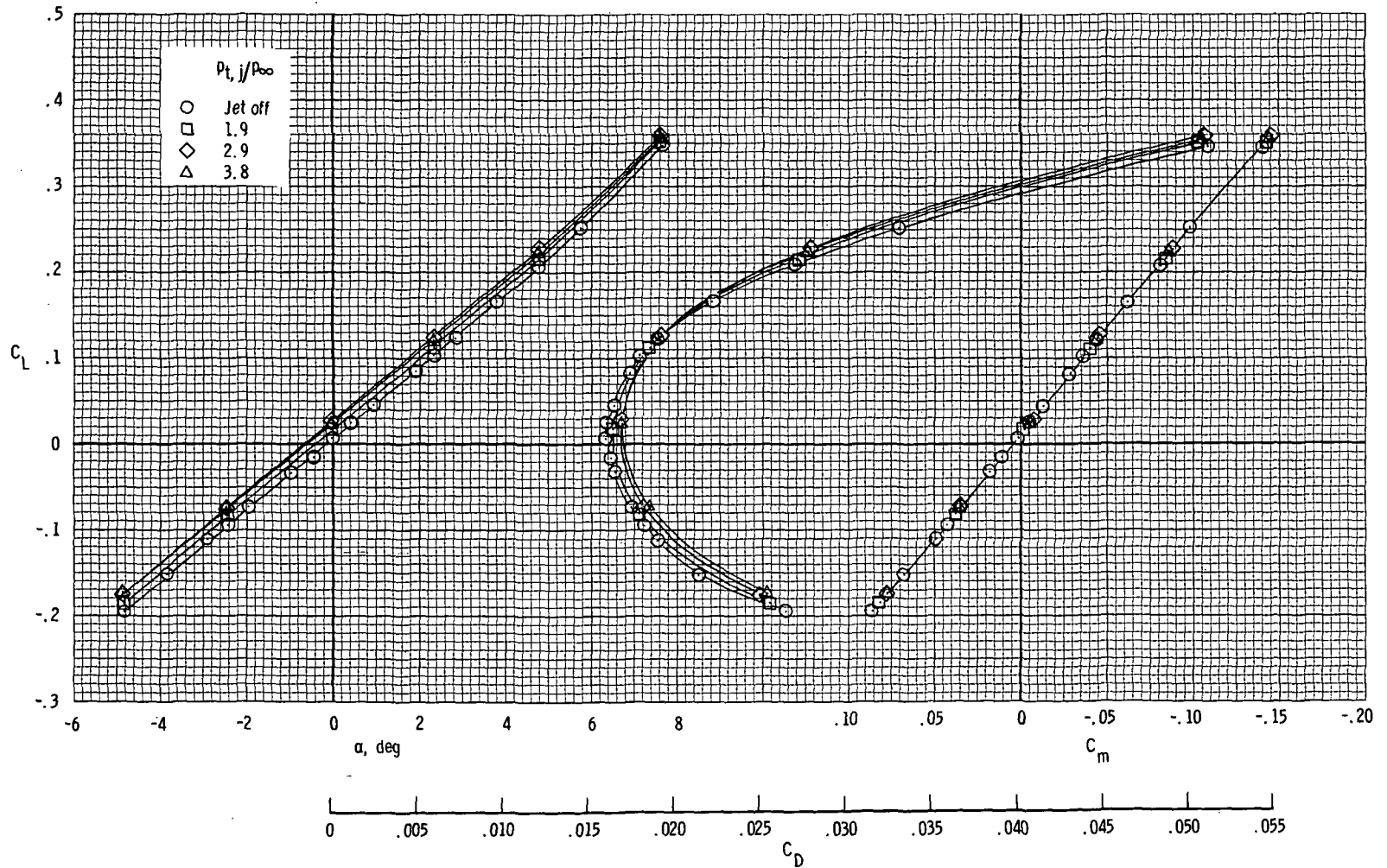
(e) $M = 0.90$.

Figure 12.- Continued.



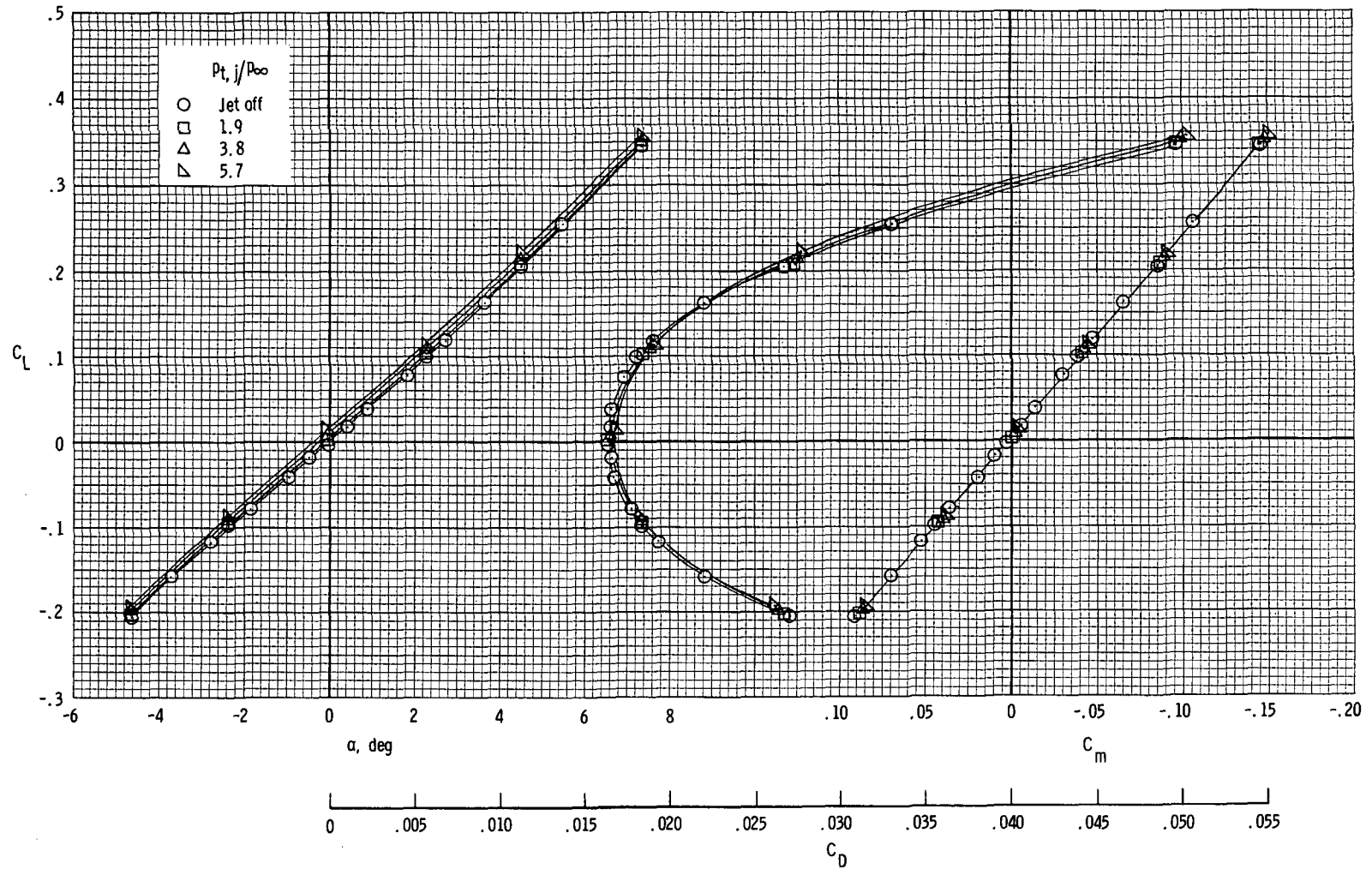
(f) $M = 0.95$.

Figure 12.- Concluded.



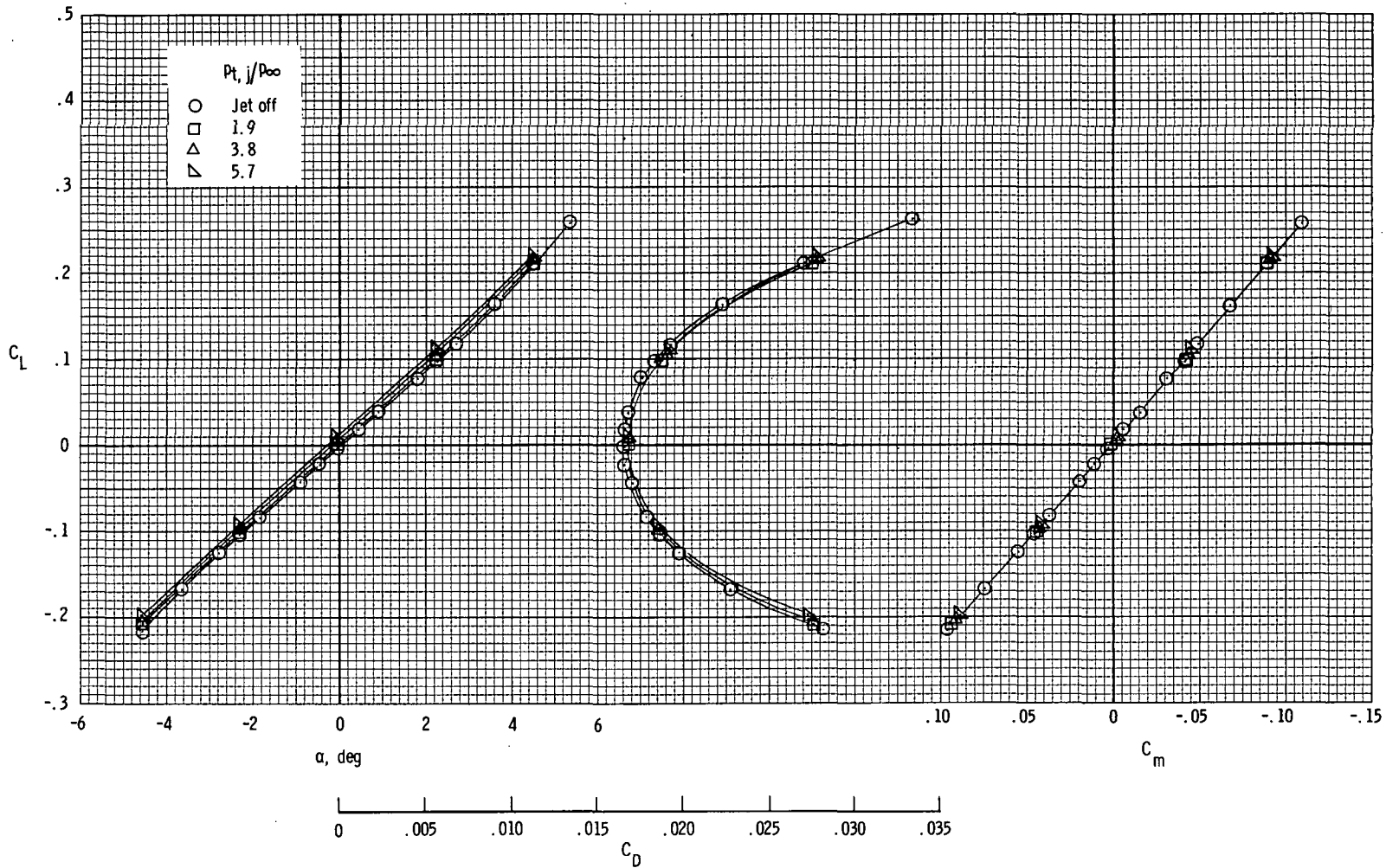
(a) $M = 0.40$.

Figure 13.- Effects of jet-total-pressure ratio on longitudinal aerodynamic characteristics of wing and afterbody of configuration with nozzle exit in high-aft position ($h/d_e = 1.50$; $l/d_e = 2.59$).



(b) $M = 0.60$.

Figure 13.- Continued.



(c) $M = 0.70$.

Figure 13.- Continued.

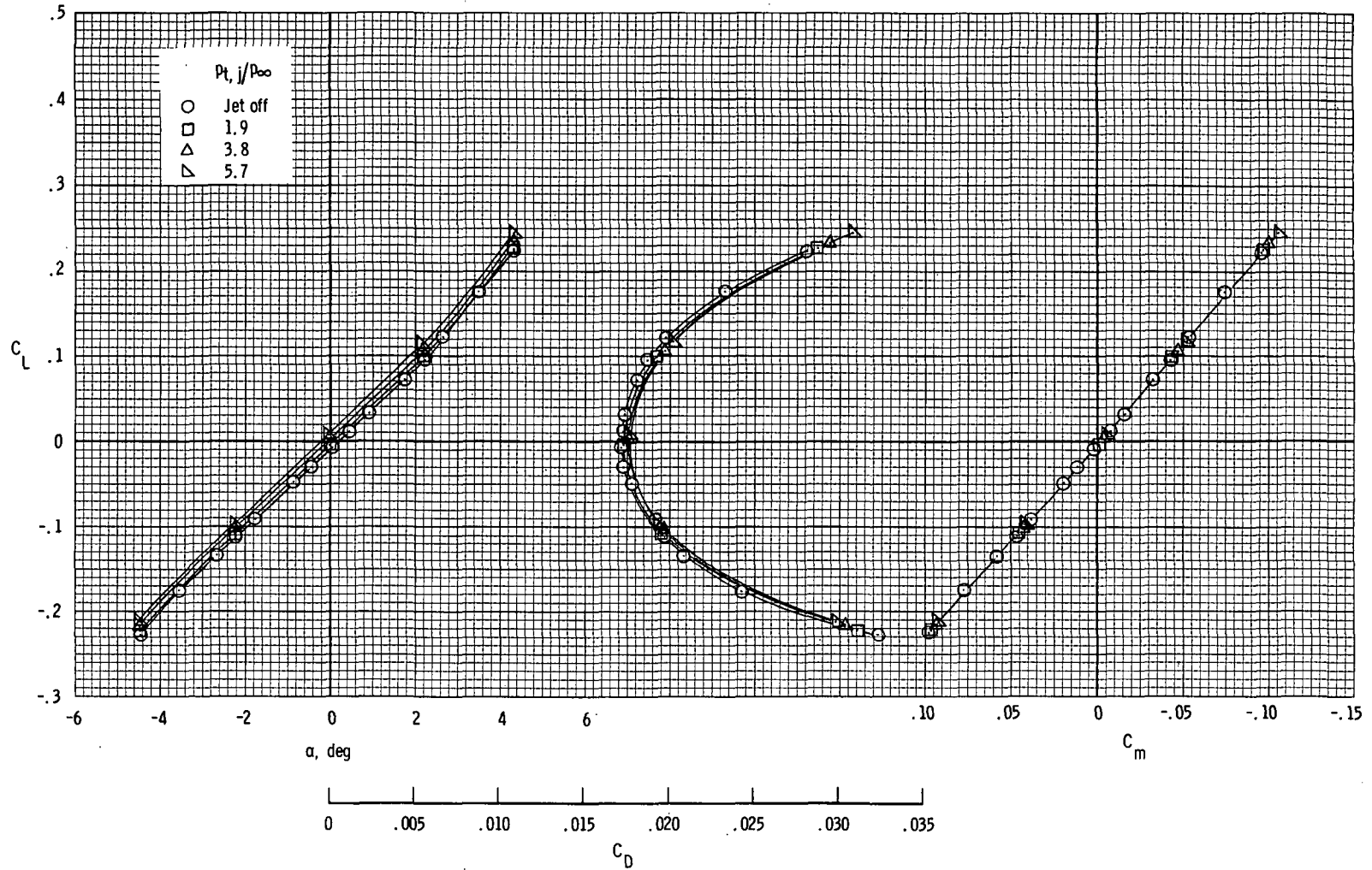
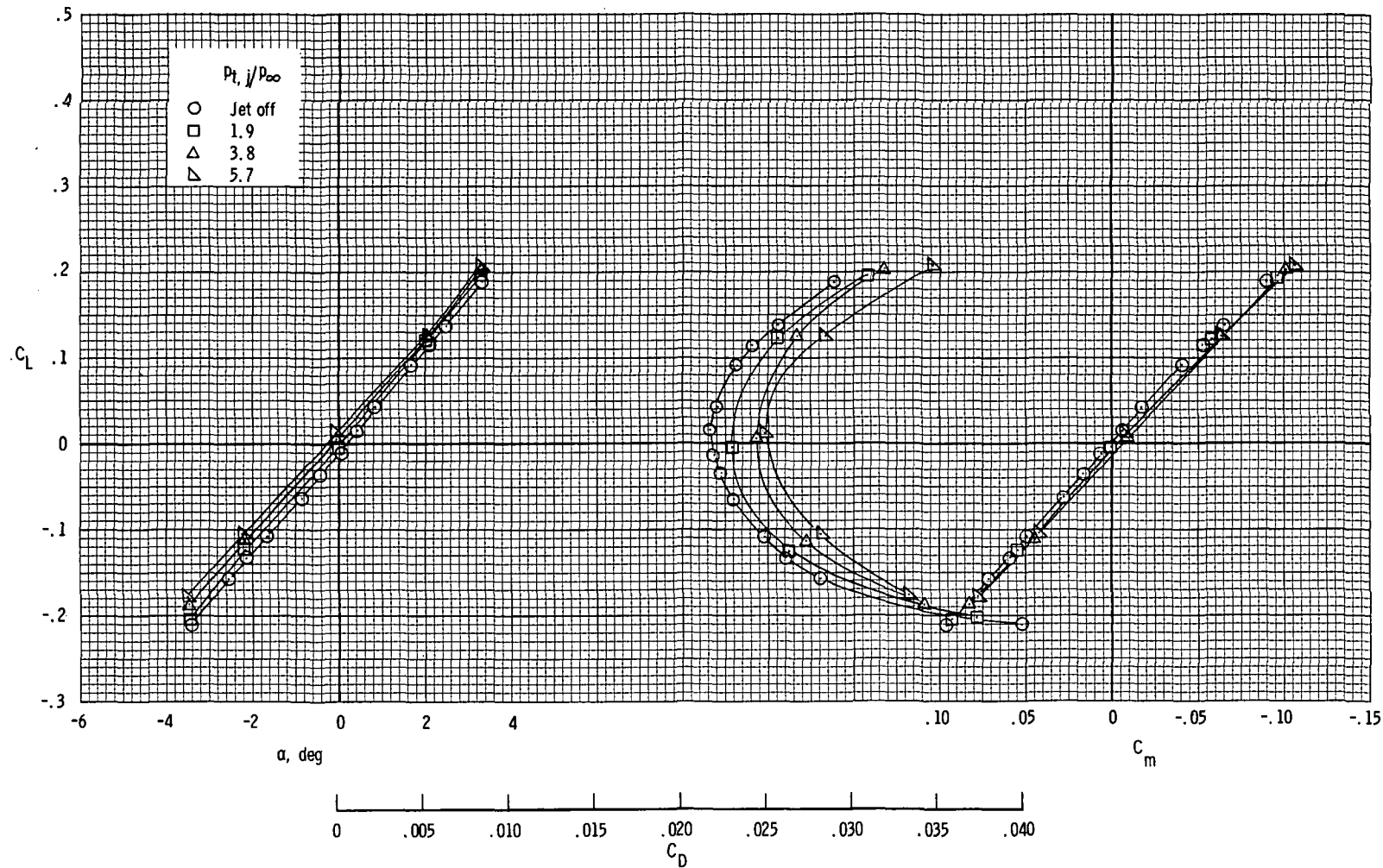
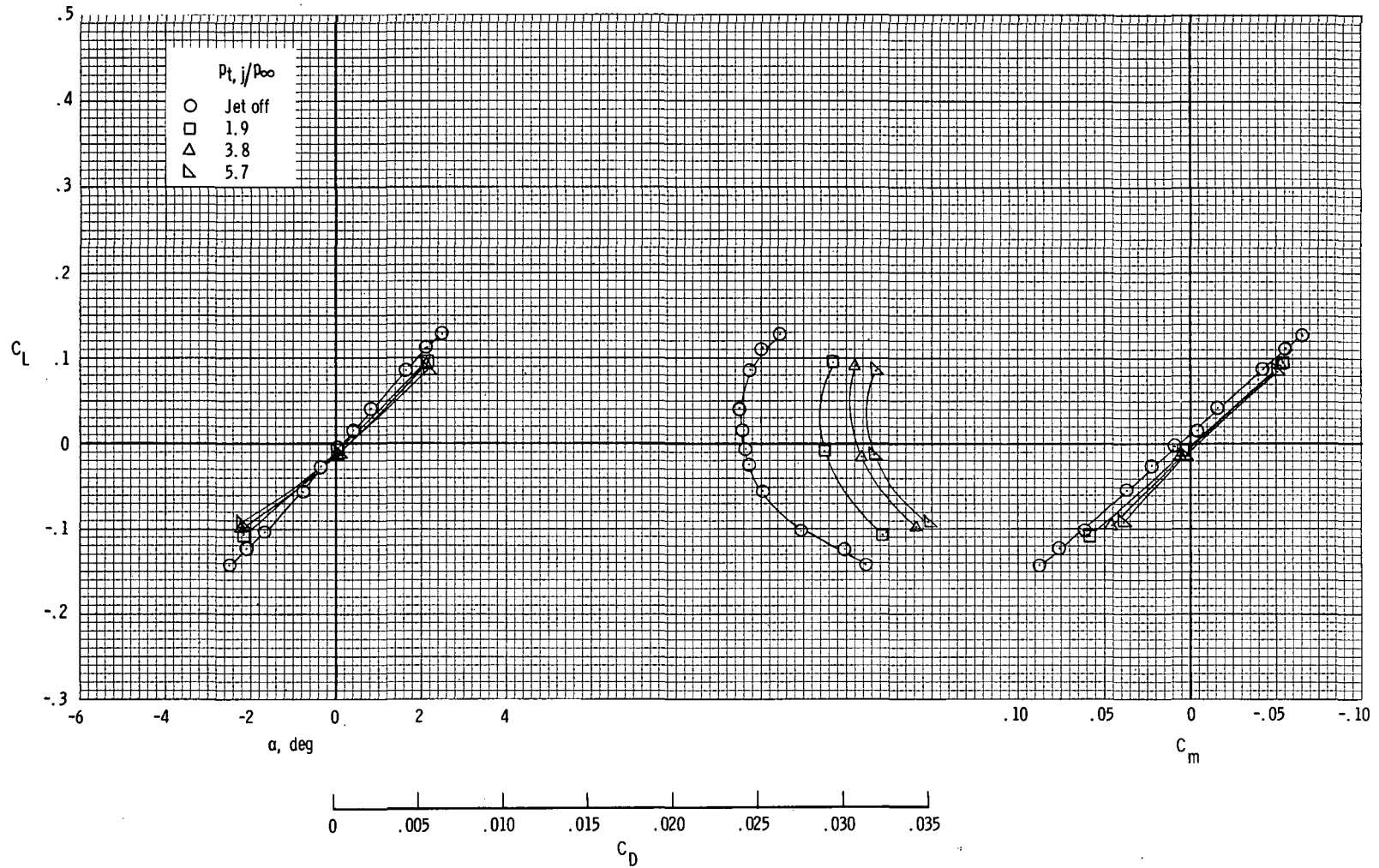
(d) $M = 0.80$.

Figure 13.- Continued.



(e) $M = 0.90$.

Figure 13.- Continued.



(f) $M = 0.95$.

Figure 13.- Concluded.

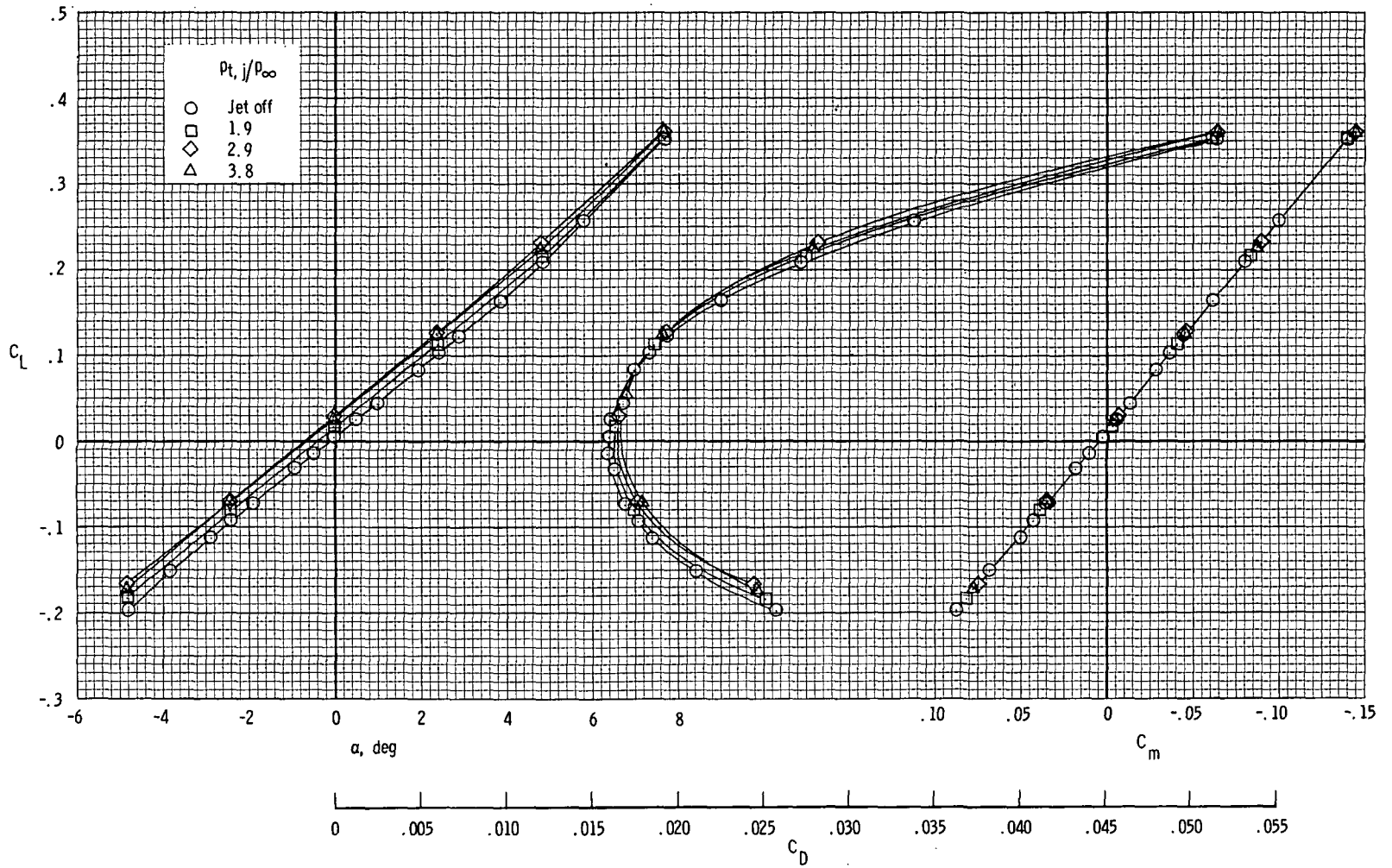


Figure 14.- Effects of jet-total-pressure ratio on longitudinal aerodynamic characteristics of wing and afterbody of configuration with nozzle exit in high-forward position ($h/d_e = 1.50$; $l/d_e = 4.59$).

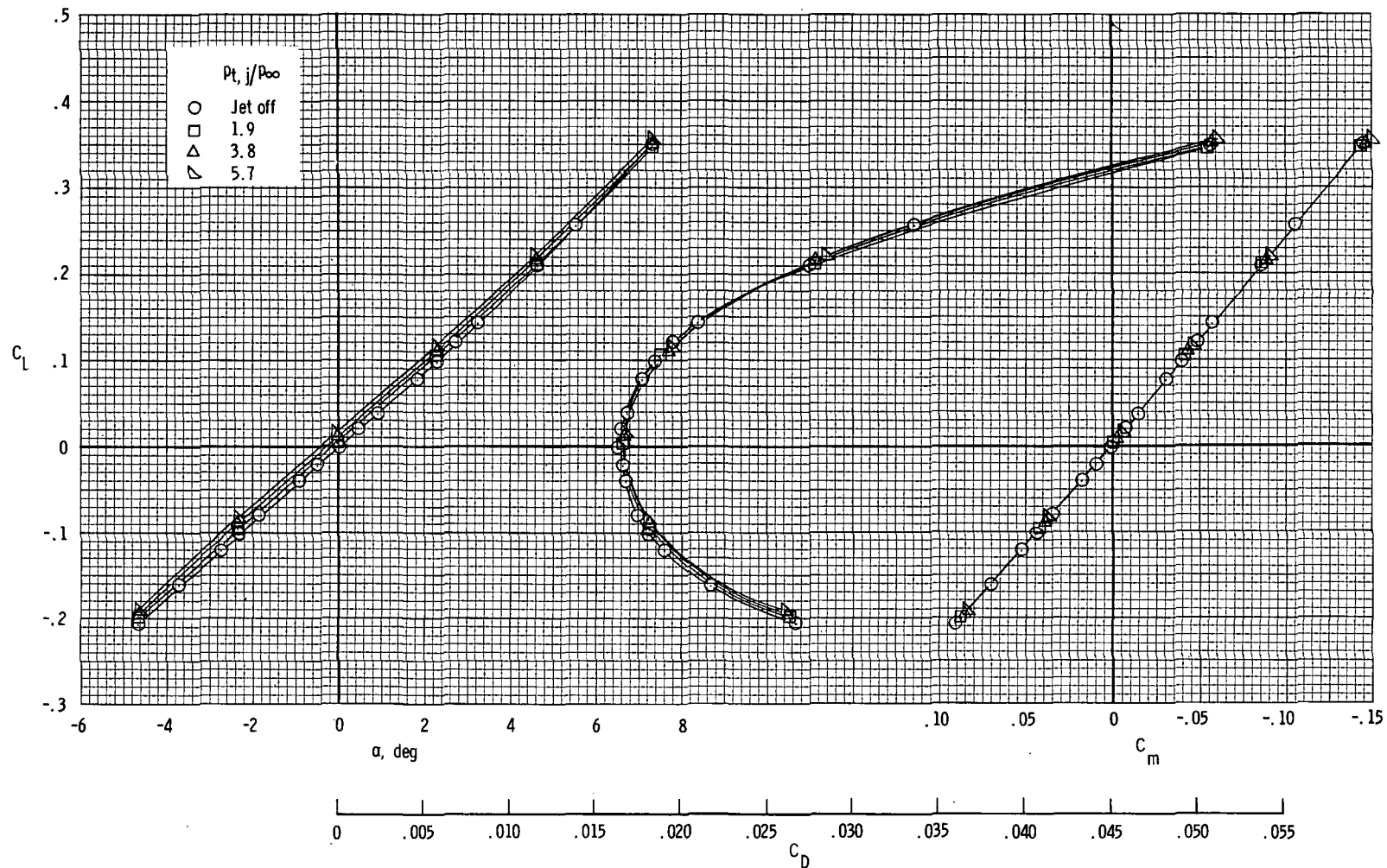
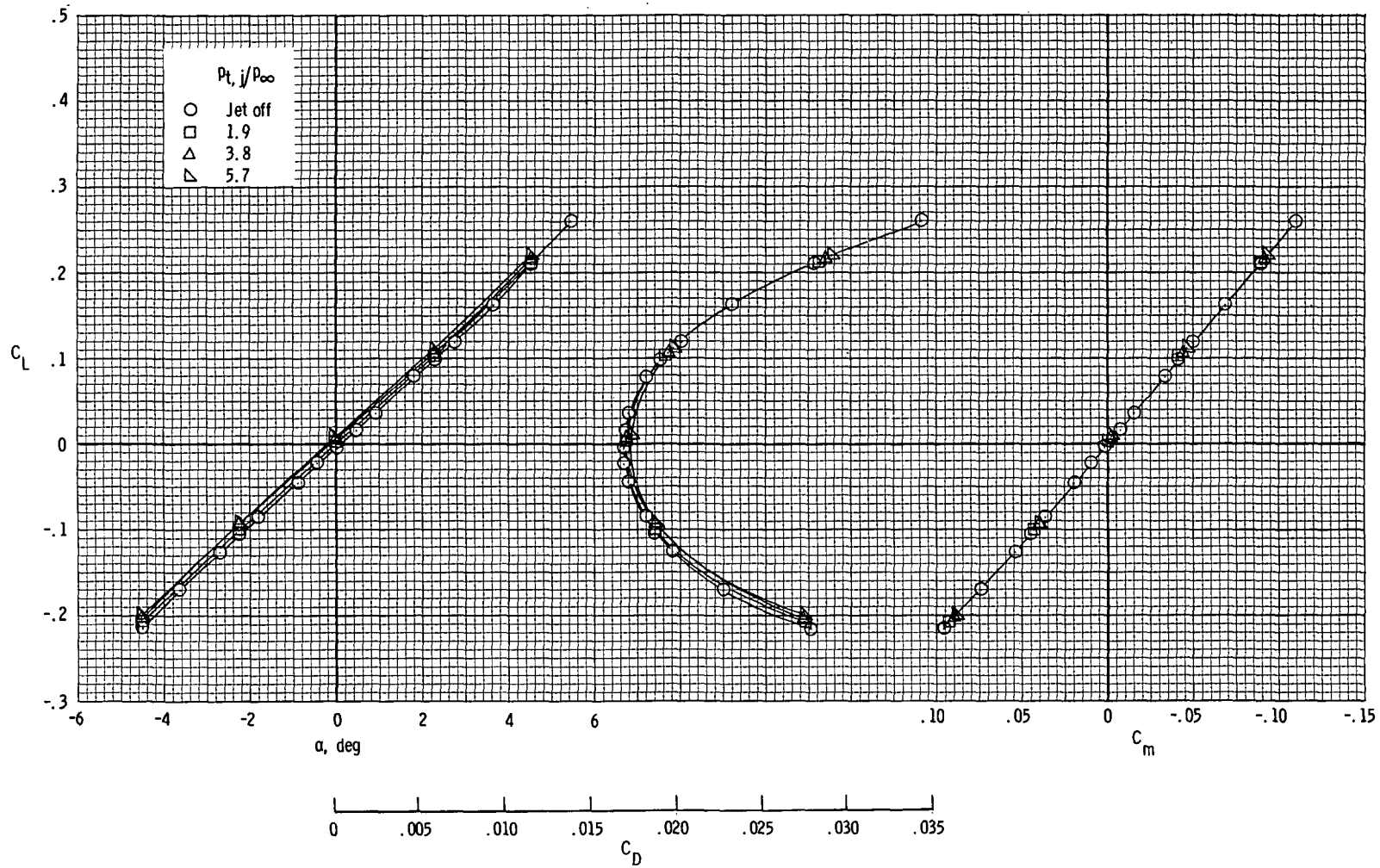
(b) $M = 0.60$.

Figure 14.- Continued.



(c) $M = 0.70$.

Figure 14.- Continued.

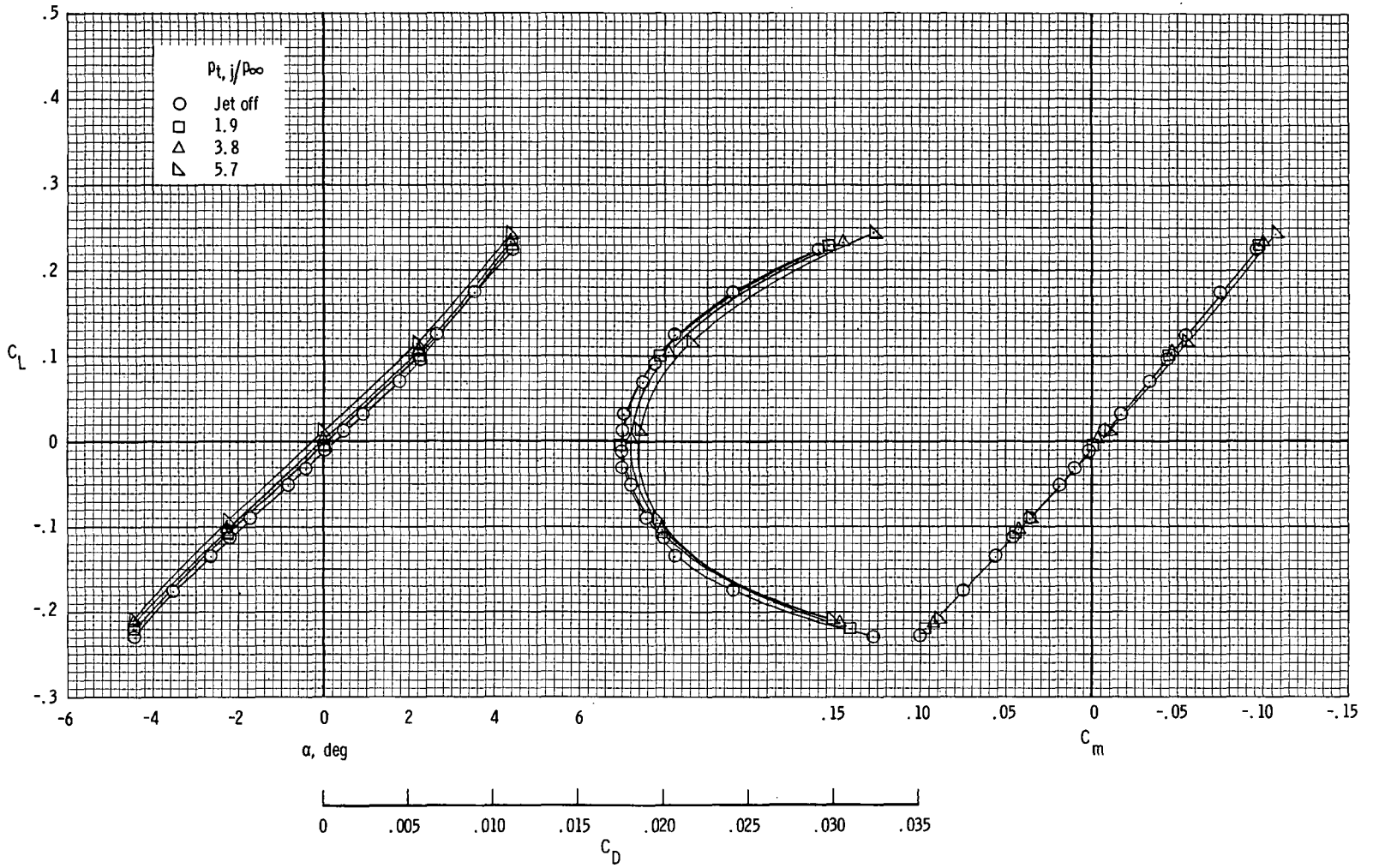
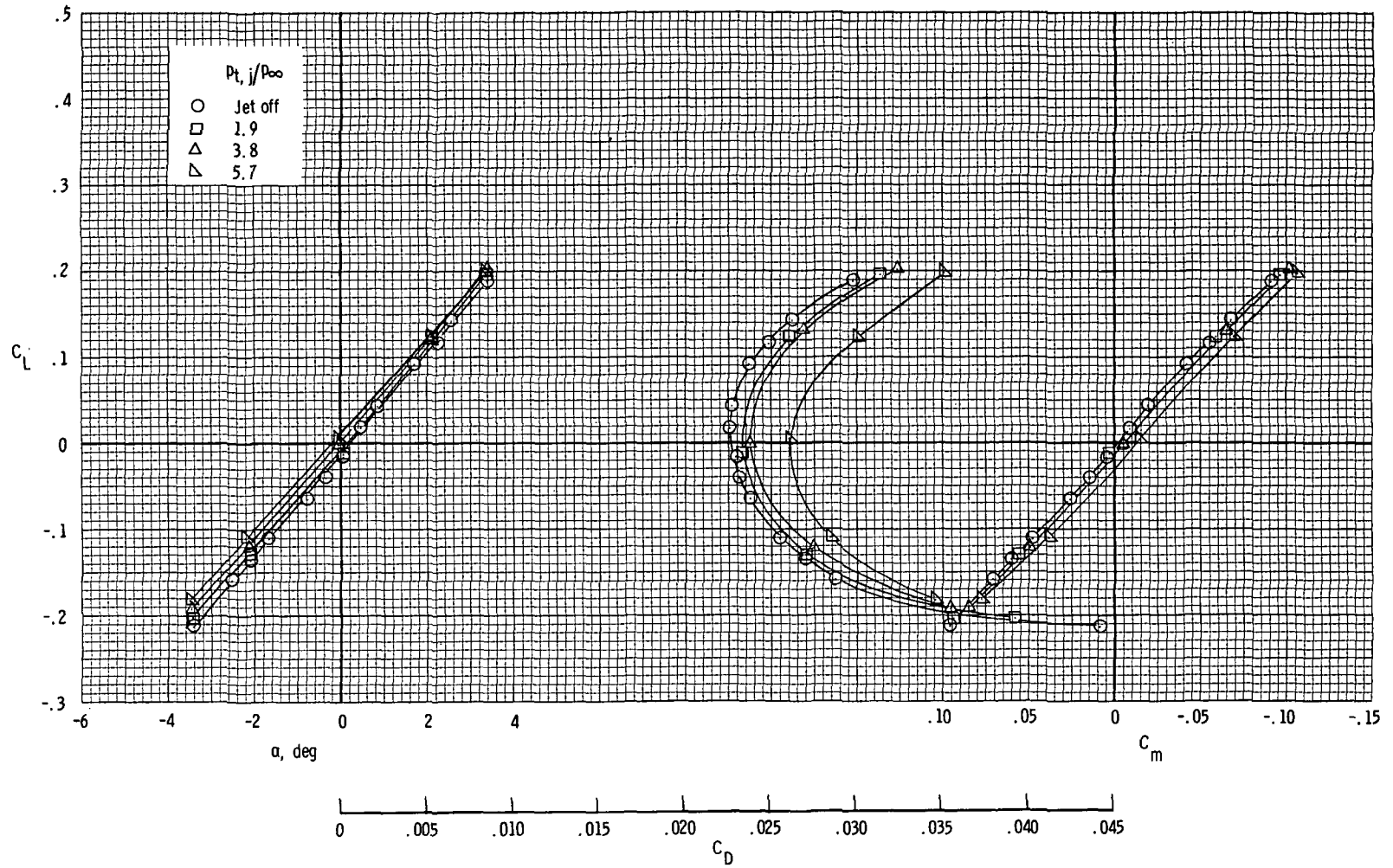
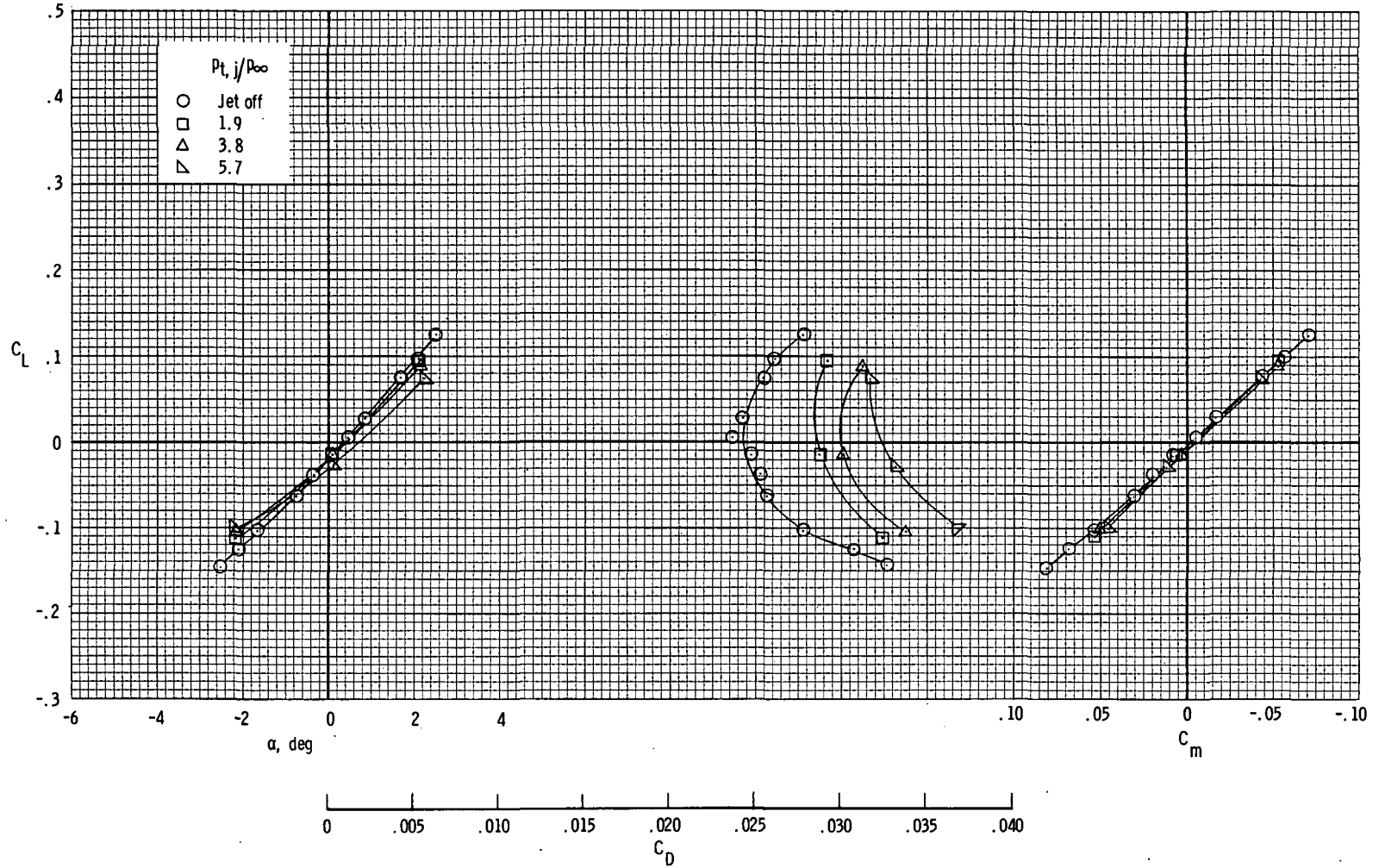
(d) $M = 0.80$.

Figure 14.- Continued.



(e) $M = 0.90$.

Figure 14.- Continued.



(f) $M = 0.95$.

Figure 14.- Concluded.

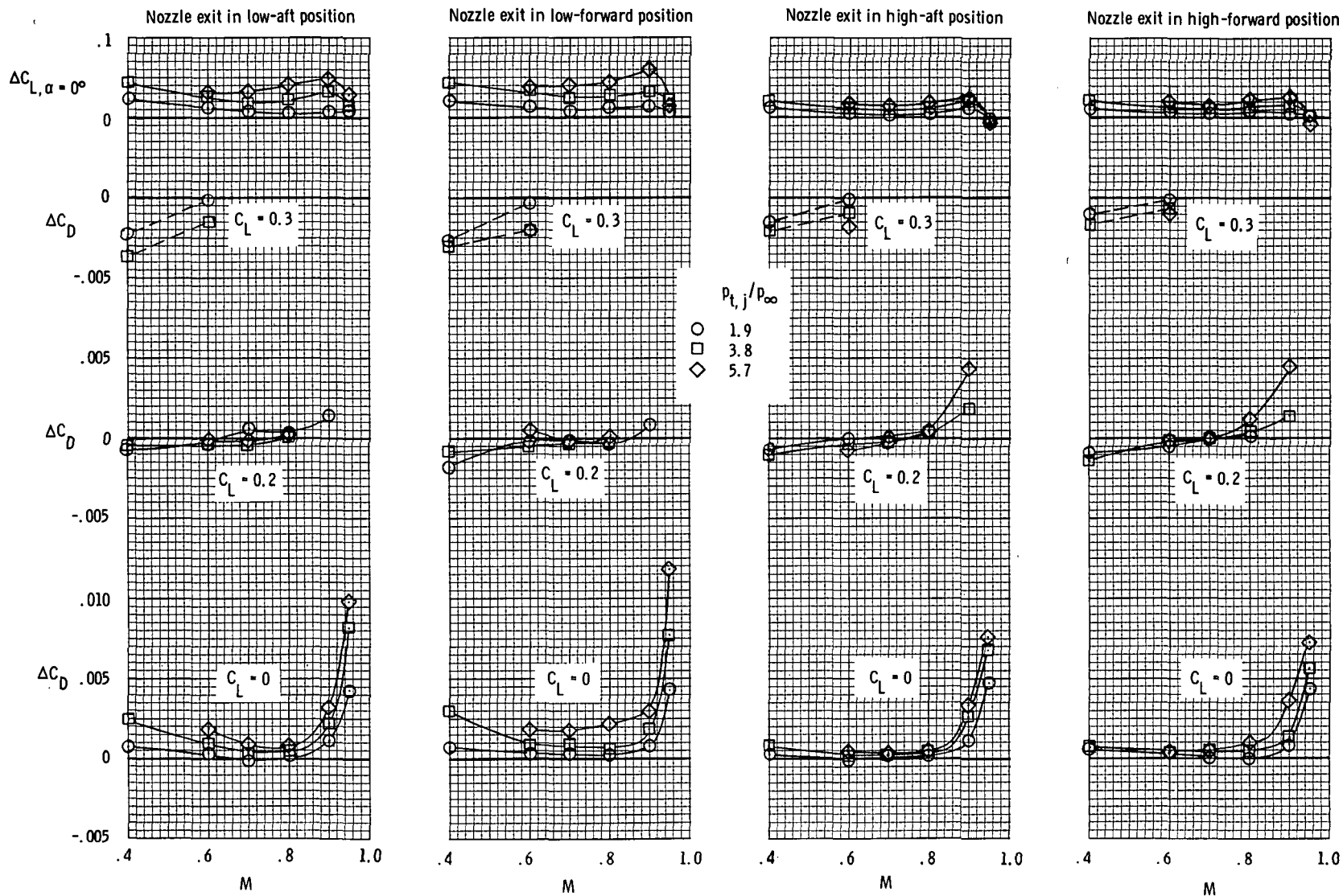


Figure 15.- Summary of effects of jet-total-pressure ratio on lift coefficient and drag coefficient of wing and afterbody. (Symbols denote data obtained from faired curves.)

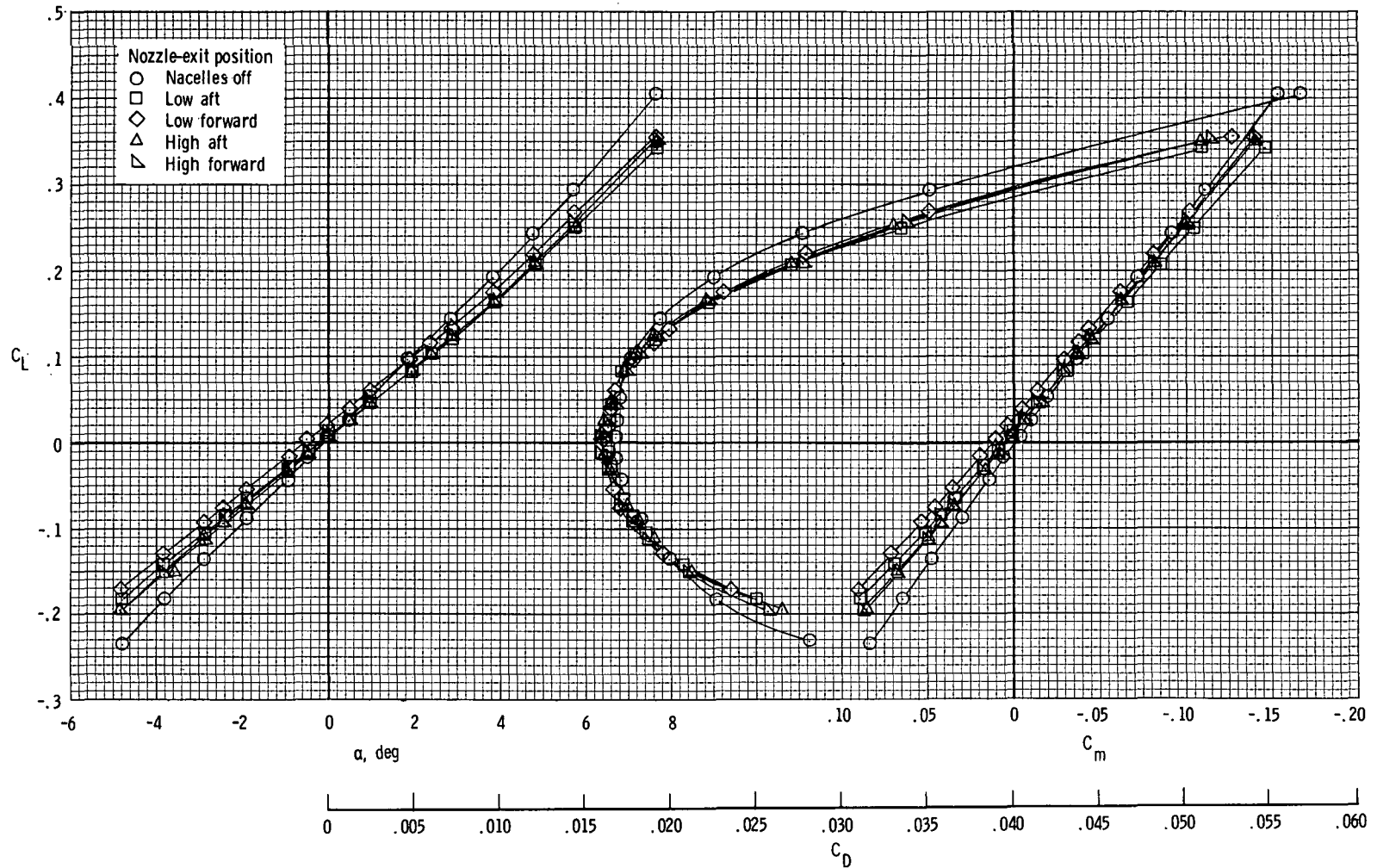
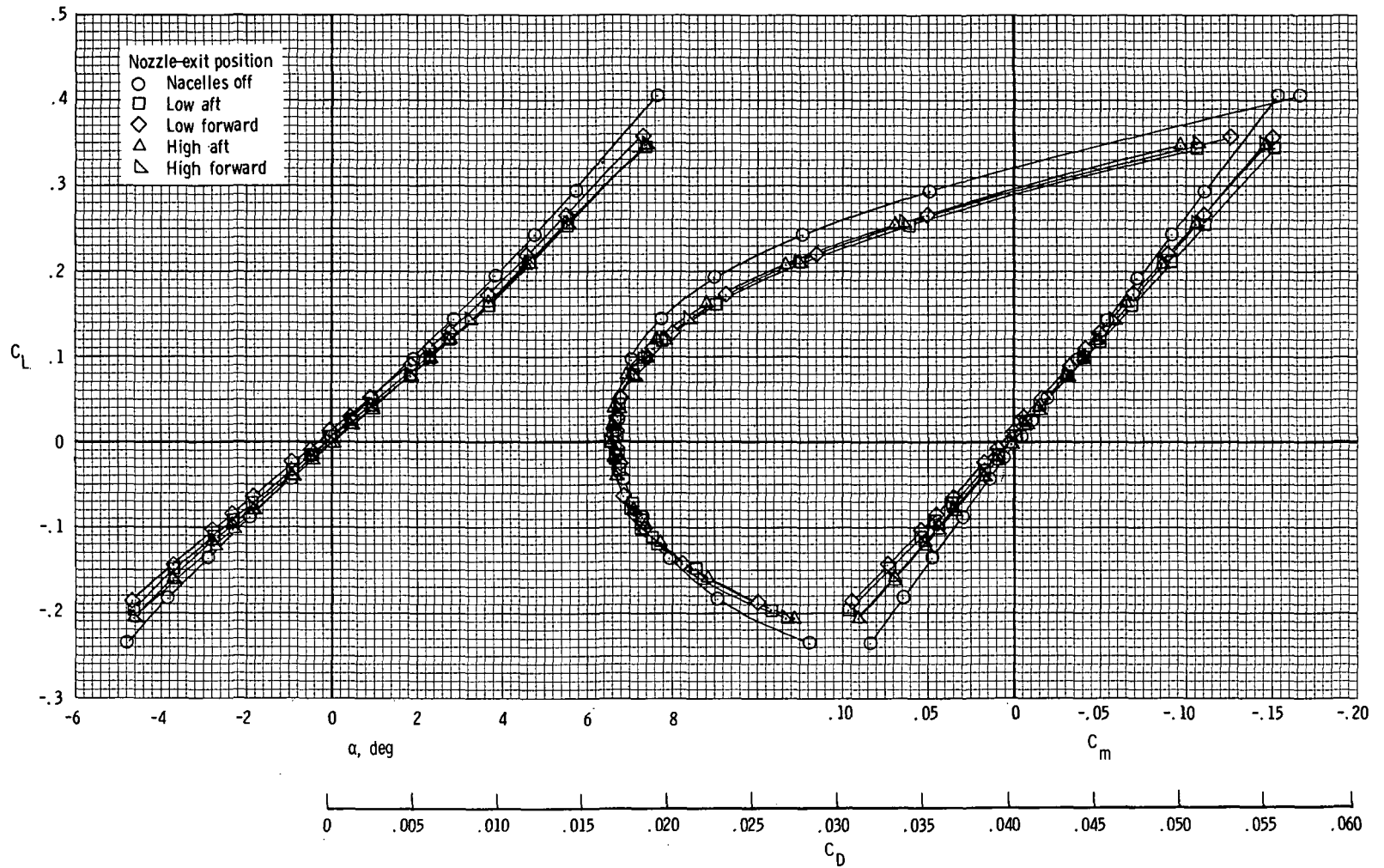
(a) $M = 0.40$.

Figure 16.- Effects of nacelle and pylon addition to configuration forebody on longitudinal aerodynamic characteristics of wing and afterbody. Jet off.



(b) $M = 0.60$.

Figure 16.- Continued.

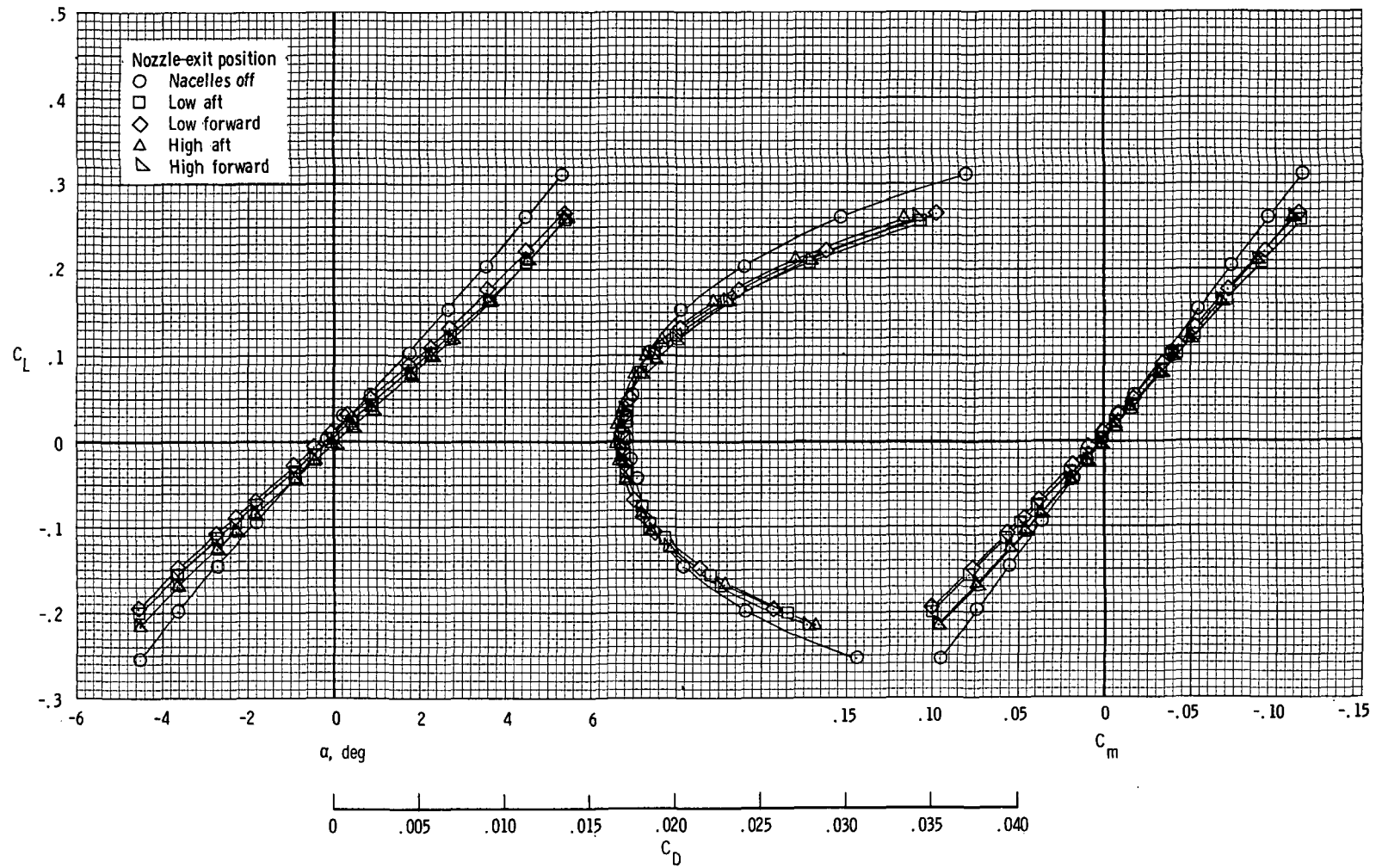
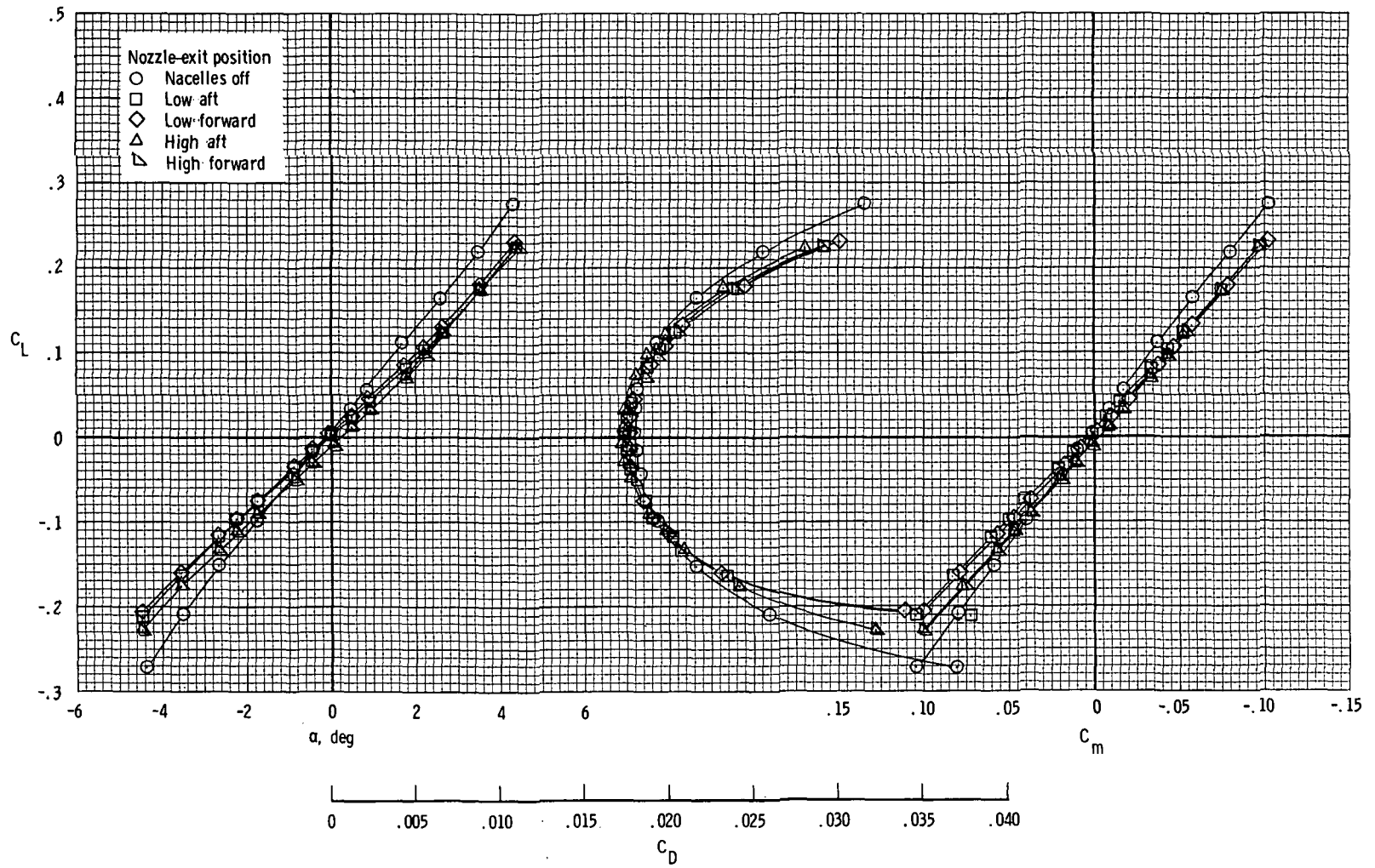
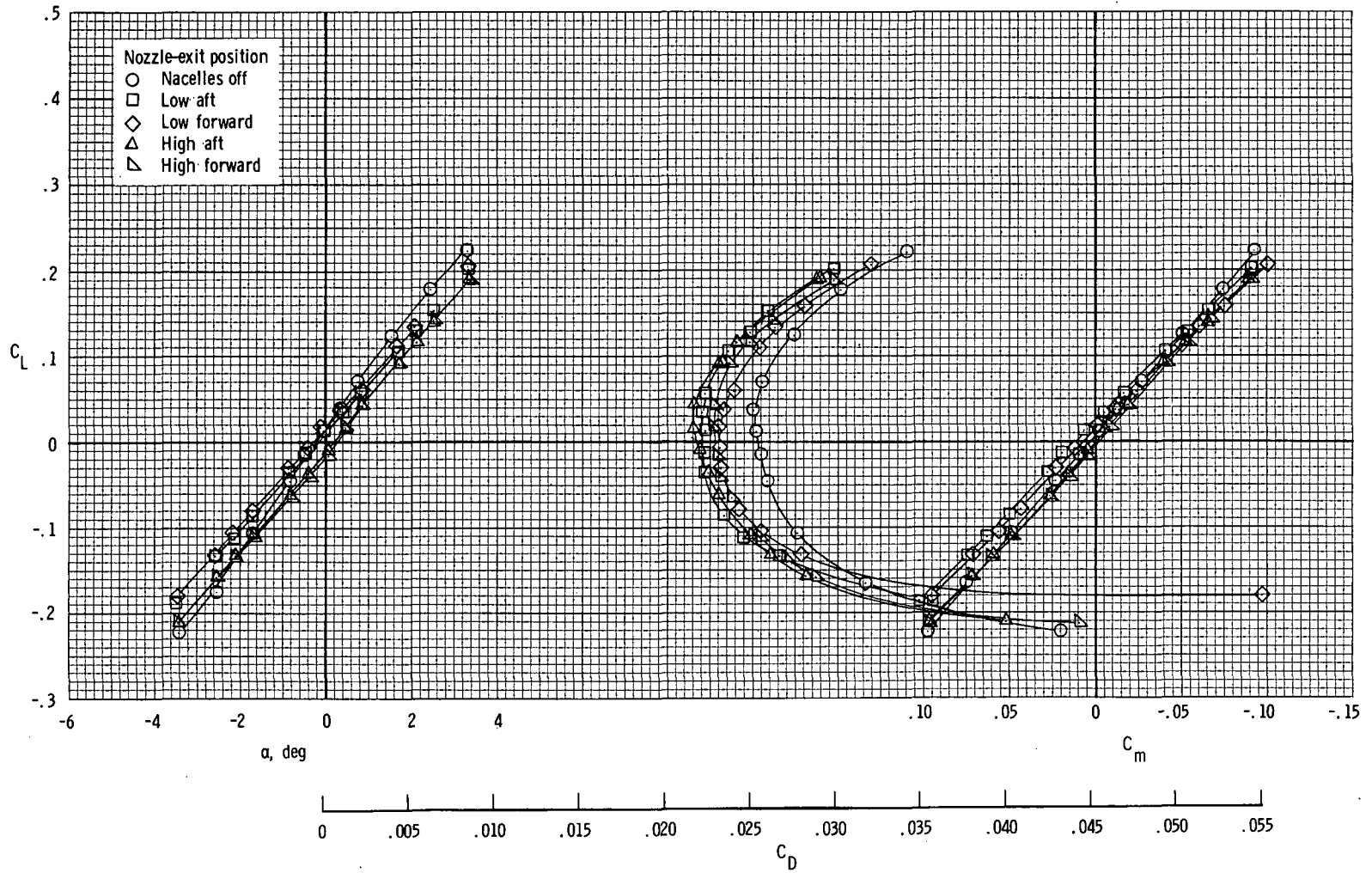
(c) $M = 0.70$.

Figure 16.- Continued.



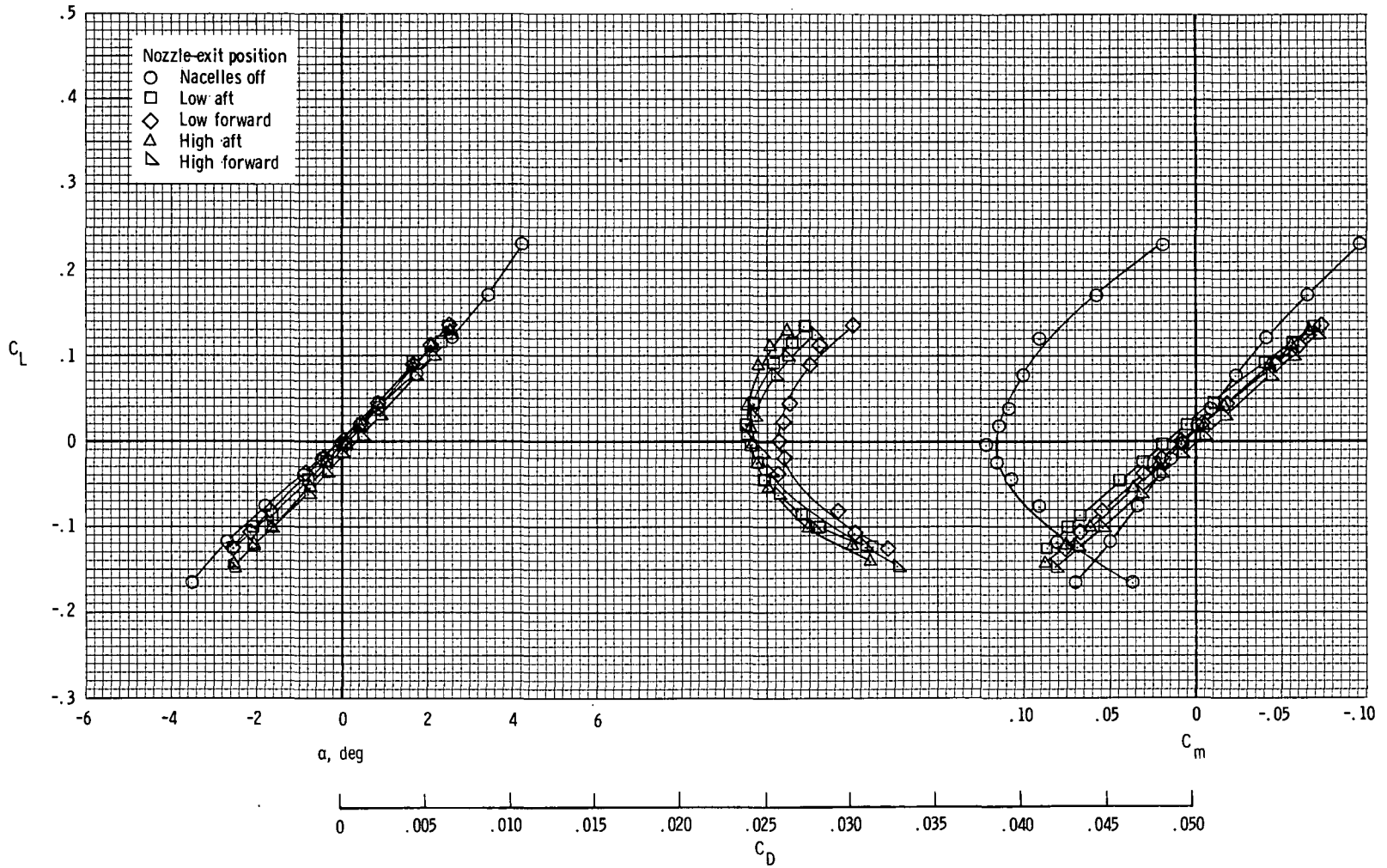
(d) $M = 0.80$.

Figure 16.- Continued.



(e) $M = 0.90$.

Figure 16.- Continued.



(f) $M = 0.95$.

Figure 16.- Concluded.

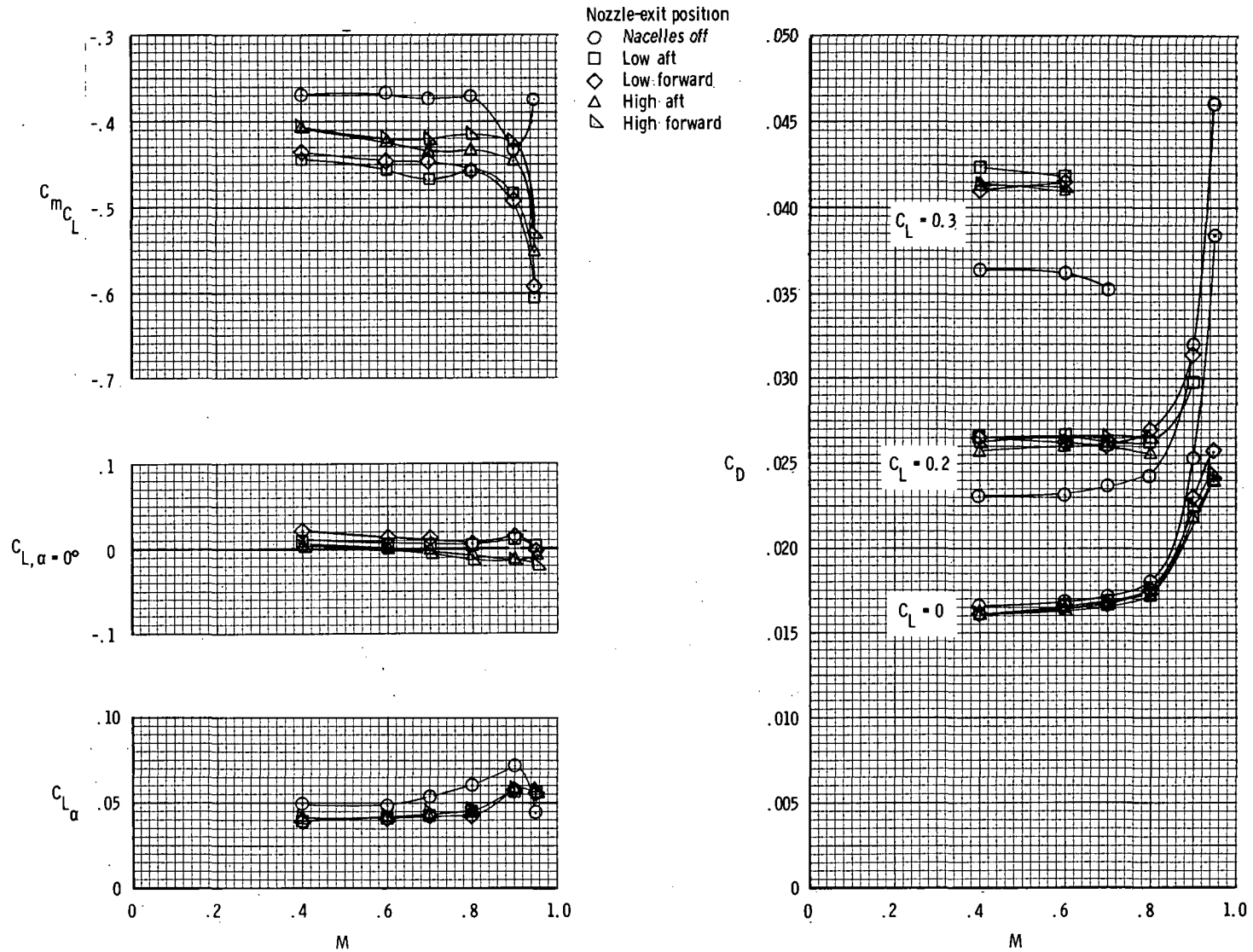


Figure 17.- Summary of effects of nozzle-exit position on longitudinal aerodynamic characteristics of wing and afterbody. Jet off. (Symbols denote data obtained from faired curves.)

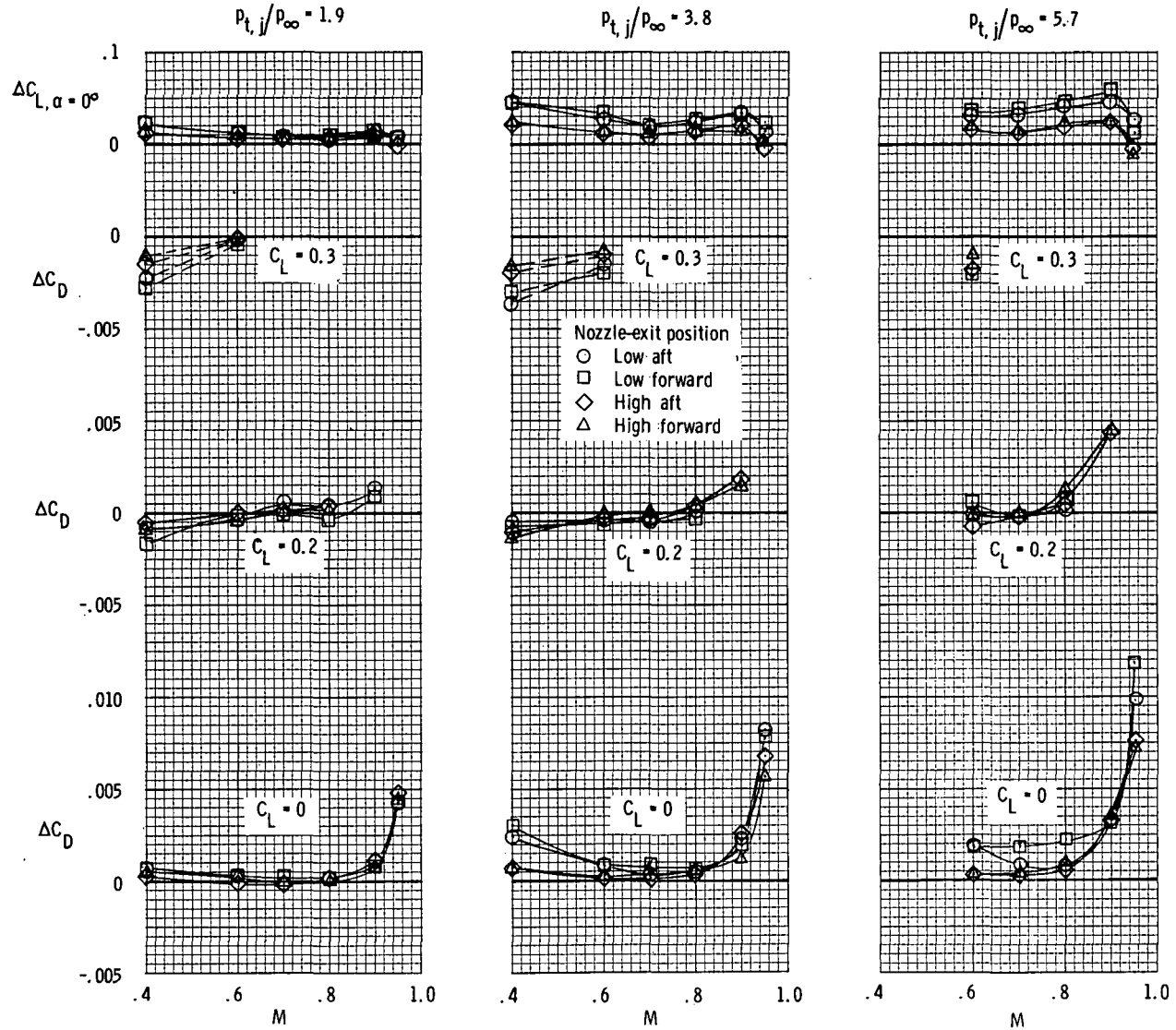


Figure 18.- Summary of effects of nozzle-exit position on lift-coefficient and drag-coefficient increments due to jet blowing. (Symbols denote data obtained from faired curves.)



POSTMASTER: If Undeliverable (Section 158
Postal Manual) Do Not Return

"The aeronautical and space activities of the United States shall be conducted so as to contribute . . . to the expansion of human knowledge of phenomena in the atmosphere and space. The Administration shall provide for the widest practicable and appropriate dissemination of information concerning its activities and the results thereof."

—NATIONAL AERONAUTICS AND SPACE ACT OF 1958

NASA SCIENTIFIC AND TECHNICAL PUBLICATIONS

TECHNICAL REPORTS: Scientific and technical information considered important, complete, and a lasting contribution to existing knowledge.

TECHNICAL NOTES: Information less broad in scope but nevertheless of importance as a contribution to existing knowledge.

TECHNICAL MEMORANDUMS: Information receiving limited distribution because of preliminary data, security classification, or other reasons. Also includes conference proceedings with either limited or unlimited distribution.

CONTRACTOR REPORTS: Scientific and technical information generated under a NASA contract or grant and considered an important contribution to existing knowledge.

TECHNICAL TRANSLATIONS: Information published in a foreign language considered to merit NASA distribution in English.

SPECIAL PUBLICATIONS: Information derived from or of value to NASA activities. Publications include final reports of major projects, monographs, data compilations, handbooks, sourcebooks, and special bibliographies.

TECHNOLOGY UTILIZATION PUBLICATIONS: Information on technology used by NASA that may be of particular interest in commercial and other non-aerospace applications. Publications include Tech Briefs, Technology Utilization Reports and Technology Surveys.

Details on the availability of these publications may be obtained from:

SCIENTIFIC AND TECHNICAL INFORMATION OFFICE

NATIONAL AERONAUTICS AND SPACE ADMINISTRATION

Washington, D.C. 20546